UNIVERSITY OF CALIFORNIA

Santa Barbara

Late Cretaceous tectonic evolution of the Deep Creek-Kern Mountains, eastern Nevada and western Utah: Magmatically induced large-scale folding, dynamothermal metamorphism and ductile strain at mid- to upper-crustal levels in the Sevier hinterland

A dissertation submitted in partial satisfaction of the

requirements for the degree Doctor of Philosophy

in Earth Science

by

Evan Burns Monroe

Committee in charge:

Professor Phillip B. Gans, Chair

Professor Francis Macdonald

Professor Matthew Rioux

June 2023

The dissertation of Evan Burns Monroe is approved.

_____

Francis Macdonald

_____

Matthew Rioux

_____

Phillip B. Gans

May 2023

VITA OF EVAN BURNS MONROE
May 2013

EDUCATION

Bachelor of Science in Geology, University of California, Santa Barbara, June 2013 (High Honors)

PROFESSIONAL EMPLOYMENT

2017-2023: Teaching Assistant, Department of Earth Science, University of California, Santa Barbara

AWARDS

Outstanding Graduating Senior, UCSB Earth Science, 2013
Outstanding Academic Achievement, UCSB Earth Science, 2013
Distinction in the Major, UCSB Earth Science, 2013

FIELDS OF STUDY

Structural Geology
Geologic Mapping
Tectonics
Geochronology

ABSTRACT

Late Cretaceous tectonic evolution of the Deep Creek-Kern Mountains, eastern Nevada and western Utah: Magmatically induced large-scale folding, dynamothermal metamorphism and ductile strain at mid- to upper-crustal levels in the Sevier hinterland

by

Evan Burns Monroe

Deformation and metamorphism in the hinterland of the Cretaceous Sevier Orogeny in western North America has often been attributed to be a result of the same retroarc shortening that caused deformation in the fold-and-thrust belt to the east. However, new data presented in this dissertation from the Kern Mountains and Deep Creek Range of western Utah and eastern Nevada suggests that, at least in this area, much of the deformation and metamorphism can be attributed to the emplacement of Late Cretaceous leucogranite plutons. The third and final chapter of this dissertation focuses on a different topic: a series of virtual field trips that were made for upper division Structural Geology and Physical Volcanology classes.

Chapter 1 focuses on the Trout Creek Intrusive Complex (TCIC) on the eastern flank of the Deep Creek Range, which forms the center of a Late Cretaceous granite cored gneiss dome. The TCIC is composed of several leucogranite stocks and numerous dikes and sills exposed over an area of ~2 km^2 and is surrounded by a structural dome with a diameter of ≥5 km and ~1-1.5 km of structural relief. Within a few hundred meters of the TCIC, rocks exhibit an intensification of penetrative strain and increase in metamorphic grade from

greenschist to amphibolite facies. Integrated geologic mapping, structural analysis and U-Pb geochronology of igneous zircon from the granite and metamorphic monazite from surrounding country rock indicates that peak metamorphism, doming of the country rock, and penetrative deformation occurred approximately synchronously with, and were a direct result of emplacement of the 80 ± 2 Ma TCIC. A regional foliation (S_1) developed prior to emplacement and was passively rotated during doming, while a younger more localized cleavage (S_2) was actively developing and upgraded during emplacement, ultimately resulting in a penetrative transposition foliation along the immediate margins.

Chapter 2 focuses on the southern flank Deep Creek Range and Kern Mountains and proposes that the Water Canyon Anticline, a major recumbent fold that has been previously interpreted to reflect Sevier-age tectonic shortening, formed in response to the emplacement of the Tungstonia Granite, a large highly peraluminous Late Cretaceous pluton that underlies most of the Kern Mountains. The Tungstonia Granite is surrounded by a deformational aureole with a well-developed foliation along its margins that parallels intrusive contact and decreases in intensity and dies out completely within a few hundred meters both outward into the country rock and inward towards to core of the pluton. This deformational aureole coincides with deflections of bedding into parallelism with the intrusive contact, the largest of which is the Water Canyon Anticline, where stratigraphy in the overturned limb is highly attenuated and parallels the northeastern margin of the pluton. U-Pb zircon geochronology from the Tungstonia suggests it was emplaced at ~70 Ma but that its upper and outer margins crystallized prior to its interior and deeper portions. Zircon ages show a continuous spectrum of ages from ~70 Ma to 80-90 Ma, suggesting a period of protracted crustal

anatexis and crystallization prior to final emplacement. U-Pb geochronology of monazite from two amphibolite facies metamorphic aureoles in the southern Deep Creek Range indicates a prolonged period of monazite crystallization from ~80-90 Ma followed by another episode of crystallization at 70 ± 2 Ma. We interpret the earlier period to reflect a protracted prograde metamorphism, anatexis, and fluid flow that is also reflect in the zircon ages from the Tungstonia, with the 70 ± 2 Ma peak possibly reflecting final ascent of the Tungstonia magma/crystal mush. We propose that the area now occupied by the southern Deep Creek Range and Kern Mountains served as a long lived "channel" during the Late Cretaceous, where leucogranite melts and fluids were funneled upward, resulting in localized metamorphism and culminating in the emplacement of the largest Late Cretaceous pluton in eastern Nevada—the Tungstonia Granite.

The third chapter discusses eight virtual field trips were produced for upper division Structural Geology and Volcanology classes that integrate high-quality videos taken at classic field sites with focused assignments requiring data analysis and interpretation. Virtual field trips help alleviate the logistical, financial, and accessibility issues associated with in-person trips, and allow students to work at their own pace, view annotations that clarify geologic relationships, and can provide superior audio and outcrop viewing experiences. Major drawbacks of virtual field exercises are that students don't get the same hands-on experiences observing rocks and collecting data, deciphering ambiguous relationships, and group bonding. We believe these virtual field trips are best used in conjunction with in-person trips in order to reinforce the material, provide more opportunities for field-experiences, and provide an alternative for students who can't attend a trip in-person.

I. Late Cretaceous magmatic perturbation of the thermal-mechanical architecture of the Sevier hinterland middle crust in western Utah

Introduction

The hinterland region of the Sevier Orogen in western Utah and eastern Nevada hosts numerous Late Cretaceous leucogranite plutons with isotopic compositions that indicate they formed from nearly pure crustal melts (Barton and Anderson, 1990; Best et al., 1974; Farmer and De Paolo, 1983; Miller and Bradfish, 1980). These leucogranites often form the core of structural and deformational culminations that resemble gneiss domes. Metamorphic fabrics in these domes have commonly been interpreted as reflecting regional strain; however, many of these domes display abrupt lateral increases in metamorphism and intensification of strain in the immediate surroundings of Late Cretaceous granites. In these settings, distinguishing between regional tectonite fabrics and those related to granite emplacement is challenging, and yet the distinction is critical for regional tectonic interpretations. The role of these granite cored gneiss domes on the thermal and deformational architecture of the hinterland crust during the Late Cretaceous remains enigmatic.

The Deep Creek Range of western Utah experienced significant deformation, metamorphism, and plutonism during the Late Cretaceous and is an ideal place to investigate these problems. The range has been tilted approximately 40-50° to the west during slip on a range bounding normal fault so that paleodepth increases to the east (Rodgers, 1987), providing a cross-section of the upper to middle crust and the opportunity to investigate the interplay between pluton emplacement and deformation at different

structural levels. A domal structural culmination centered on the Late Cretaceous Trout Creek Intrusive Complex (TCIC) is characterized by an abrupt increase in metamorphic grade and strain in the country rock and has all of the trademark features of a granite cored gneiss dome. In this study, we present the results of integrated geologic mapping, microstructural analysis, and metamorphic and igneous geochronology to constrain the age of emplacement of the TCIC and its role in deformation and metamorphism in the country rock.

Geology of the Deep Creek Range

The Deep Creek Range is a N-S trending mountain range on the Nevada-Utah border in the eastern Great Basin located in the heart of the Sevier hinterland, where mid- to lower-crustal thickening above an inferred west-dipping basal detachment surface accommodated east-directed thin-skinned shortening in the fold-and-thrust belt in central Utah (Figure 1a; Armstrong, 1968; DeCelles & Coogan, 2006; Miller and Gans, 1989; Taylor et al, 2000). Crustal thickening in the hinterland led to prograde metamorphism and anatexis in the lower crust, ultimately resulting in the emplacement of leucogranite plutons with isotopic compositions indicative of nearly pure crustal melts (Douce et al., 1990; Farmer and DePaolo, 1983; Lee et al., 2003; Miller and Bradfish, 1980; Wright and Wooden, 1991). Metamorphism and plutonism were geographically dispersed and diachronous but peaked in the Late Cretaceous (90-70 Ma; Camilleri and Chamberlain, 1997; Cruz-Uribe et al., 2015; Kelly et al., 2015; McGrew et al., 2000; Miller et al., 1988; Miller and Gans, 1989).

The geologic framework of the southern Deep Creek Range was laid out by Rodgers (1987), who focused on the deformational and thermal history and provided important

context for this project. The eastern Deep Creek Range is underlain by the Neoproterozoic Trout Creek and McCoy Creek groups, composed of interbedded quartzite, metapelite, schist, metadiamictite, and minor marble. The western part of the range is underlain by upper-crustal Paleozoic carbonates and Eocene volcanic rocks (Figure 1b and c). The Eocene Ibapah pluton intrudes the older succession in the central part of the range and has a narrow contact metamorphic aureole that overprints penetrative cleavages that are

interpreted to have formed during the Cretaceous. The first is reflected in a west dipping cleavage (S_1) that is also present in many other nearby ranges and is interpreted to have formed as a result of east directed layer parallel shear (Miller et al., 1988; Rodgers, 1987). During the second event, rocks on the southern flank of the range were folded into the Water Canyon Anticline, a large recumbent fold that closes to the west and has a gently north plunging fold axis. A locally developed cleavage (S_2) that appears to be axial planar to the

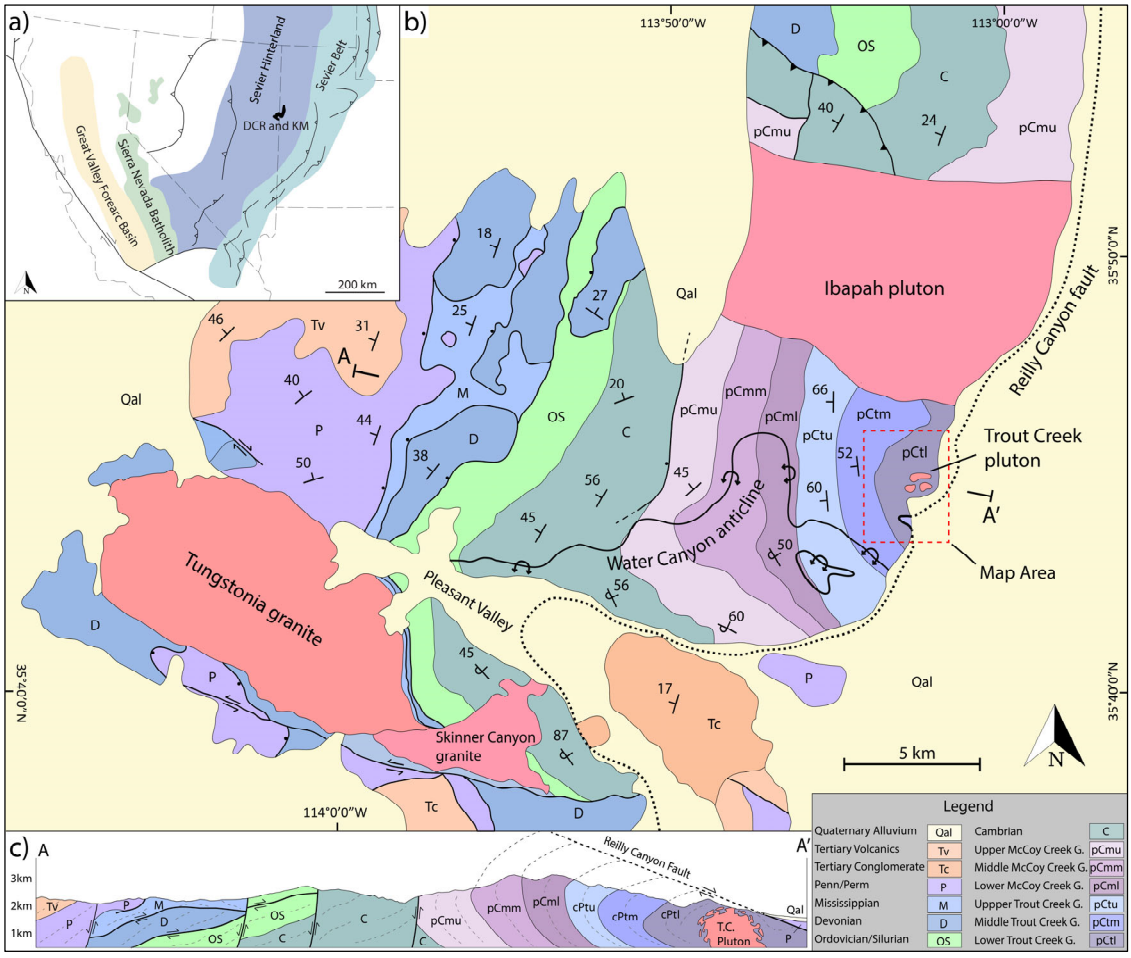

Figure 1: a) Simplified tectonic map of a portion of the western U.S. showing the location of major tectonic features of the Sevier orogen. The Deep Creek Range is located on the Nevada-Utah border and lies within the hinterland of the Sevier orogen approximately 100 km west of the frontal portion of the fold-and-thrust belt (modified from DeCelles and Coogan, 2006). b) Simplified geologic map of the Deep Creek Range and Kern Mountains based on mapping by Hose and Blake (1976), Rodgers (1987), and Nutt and Thorman (1994). c) Simplified WNW-ESE cross section across the southern Deep Creek Range based on mapping by Rodgers (1987) and Nutt and Thorman (1994).

Water Canyon Anticline also developed during this event. Metamorphism increases down section from unmetamorphosed Paleozoic carbonates in the west to upper greenschist grade within the stratigraphically lowest units and locally to amphibolite grade in several metamorphic culminations. The Trout Creek culmination, and associated Trout Creek pluton, are situated at the deepest exposed structural levels on the eastern flank of the range and are the primary focus of this study (Figures 1 and 2).

Geology of the Trout Creek Culmination

Rodgers (1987) briefly discusses the Trout Creek area and speculated that the doming and increase in deformation and metamorphism was a result of pluton emplacement. Three weeks of field study for this project built upon his work by mapping contacts in greater detail, collecting a dense array of bedding and cleavage orientations, and sampling key units for petrographic and geochronologic analysis. This new work is illustrated in a detailed map of a ~15 km^2 area centered around the Trout Creek pluton, as well as two perpendicular cross sections across the map area (Figures 2 and 3).

The Trout Creek intrusion consists of a medium- to fine-grained leucogranite that intrudes the basal schist member of the ~4500 m thick Trout Creek Group (Figure 4a). The

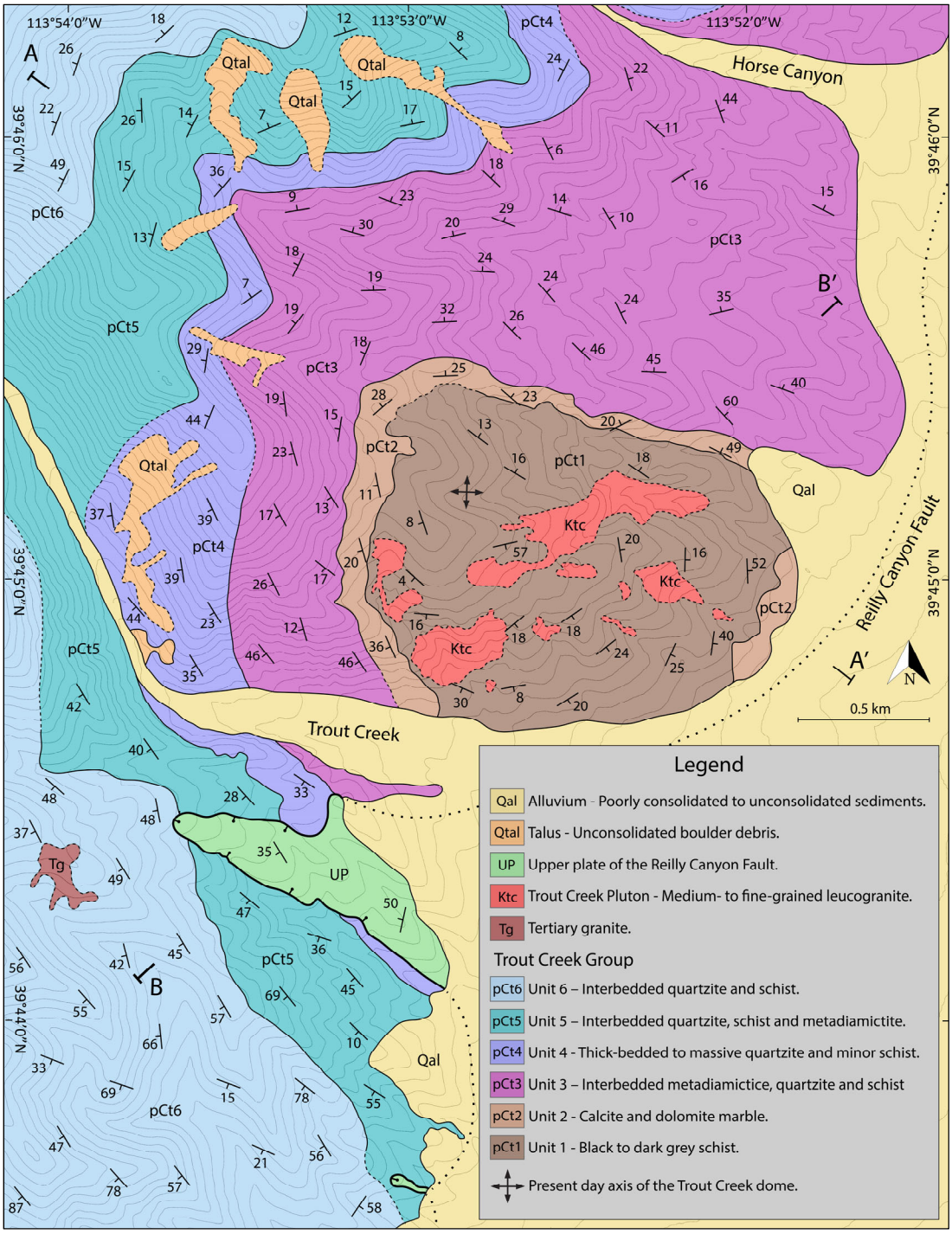

Figure 2: Geologic map of the Trout Creek culmination.

exposed pluton isn't composed of a single body, but instead is exposed over a ~2 km^2 area as abundant dikes and sills (not shown in Figure 2) that radiate from several small stocks,

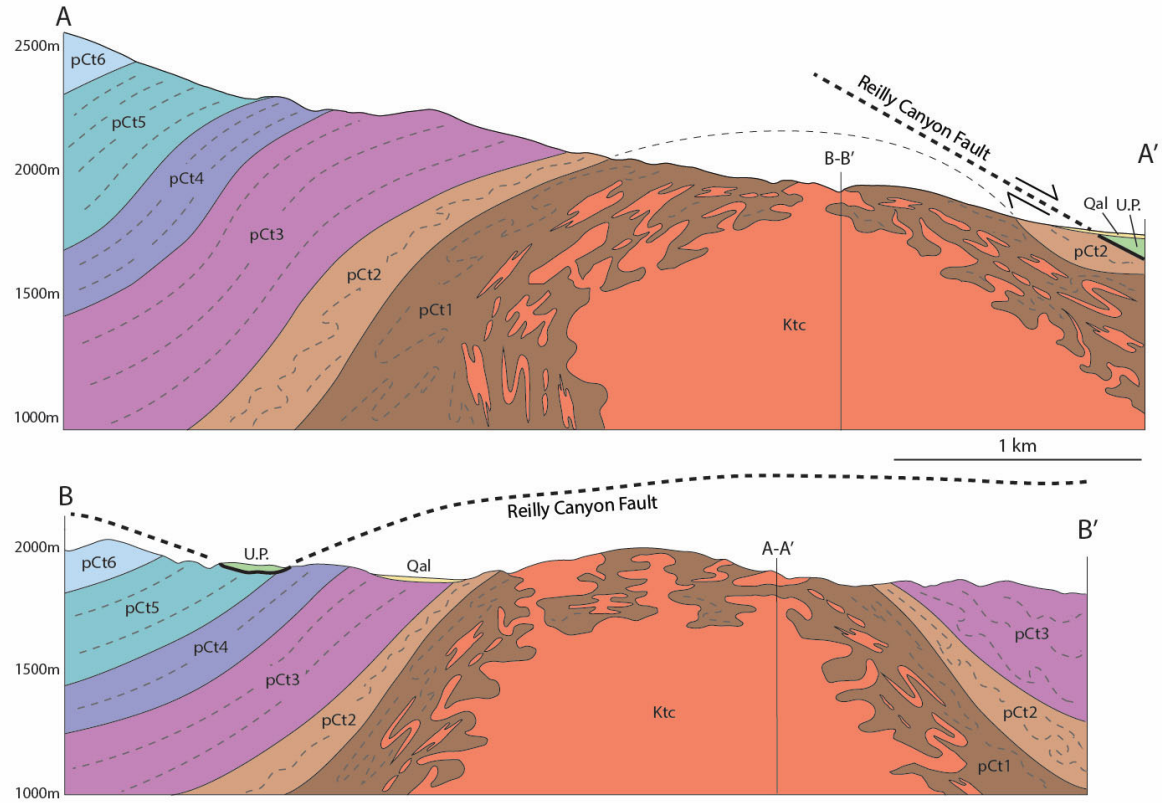

Figure 3: Mutually perpendicular cross sections along lines A-A' (NW-SE) and B-B' (SW-NE) on the geologic map. Both cross sections have a similar geometry, highlighting the fact that the culmination has a domal and not cylindrical geometry. However, A-A' is approximately perpendicular to the axis of Cenozoic tilting of the range and therefore the geometry of the culmination when it formed during the Cretaceous is tilted to the west.

and will hereafter be referred to as the Trout Creek Intrusive Complex (TCIC). Bedding and both the S_1 and S_2 foliations dip gently to moderately away from the TCIC, forming a structural dome that is at least 5 km in diameter. Projection of unit contacts above the dome indicates that the dome has approximately 1-1.5 km of structural relief. The degree of penetrative deformation in the country rock increases markedly in the vicinity of the TCIC, grading over a distance of ~500 m from quartzites and phyllite with only weakly developed cleavages in shale beds and well-preserved sedimentary structures in quartzites, to highly strained tectonites with an intense transposition of foliation in the lower half of pCm3 and

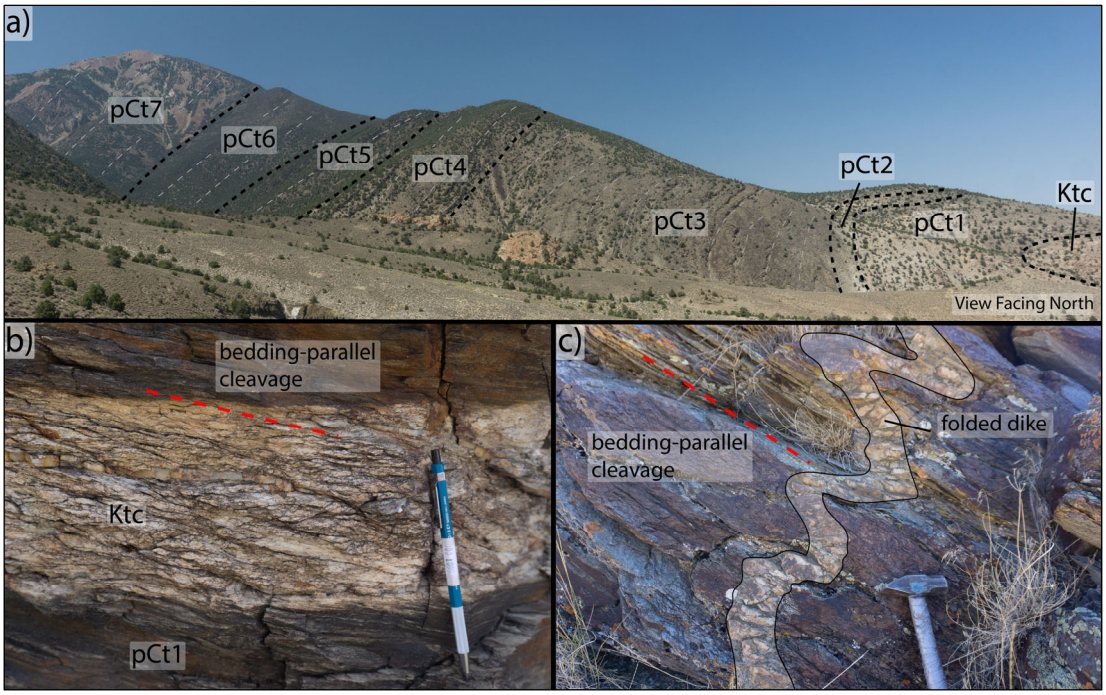

Figure 4 a) View north across Trout Creek Canyon showing the approximate contacts of the Trout Creek Group units (pCt1-pCt7) and the TCIC (Ktc). Bedding in general dips to the west in this part of the range and moves upsection westward towards the crest of the range, which is underlain by the uppermost unit of the Trout Creek Group. Distance across the field of view of the photo is approximately 8 km. b) Sill from the TCIC with a well-developed foliation that is continuous with the country rock. c) Folded TCIC dike with an axial surface approximately parallel to the bedding-parallel cleavage.

below. Metamorphic grade also increases within a few hundred meters of the TCIC from greenschist facies phyllite and fine-grained biotite-muscovite schist to amphibolite facies coarse-grained schist with conspicuous large porphyroblastic biotite, garnet, andalusite, and staurolite irregularly distributed within the basal schist (pCt1).

Two cleavages are present in schistose horizons of units 3, 5 and 6 of the Trout Creek Group in the periphery of the domal culmination. The first cleavage (S_1) is consistently more west dipping than bedding with an intersection angle of approximately 20-40° (Figure 5). This relationship with bedding is consistent around all sides of the culmination, suggesting that the cleavage formed prior to the development of the structural

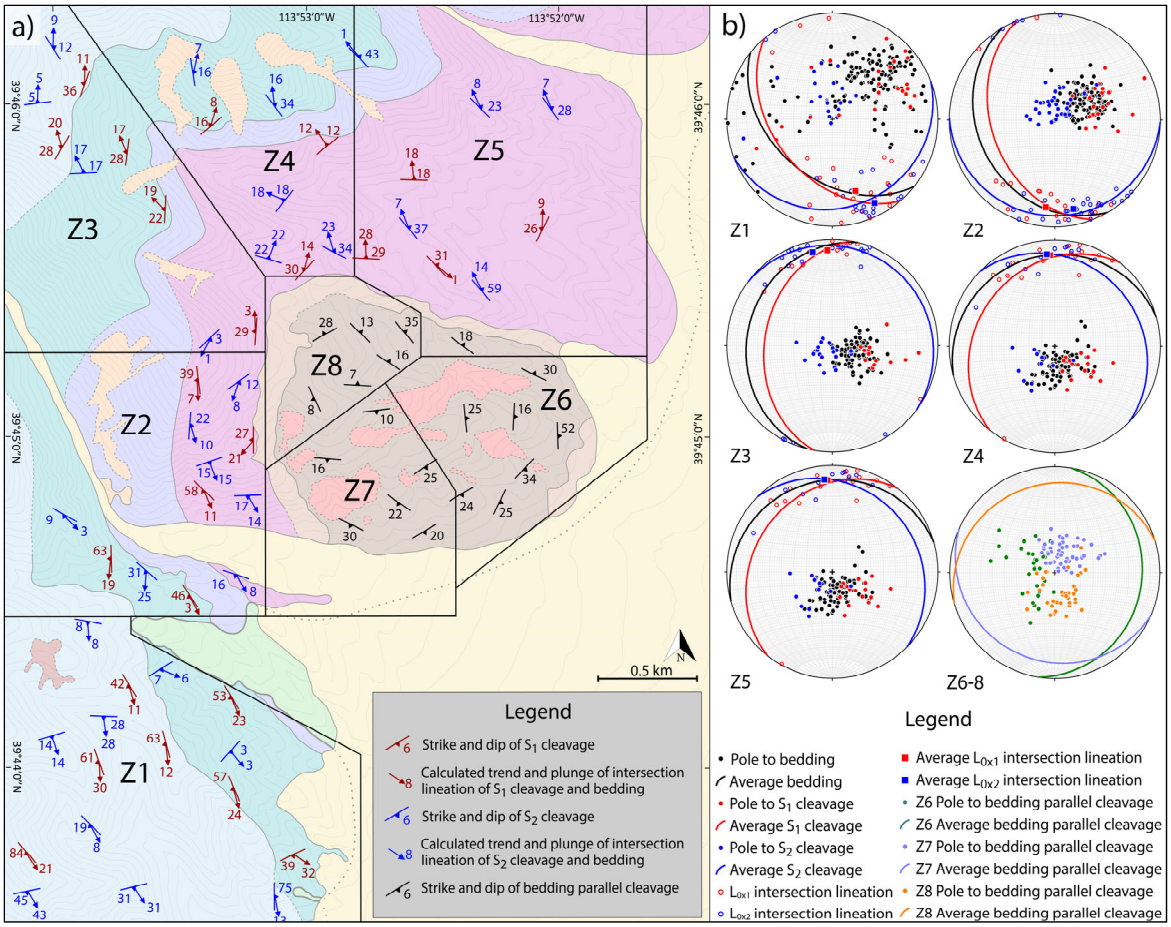

Figure 5: a) Map showing the orientations of the S_1, S_2 and bedding parallel cleavages and their intersection lineations with bedding. S_1 is consistently more west dipping than bedding and in general dips away from the Trout Creek pluton. The L_{0x1} intersection lineation plunges gently to the NNW in the northern half of the map area and to the SSE in the southern half. S_2 typically dips gently to moderately away from the center of the dome, with an L_{0x2} intersection lineation that plunges gently to moderately to the north to northwest in the northern half of the map area and to the south to southeast in the southern half. b) Zoned stereonets showing the orientations of poles to bedding, S_1, S_2 and the bedding parallel cleavage as well as calculated intersection lineations.

dome and was passively rotated during doming. This cleavage is widespread through the southern Deep Creek Range and increases in intensity and metamorphic grade from a spaced slaty cleavage in stratigraphically higher units near the crest of the range, to a penetrative biotite-grade schistosity in the deepest stratigraphic levels. A similar west-dipping cleavage is present in many of the surrounding ranges and thus appears to reflect a relatively

widespread deformational event in the Sevier hinterland (Miller et al., 1988, Miller and Gans, 1989). Previous workers interpreted this cleavage to be a result of east directed layer parallel shear when the section was approximately flat lying based on the observations that 1) the cleavage is consistently more west dipping than bedding and generally intersects bedding at an angle of less than 45 degrees, 2) the cleavage becomes more well developed and the intersection angle with bedding decreases with depth, and 3) folds associated with the cleavage are rare, suggesting that bedding was never in the shortening field (Miller et al., 1988; Miller and Gans, 1989; Rodgers, 1987).

The second cleavage (S_2) crenulates S_1 and generally dips east with respect to bedding, with an intersection angle of 15-45 degrees (Figure 5). This cleavage is only present at deeper structural levels in the Deep Creek Range and was interpreted by Rodgers (1987) to be an axial planar cleavage to the Water Canyon Anticline. However, second cleavages are sporadically developed in different parts of the range and may have developed at different times and have different origins. Within the Trout Creek culmination, the second cleavage dips away from exposures of the TCIC and is generally more gently dipping than bedding, suggesting it was at least partially developed prior to emplacement of the TCIC and was passively rotated during doming. However, it also increases in intensity and metamorphic grade in the vicinity of the TCIC within pCt3 and below, suggesting that it was actively developing during the time of emplacement and was upgraded due to the thermal effects of the magmas. In the basal micaceous schist unit of the Trout Creek sequence, there is a single very well-developed foliation that is parallel to bedding and contains numerous isoclinal folds with axial surfaces parallel to the foliation. It appears that the additional strain in the basal schist likely transposed bedding, S_1 and (early) S_2 into parallelism to form a

single penetrative foliation. This foliation forms the core of the dome and is subhorizontal at the dome axis and dips gently to moderately away from the dome around its margins (Figure 5). It is unclear whether this high-strain transposition foliation is an entirely new cleavage or simply an intensification of the S_2 cleavage described above.

The age of the penetrative strain and strain intensification appears closely related to the emplacement of the TCIC. Although the larger stocks appear undeformed, their margins have a well-developed deformational fabric that is continuous with and parallel to the fabric in the country rock (Figure 4b). Additionally, dikes and sills that radiate from the pluton are folded and boudinaged (Figure 4c). The lack of deformation in the interior of the stocks is likely due to the rheological contrast with the country rock. such that strain was strongly partitioned into the schist. The close spatial association of the highest strain rocks with the TCIC and the variable strain observed in the TCIC suggest the TCIC and high strain deformation were broadly synchronous. The highest intensity fabrics have a very well-developed foliation, but lineations are either absent or very weakly developed, suggesting strain was primarily in the flattening field.

Microstructures and Metamorphic Assemblages

Twenty-eight oriented samples of schist from Trout Creek Group units 1, 3, 5 and 6 were collected and examined petrographically to characterize deformational fabrics, metamorphic assemblages, porphyroblast-cleavage relationships and recrystallization mechanisms. These samples range from micaceous quartzite to pelites and contain varying proportions of quartz, muscovite, biotite and chlorite. More pelitic horizons near the base of pCt3 and pCt1 contain porphyroblasts of garnet ± andalusite ± staurolite.

The S_1 cleavage is best developed in pelitic horizons in Trout Creek units 3, 5, and 6 and is absent in the intervening quartzite units. It is defined by fine-grained syn-kinematic biotite and muscovite, which is partially retrograded to chlorite, as well as a weak grain or aggregate shape preferred orientation of quartz (Figure 6b). Sparse, small garnets in pCt3 have trails of quartz and oxide inclusions continuous with S_1, suggesting syn- to post-kinematic growth, however this relationship is obscured by D_2 deformation. The presence of synkinematic biotite and possibly garnet suggests that this cleavage formed at upper greenschist to lower amphibolite facies in this part of the range.

In the distal parts of the Trout Creek dome, S_2 is a spaced cleavage defined by distinct bands of aligned biotite, muscovite and chlorite and insoluble concentrations of oxides along dissolution seams (Figure 6b). Here, rocks appear only weakly strained and sedimentary structures in many outcrops are still recognizable. The S_2 cleavage domains are spaced 200-400 um apart and separate quartz-rich microlithons that preserve the S_1 cleavage. The growth of micas along dissolution seams suggests that the cleavage began to form by crenulation of the S_1 cleavage and dissolution/precipitation of quartz along the cleavage domains, followed by new mica growth at a higher metamorphic grade. In the lower portions of pCt3 in the vicinity of the TCIC, the S_2 cleavage is better developed and defined by penetrative mica growth, largely obscuring the S_1 cleavage (Figure 6c). Cleavage domains of S_2 are still recognizable but more closely spaced and overprinted by penetrative mica growth. In outcrop, these rocks appear progressively more flaggy and strained from the middle of pCt3 toward its base, with sedimentary structures becoming unrecognizable.

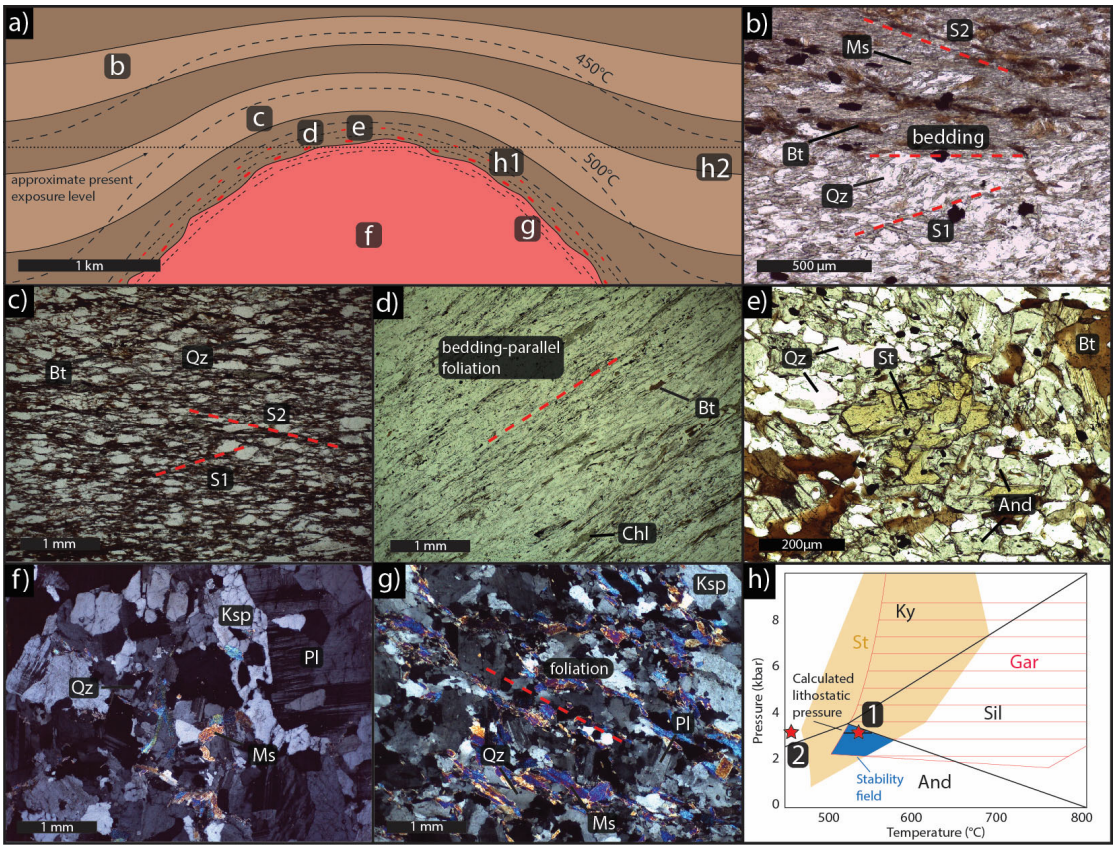

Figure 6: a) Schematic cross section of the Trout Creek culmination during the Late Cretaceous showing doming of the country rock, elevated isotherms, and the approximate present exposure level. The high strain fabric along the pluton margins is shown schematically as dashed lines and metamorphism is shown as red rectangles. b) Photomicrograph with a view facing north showing bedding, S_1 and S_2. S_1 dips toward the west (left) and is defined by aligned muscovite which is most obvious in the lower half of the image and in the upper half within microlithons of the S_2 cleavage. The S_2 cleavage dips to the right (east) and is a spaced cleavage defined by cleavage domains of aligned synkinematic biotite (PPL). c) Sample from pCt3 showing a very well developed S_2 cleavage (PPL). d) High-strain bedding parallel foliation in pCt1 defined by highly aligned micas and a grain shape preferred orientation in quartz (PPL). e) Sample from pCt1 with porphyroblastic biotite, staurolite, and andalusite (PPL). f) Undeformed TCIC leucogranite from the interior of the stock. g) Deformed TCIC leucogranite from the margins of a dike. h) P-T diagram showing the stability fields of garnet, staurolite and the aluminosilicates. The assemblage of garnet+staurolite+andalusite in the Trout Creek schist indicates pressures of ~2-3.8 kbar and temperatures of ~500-600°C (stability field shown in blue). Calculated lithostatic pressure for a 13.5 km section of rock with an average density of 2.6 g/km^3 shown as horizontal line in the blue stability field for the assemblage.

The basal schist of the Trout Creek Group is highly strained with a single well-developed bedding-parallel penetrative cleavage defined by aligned micas and a grain and aggregate shape preferred orientation in quartz (Figure 6d). In outcrop, these rocks are

flaggy and sedimentary structures have been completely overprinted by deformation. The additional strain within this unit obscured S_1-S_2 relations by transposing them into parallelism with each other and with bedding. Conspicuous porphyroblastic garnet, biotite, andalusite and staurolite are irregularly distributed in close proximity to the TCIC. Garnet typically occurs as 1-2 mm porphyroblasts that are partially to completely replaced by post-kinematic sericite or chlorite. Cores have fine-grained inclusions that make them appear "dirty" whereas the rims are clear, suggesting two stages of growth or a change in reaction during a single stage of growth. Micas are aligned with the foliation and present in strain shadows of garnet porphyroblasts, indicating synkinematic growth of mica and pre- to synkinematic garnet growth. In some samples there is also decussate biotite that cuts the foliation, indicating post-kinematic static growth. Andalusite occurs as porphyroblasts up to ~2 cm across with strain fabric-parallel quartz inclusions, suggesting syn- to post-kinematic growth (Figure 6e). Andalusite pseudomorphs composed of fine-grained micas and quartz up to 5 cm across are more common and indicate that andalusite was widespread within pCt1. Staurolite occurs as 100-500 um porphyroblasts but the timing of growth is ambiguous (Figure 6e). Quartz occurs as weakly aligned aggregates with equant to slightly elongate grains exhibiting polygonal grain boundaries suggestive of static recrystallization. The highly variable quartz grain-size and similar extinction angle of adjacent subgrains suggests that subgrain rotation recrystallization was dominant. However, pinning structure between micas and quartz was also observed, suggesting a component of grain boundary migration.

The Trout Creek pluton is largely undeformed in its interior but has a well-developed foliation around its margins and in dikes and sills that is continuous with the country rock

(Figures 6f and 6g). The foliation decreases in intensity with distance from the pluton margins and is defined by aligned muscovite and a grain-shape preferred orientation in quartz. Feldspar is relatively undeformed except for moderate deformation twinning and minor recrystallization around grain boundaries, indicating that the majority of strain was partitioned into the quartz and micas.

Textural relationships between porphyroblasts and the deformational fabric and their spatial coincidence suggests that peak metamorphism occured during the formation of the high strain fabric in the basal unit of the Trout Creek Group. The presence of garnet, andalusite and staurolite indicates that peak P-T conditions were between ~2-3.8 kb and ~500-600°C (Figure 6h; Spear, 1993). Additionally, the dominant recrystallization mechanism observed in quartz is subgrain rotation with minor grain boundary migration, suggesting temperatures of approximately 500-550°C (Hirth and Tullis, 1992). Pressures of ~2-3.8 kbar require no burial beyond the stratigraphic depth for the lower Trout Creek Group; using a stratigraphic depth of 13.5 km and an average rock density of 2.7 g/cm^3, the pressure would be ~3.6 kbar, in the upper part of the stability field. Temperatures of 500-550°C at this depth would require an average geothermal gradient of approximately 35-40°C/km, which is quite high even for orogenic systems. It is more likely that the increase in temperature is localized around the TCIC and is a direct result of heat from the magma itself, rather than a regionally elevated geothermal gradient.

U-Pb Geochronology

Methods

U-Pb geochronology was performed on zircon from the main phase of the TCIC and monazite from the basal unit of the Trout Creek Group using the Laser-Ablation Split-Stream facility at UC Santa Barbara following the methods described in Kylander-Clark et al. (2013). Zircon crystals from a sample of the TCIC were separated using standard magnetic and density techniques, mounted on an epoxy puck, and imaged using the cathodoluminescence detector on UCSB's FEI Quanta 400F field emission source SEM prior to analysis. Monazite was analyzed in thin section to evaluate the petrographic context of mineral growth and stability. Unfortunately, grains were too small (<15um) for EPMA mapping or to perform multiple analyses per grain. Samples were ablated with a Photon Machines Excite 193 nm excimer laser using a spot size and repetition rate of 24 μm and 4 Hz, and 8 μm and 3 Hz for zircon and monazite respectively. U-Pb isotopes were measured with a Nu Instruments Plasma HR multi-collector ICP for both zircon and monazite, and element concentrations for monazite were measured concurrently using an Agilent 7700X quadrupole ICPMS . The primary reference material (RM) for zircon U-Pb was 91500 (Wiedenbeck et al., 1995) and GJ1 (Horstwood et al., 2016) and Plešovice (Sláma et al., 2008) were employed for accuracy and yielded ages within 2% of their expected values. Monazite 44069 was used as the primary RM for U-Pb normalization and Bananiera (Palin et al., 2013), FC-1 (Horstwood et al., 2003) and Trebilcock (Tomascak et al., 1996) yielded U-Pb ages within 2% of their expected values. Bananiera (Kylander-Clark et al., 2013) was used as the primary trace-element RM, assuming 12.9% P in monazite. Twenty-seven spot analyses were performed for zircon and a final age was calculated from a single population of nine ages. Spot analyses on fifty-one monazite grains were performed. Isotope data was reduced using Iolite software and plotted with Isoplot software (Paton et al., 2011).

Results

Prior to this study, the TCIC and associated amphibolite-facies metamorphism had no credible age constraints. Rodgers (1987) performed $^{40}Ar/^{39}Ar$ analyses on muscovite and microcline from the TCIC that yielded ages of 25-29 Ma and 17-26 Ma, respectively. However, these ages reflect final cooling of these minerals to temperatures of <350°C, not the crystallization or metamorphic age. Our new U-Pb analysis of zircon from the interior of one of the large stocks indicates a crystallization age of 80 ± 2 Ma, calculated from a single population of nine concordant analyses (Figure 7a; Monroe et al., 2023a). Older Mesozoic and Proterozoic ages (not shown in diagram) are interpreted to be inherited and the two younger ages are interpreted to be due to minor lead loss.

Metamorphic monazite from the Trout Creek schist yielded a wide range of 207-corrected ages between ca. 100–38 Ma (Figure 7b and 7c; Monroe et al., 2023b). Although this may suggest multiple (re)crystallization events or prolonged (re)crystallization, a cluster of dates at ~80 Ma suggests peak metamorphism at approximately the same time as pluton emplacement. The presence of two small bodies of ~39 Ma granite in the map area as well as the nearby much larger ~39 Ma Ibapah pluton suggests that the ~39 Ma monazite ages may reflect an important Eocene reheating event. It is possible that the intermediate ages reflect mixed analyses between older (~80 Ma) cores and Eocene rims in a single laser spot. The peak of ages at ~58 Ma appears to be statistically significant and may represent a (re)crystallization event whose significance is unclear. The REE profile for all the monazite analyses is typical for metamorphic monazite and the depletion of the HREEs indicates garnet stability during monazite growth (Figure 7d).

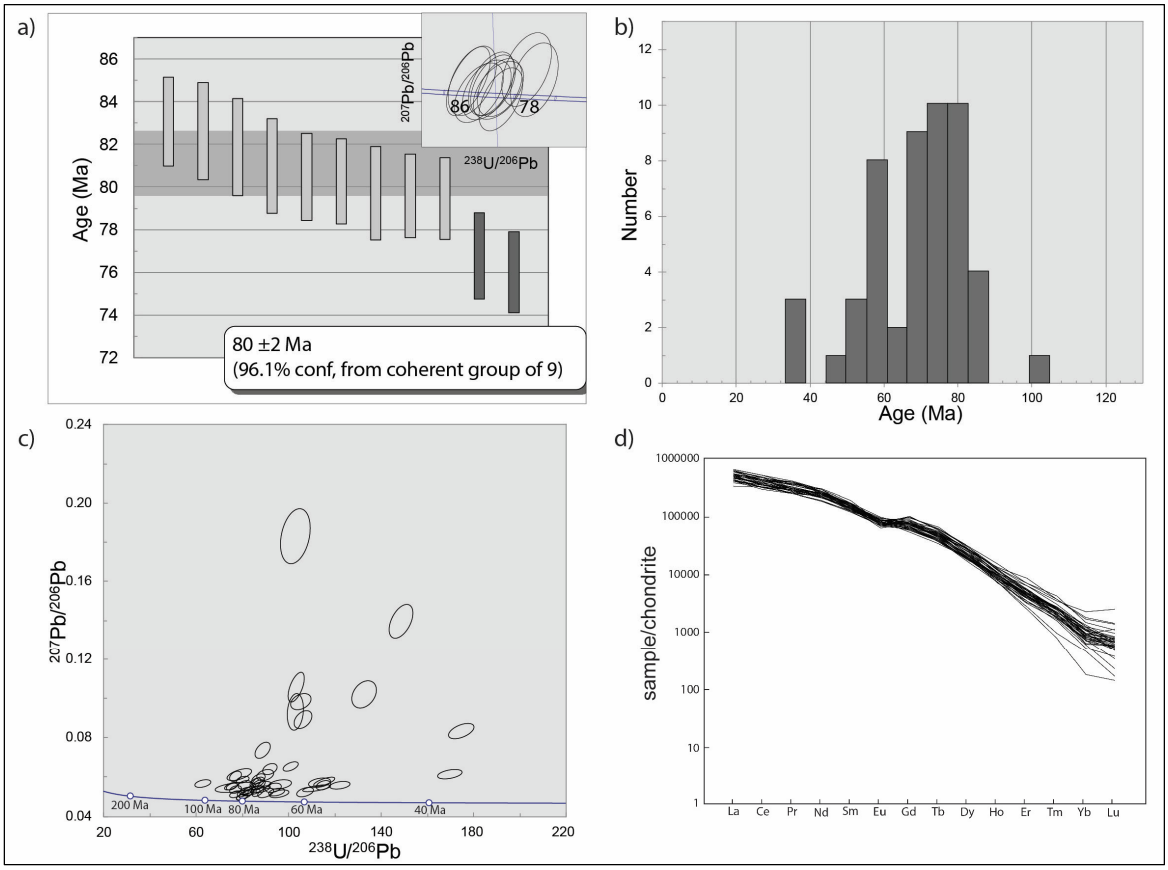

Figure 7: a) Plot showing the ages with errors of individual zircon analyses. Light grey bars represent ages that fit within a single population are were used in the final age calculation. Terra-Wasserberg concordia diagram (inset) shows that all U-Pb ratios are concordant. b) Histogram showing the distribution of monazite ages obtained from analysis of the Trout Creek schist. c) Terra-Wasserberg concordia plot of the monazite analyses showing a wide range of concordance values. d) REE plot from the monazite showing a depletion in HREEs indicating monazite growth in the presence of garnet.

Discussion

The structural and geochronological data gathered from the Trout Creek culmination permits a reinterpretation of the timing and nature of metamorphism. The regionally developed S_1 cleavage that dips more westward than bedding is present throughout the culmination but does not appear to be upgraded near the TCIC and is interpreted to have formed prior to doming and the emplacement of the TCIC. A second cleavage that generally

dips more eastward with respect to bedding was upgraded in the vicinity of the TCIC and is interpreted to have been actively forming during doming. In the core of the dome, the two cleavages and bedding are transposed into a single high-strain amphibolite facies fabric. This zone of upgraded metamorphism and high strain is pervasively intruded by the TCIC, which is characterized by abundant folded and boudinaged dikes and sills with a tectonite fabric that passes continuously into the country rock. Thus, it appears that metamorphism, development of the high strain fabric and doming of the country rock occurred approximately synchronously with intrusion of the ~80 Ma TCIC. Further evidence to support this interpretation comes from the U-Pb geochronology data that indicates monazite growth in the schist began at approximately the same time as crystallization of TCIC. Thus, we conclude that emplacement of the TCIC was the primary cause of structural doming, localization of fabrics and increased metamorphic grade.

When a pluton is emplaced in the crust, space must be made to accommodate the additional volume of the ascending magma body (e.g. Hutton, 1996). Some of the hypothesized mechanisms for creating this space include fracturing and diking, stoping, ductile flow, folding of the country rocks, and tectonic accommodation along faults or ductile shear zones (e.g. Clemens and Mawer 1992; Glazner, 2004; Paterson and Farris, 2008; Paterson and Fowler 1993; Miller and Paterson, 1999). Ductile emplacement mechanisms are more likely to dominate at mid-crustal levels. In the case of the TCIC, the space occupied by the intrusion appears to have been accommodated by a combination of doming of its roof rocks and ductile flow immediately above and along the margins of the intrusion. The structural dome surrounding the TCIC has a diameter of at least 5 km with

~1-1.5 km of structural relief which could accommodate an estimated ≥6 km^3 of additional space. We suggest that the exposures of the TCIC at the surface are small bodies near the roof of a larger pluton at depth, as illustrated in Figure 3. Thermal rheologic weakening within the metamorphic aureole appears to have helped localize strain to within ~500 m of the TCIC and allowed for the pluton to more easily deform the country rock during emplacement. Although it is apparent that doming and ductile attenuation occurred above the roof of the pluton, it is unclear what mechanisms dominated along its sides and lower margins as only the uppermost parts of the pluton are exposed at the current level.

Impact of Late Cretaceous plutons on the Sevier hinterland

The TCIC is one of many Late Cretaceous leucogranites in the Sevier hinterland and provides a striking example of how plutons can affect the deformational and thermal architecture of their surroundings (Figure 8). Heat and fluids advected from depth by the ascending magma body resulted in elevated temperatures and strain localization at relatively shallow levels in the crust. Isotherms which are commonly thought to be horizontal apparently had significant topography, resulting in high lateral thermal gradients. In the Trout Creek culmination, background temperatures are estimated to have been ~400°C, but were upgraded to 550-600°C in the vicinity of the pluton. The complex strain field in the vicinity of the TCIC resulted from superposition of tectonite fabrics related to regional shortening and the local effects associated with pluton emplacement. Although the Trout Creek culmination is a relatively small-scale case, there are numerous other larger Cretaceous leucogranites in the Sevier hinterland that show a similar intensification of strain and metamorphism, including the ~71 Ma Tungstonia granite in the Kern Mountains (Best

et al., 1974; Gottlieb, et al., 2022) and the 94 ± 2 Ma Lexington Creek pluton in the Southern Snake Range (Gottlieb et al., 2022; Lee and Christiansen, 1983). Exposures of high strain dynamothermally metamorphosed rocks such as are exposed in the vicinity of the TCIC would, in isolation, likely be interpreted as a product of a regional Barrovian metamorphic and deformational event, not the local deformational and thermal effects of a nearby pluton. This study emphasizes the need for caution in making "tectonic" interpretations from rocks that may instead be recording very local thermal and structural events.

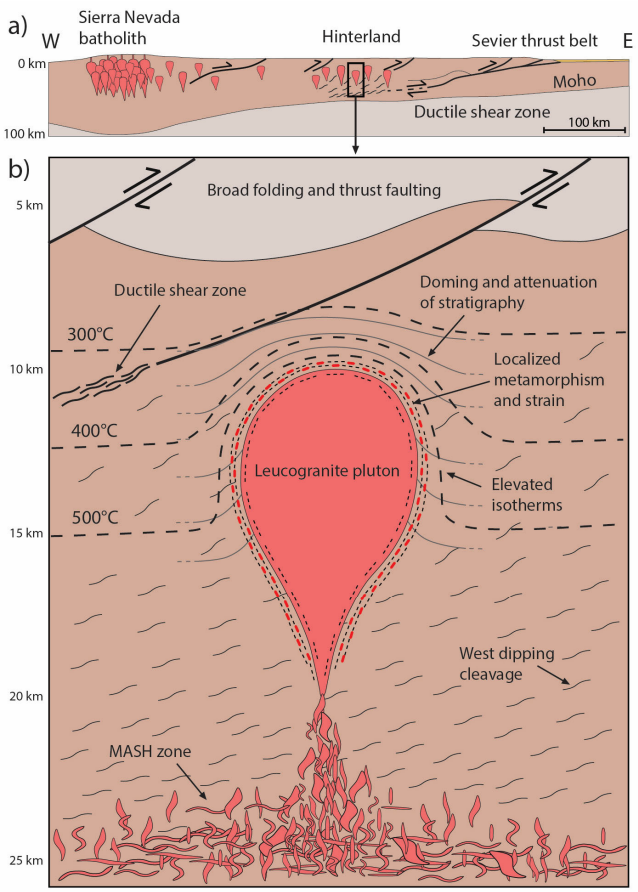

Figure 8: a) Schematic E-W cross section across the Sevier orogen during the Late Cretaceous showing the location of the hinterland region relative to the magmatic arc and the fold-and-thrust belt. Approximate area of cross section b shown as the black box. b) Schematic cross section of the Sevier hinterland during the Late Cretaceous highlighting the impacts of plutons on the thermal and deformational architecture of the crust. Isotherms have significant topography and are closely spaced around leucogranite plutons that are being intruded at different depths in the crust. Emplacement of these plutons causes localized strain and metamorphism around their margins and can result in doming of the country rock. These complex deformational and thermal structures are superimposed on an area undergoing more regional deformation associated with E-W shortening, reflected in the west dipping cleavage at deeper crustal levels and broad folding and thrust faulting at shallower crustal levels.

Effect of fluids during pluton emplacement

One of the puzzles of the metamorphic culminations in the

Sevier hinterland is that they are commonly associated with Late Cretaceous plutons; Jurassic and Eocene plutons in the same areas and at the same inferred structural depths typically only have narrow static metamorphic aureoles, even for intrusions that are much larger than the TCIC and were emplaced at the same structural/stratigraphic depth (Miller et al., 1988). *Why do some plutons have such profound effects on their country rocks while others appear to have very little? What was different during the Cretaceous that tended to produce granite cored metamorphic and deformational culminations?*

The Late Cretaceous plutons of eastern Nevada are all 2-mica leucogranites with an isotopic composition that suggests they are nearly pure crustal melts (e.g. Best et al, 1974; Miller and Bradfish, 1980; Wright and Wooden, 1991). These rocks were largely derived from the prograde metamorphism and melting of sedimentary rocks which would result in magmas with a high volatile content. More speculatively, these magmas were likely rising in concert with fluids released from dehydration reactions in the zone of prograde metamorphism. The presence of abundant fluids associated with the rise of these magmas would have drastically reduced rock strength as well as increased diffusivity and decreased nucleation rates, allowing rapid growth of large porphyroblasts. These changes would allow a pluton to more easily deform the country rock during emplacement and allow the rapid growth of large porphyroblasts in its aureole. Perhaps it was this fluid rich environment that allowed Late Cretaceous plutons to more easily deform and metamorphose their country rock and form these types of gneiss dome culminations.

References

Ahlborn, R. C. (1977). Mesozoic-Cenozoic Structural Development of the Kern Mountains, Eastern Nevada-Western Utah. *Brigham Young University Geology Studies, 24*(2), 117-131.

Armstrong, R. L. (1968). Sevier orogenic belt in Nevada and Utah. *Geological Society of America Bulletin, 79*(4), 429-458.0. https://doi.org/10.1130/0016-7606(1968)79[429:SOBINA]2.0.CO;2

Barton, M. D., & Anderson, J. L. (1990). Cretaceous magmatism, metamorphism, and metallogeny in the east-central Great Basin. *The nature and origin of Cordilleran magmatism: Geological Society of America Memoir*, *174*, 283-302.

Best, M. G., Armstrong, R. L., Graustein, W. C., Embree, G. F., & Ahlborn, R. C. (1974). Mica granites of the Kern Mountains pluton, eastern White Pine County, Nevada: Remobilized basement of the Cordilleran miogeosyncline?. *Geological Society of America Bulletin*, *85*(8), 1277-1286. https://doi.org/10.1130/0016-7606(1974)85<1277:MGOTKM>2.0.CO;2

Bick, K. F. (1966). Geology of the Deep Creek Mountains, Tooele and Juab Counties, Utah. *Utah Geological and Mineralogical Survey Bulletin, 77.*

Caggianelli, A., Ranalli, G., Lavecchia, A., Liotta, D., & Dini, A. (2014). Post-emplacement thermo-rheological history of a granite intrusion and surrounding rocks: the Monte Capanne pluton, Elba Island, Italy. *Geological Society, London, Special Publications*, *394*(1), 129-143. https://doi.org/10.1144/SP394.1

Camilleri, P. A., & Chamberlain, K. R. (1997). Mesozoic tectonics and metamorphism in the Pequop Mountains and Wood Hills region, northeast Nevada: Implications for the architecture and evolution of the Sevier orogen. *Geological Society of America Bulletin*, *109*(1), 74-94. https://doi.org/10.1130/0016-7606(1997)109<0074:MTAMIT>2.3.CO;2

Clemens, J. D., & Mawer, C. K. (1992). Granitic magma transport by fracture propagation. *Tectonophysics*, *204*(3-4), 339-360. https://doi.org/10.1016/0040-1951(92)90316-X

Cruz-Uribe, A. M., Hoisch, T. D., Wells, M. L., Vervoort, J. D., & Mazdab, F. K. (2015). Linking thermodynamic modelling, Lu–Hf geochronology and trace elements in garnet: New P–T–t paths from the Sevier hinterland. *Journal of Metamorphic Geology*, *33*(7), 763-781. https://doi.org/10.1111/jmg.12151

DeCelles, P. G., & Coogan, J. C. (2006). Regional structure and kinematic history of the Sevier fold-and-thrust belt, central Utah. *Geological Society of America Bulletin*, *118*(7-8), 841-864. https://doi.org/10.1130/B25759.1

Douce, P., Humphreys, E. D., & Johnston, A. D. (1990). Anatexis and metamorphism in tectonically thickened continental crust exemplified by the Sevier hinterland, western North America. *Earth and Planetary Science Letters*, *97*(3), 290-315. https://doi.org/10.1016/0012-821X(90)90048-3

Farmer, G. L., & DePaolo, D. J. (1983). Origin of Mesozoic and Tertiary granite in the western United States and implications for Pre-Mesozoic crustal structure: 1. Nd and Sr isotopic studies in the geocline of the Northern Great Basin. *Journal of Geophysical Research: Solid Earth*, *88*(B4), 3379-3401. https://doi.org/10.1029/JB088iB04p03379

Glazner, A. F., Bartley, J. M., Coleman, D. S., Gray, W., & Taylor, R. Z. (2004). Are plutons assembled over millions of years by amalgamation from small magma chambers?. *GSA today*, *14*(5-Apr), 4-11. https://doi.org/10.17615/nspy-zk53

Gottlieb, E. S., Miller, E. L., Valley, J. W., Fisher, C. M., Vervoort, J. D., & Kitajima, K. (2022). Zircon petrochronology of Cretaceous Cordilleran interior granites of the Snake Range and Kern Mountains, Nevada, USA. In J. P. Craddock et al. (Eds.), *Tectonic Evolution of the Sevier-Laramide Hinterland, Thrust Belt, and Foreland, and Postorogenic Slab Rollback (180–20 Ma), GSA Special Bulletin* (Vol. 555, pp. 21-65). Boulder, CO: Geological Society of America. https://doi.org/10.1130/2022.2555(02)

Harrison, T. M., & Clarke, G. K. (1979). A model of the thermal effects of igneous intrusion and uplift as applied to Quottoon pluton, British Columbia. *Canadian Journal of Earth Sciences*, *16*(3), 411-420. https://doi.org/10.1139/e79-03

Hirth, G., & Tullis, J. A. N. (1992). Dislocation creep regimes in quartz aggregates. *Journal of structural geology*, *14*(2), 145-159. https://doi.org/10.1016/0191-8141(92)90053-Y

Horstwood, M. S., Foster, G. L., Parrish, R. R., Noble, S. R., & Nowell, G. M. (2003). Common-Pb corrected in situ U–Pb accessory mineral geochronology by LA-MC-ICP-MS. *Journal of Analytical Atomic Spectrometry*, *18*(8), 837-846. https://doi.org/10.1039/B304365G

Horstwood, M. S., Košler, J., Gehrels, G., Jackson, S. E., McLean, N. M., Paton, C., et al. (2016). Community-derived standards for LA-ICP-MS U-(Th-) Pb geochronology–Uncertainty propagation, age interpretation and data reporting. *Geostandards and Geoanalytical Research*, *40*(3), 311-332. https://doi.org/10.1111/j.1751-908X.2016.00379.x

Hose, R. K., & Blake, M. C. (1976). Geology of White Pine County, Nevada. *Nevada Bureau of Mines and Geology Bulletin*, *85*, 1-35.

Hutton, D. H. (1996). The 'space problem' in the emplacement of granite. *Episodes Journal of International Geoscience*, *19*(4), 114-119. https://doi.org/10.18814/epiiugs/1996/v19i4/004

Kelly, E. D., Hoisch, T. D., Wells, M. L., Vervoort, J. D., & Beyene, M. A. (2015). An Early Cretaceous garnet pressure–temperature path recording synconvergent burial and exhumation from the hinterland of the Sevier orogenic belt, Albion Mountains, Idaho. *Contributions to Mineralogy and Petrology*, *170*, 1-22. https://doi.org/10.1007/s00410-015-1171-2

Kylander-Clark, A. R., Hacker, B. R., & Cottle, J. M. (2013). Laser-ablation split-stream ICP petrochronology. *Chemical Geology*, *345*, 99-112. https://doi.org/10.1016/j.chemgeo.2013.02.019

Lee, D. E., Kistler, R. W., Friedman, I., & Van Loenen, R. E. (1981). Two-mica granites of northeastern Nevada. *Journal of Geophysical Research: Solid Earth*, *86*(B11), 10607-10616. https://doi.org/10.1029/JB086iB11p1060

Lee, D. E., & Christiansen, E. H. (1983). The granite problem as exposed in the southern Snake Range, Nevada. *Contributions to Mineralogy and Petrology*, *83*(1-2), 99-116. https://doi.org/10.1007/BF00373083

Lee, S. Y., Barnes, C. G., Snoke, A. W., Howard, K. A., & Frost, C. D. (2003). Petrogenesis of Mesozoic, peraluminous granites in the Lamoille Canyon area, Ruby Mountains, Nevada, USA. *Journal of Petrology*, *44*(4), 713-732. https://doi.org/10.1093/petrology/44.4.713

McGrew, A. J., Peters, M. T., & Wright, J. E. (2000). Thermobarometric constraints on the tectonothermal evolution of the East Humboldt Range metamorphic core complex, Nevada. *Geological Society of America Bulletin*, *112*(1), 45-60. https://doi.org/10.1130/0016-7606(2000)112<45:TCOTTE>2.0.CO;2

Miller, C. F., & Bradfish, L. J. (1980). An inner Cordilleran belt of muscovite-bearing plutons. *Geology*, *8*(9), 412-416. https://doi.org/10.1130/0091-7613(1980)8<412:AICBOM>2.0.CO;2

Miller, E. L., & Gans, P. B. (1989). Cretaceous crustal structure and metamorphism in the hinterland of the Sevier thrust belt, western US Cordillera. *Geology*, *17*(1), 59-62. https://doi.org/10.1130/0091-7613(1989)017<0059:CCSAMI>2.3.CO;2

Miller, E. L., Gans, P. B., Wright, J. E., Sutter, J. F., & Ernst, W. G. (1988). Metamorphic history of the east-central Basin and Range province: Tectonic setting and relationship to magmatism. *Metamorphism and crustal evolution, western conterminous United States, Rubey*, *7*, 649-682.

Miller, R. B., & Paterson, S. R. (1999). In defense of magmatic diapirs. *Journal of Structural Geology*, *21*(8-9), 1161-1173. https://doi.org/10.1016/S0191-8141(99)00033-4

Monroe E. B., Kylander-Clark, A. R., & Gans, P. B. (2023a). U-Pb zircon geochronology of the Trout Creek Instrusive Complex, Deep Creek Range, UT [Dataset]. Harvard Dataverse. https://doi.org/10.7910/DVN/GBUGGX

Monroe E. B., Kylander-Clark, A. R., & Gans, P. B. (2023b). U-Pb monazite geochronology of the Trout Creek schist, Deep Creek Range, UT [Dataset]. Harvard Dataverse. https://doi.org/10.7910/DVN/SP4UXM

Nutt, C. J., & Thorman, C. H. (1994). *Geologic Map of the Weaver Canyon, Nevada and Utah, Quadrangle and Parts of the Ibapah Peak, Utah, and Tippett Canyon, Nevada, Quadrangles* (No. 94-635). Denver, CO: US Geological Survey. https://doi.org/10.3133/ofr94635

Palin, R. M., Searle, M. P., Waters, D. J., Parrish, R. R., Roberts, N. M. W., Horstwood, M. S., et al. (2013). A geochronological and petrological study of anatectic paragneiss and associated granite dykes from the Day Nui Con Voi metamorphic core complex, North Vietnam: constraints on the timing of metamorphism within the Red River shear zone. *Journal of Metamorphic Geology*, *31*(4), 359-387. https://doi.org/10.1111/jmg.12025

Paterson, S. R., & Farris, D. W. (2008). Downward host rock transport and the formation of rim monoclines during the emplacement of Cordilleran batholiths. *Earth and Environmental Science Transactions of The Royal Society of Edinburgh*, *97*(4), 397-413. https://doi.org/10.1017/S026359330000153X

Paterson, S. R., & Fowler Jr, T. K. (1993). Extensional pluton-emplacement models: Do they work for large plutonic complexes?. *Geology*, *21*(9), 781-784. https://doi.org/10.1130/0091-7613(1993)021<0781:EPEMDT>2.3.CO;2

Paton, C., Hellstrom, J., Paul, B., Woodhead, J., & Hergt, J. (2011). Iolite: Freeware for the visualisation and processing of mass spectrometric data. *Journal of Analytical Atomic Spectrometry*, *26*(12), 2508-2518. https://doi.org/10.1039/C1JA10172B

Rodgers, D. W. (1987). *Thermal and structural evolution of the southern Deep Creek Range, west central Utah and east central Nevada* (Doctoral dissertation). Stanford, CA: Stanford University.

Sláma, J., Košler, J., Condon, D. J., Crowley, J. L., Gerdes, A., Hanchar, J. M., et al. (2008). Plešovice zircon—a new natural reference material for U–Pb and Hf isotopic microanalysis. *Chemical Geology*, *249*(1-2), 1-35. https://doi.org/10.1016/j.chemgeo.2007.11.005

Spear, F. S. (1993). *Metamorphic phase equilibria and pressure-temperature-time paths*. Chantilly, VA: Mineralogical Society of America Monograph.

Taylor, W. J., Bartley, J. M., Martin, M. W., Geissman, J. W., Walker, J. D., Armstrong, P. A., & Fryxell, J. E. (2000). Relations between hinterland and foreland shortening: Sevier

orogeny, central North American Cordillera. *Tectonics*, *19*(6), 1124-1143. https://doi.org/10.1029/1999TC001141

Teyssier, C., & Whitney, D. L. (2002). Gneiss domes and orogeny. *Geology*, *30*(12), 1139-1142. https://doi.org/10.1130/0091-7613(2002)030<1139:GDAO>2.0.CO;2

Tomascak, P. B., Krogstad, E. J., & Walker, R. J. (1996). U-Pb monazite geochronology of granitic rocks from Maine: implications for late Paleozoic tectonics in the Northern Appalachians. *The Journal of Geology*, *104*(2), 185-195. https://doi.org/10.1086/629813

Wiedenbeck, M. A. P. C., Alle, P., Corfu, F. Y., Griffin, W. L., Meier, M., Oberli, et al. (1995). Three natural zircon standards for U-Th-Pb, Lu-Hf, trace element and REE analyses. *Geostandards newsletter*, *19*(1), 1-23. https://doi.org/10.1111/j.1751-908X.1995.tb00147.x

Wright, J. E., & Wooden, J. L. (1991). New Sr, Nd, and Pb isotopic data from plutons in the northern Great Basin: Implications for crustal structure and granite petrogenesis in the hinterland of the Sevier thrust belt. *Geology*, *19*(5), 457-460. https://doi.org/10.1130/0091-7613(1991)019<0457:NSNAPI>2.3.CO;2

Yoshinobu, A. S., Okaya, D. A., & Paterson, S. R. (1998). Modeling the thermal evolution of fault-controlled magma emplacement models: implications for the solidification of granitoid plutons. *Journal of Structural Geology*, *20*(9-10), 1205-1218. https://doi.org/10.1016/S0191-8141(98)00064-9

II. Late Cretaceous tectonic evolution of the Deep Creek Range-Kern Mountains block, eastern Nevada and western Utah: Magmatically induced large-scale folding, dynamothermal metamorphism, and ductile strain at mid- to upper-crustal levels in the Sevier hinterland

Introduction

The Kern Mountains and Deep Creek Range (KMDCR), situated on the Nevada-Utah border in the heart of the Northern Basin and Range, display a rich Late Cretaceous history of metamorphism, magmatism and deformation. The position of these ranges to the west of the east-vergent Sevier fold-and-thrust belt (Armstrong, 1968), and the overlapping age(s) of the Late Cretaceous magmatism, metamorphism and penetrative strain in the hinterland with shortening in the foreland (e.g., DeCelles & Coogan 2006; Miller & Bradfish, 1980; Douce et al., 1990) have led most workers to conclude that the hinterland tectonism is a direct manifestation of the same Mesozoic retroarc shortening that produced the better known thrust belt to the east. One perspective is that the isolated metamorphic/magmatic culminations in the hinterland provide windows into the Late Cretaceous lower to middle crustal mush/migmatite zone of broadly distributed penetrative deformation and thickening, prograde metamorphism and anatexis (e.g., Price & Mountjoy 1970; Miller & Gans, 1989) – effectively the middle to lower crustal accommodation of upper crustal shortening to the east. The alternative view is that these culminations are isolated features, perhaps reflecting areas of localized crustal thickening (e.g., Coney & Harms, 1984; Wrobel et al. 2021), lower crustal diapirism (e.g., Zuza & Cao, 2022), or lithospheric delamination (Wells & Hoisch, 2008). Although the Sevier fold-and-thrust belt is one of the best-studied in the world, its hinterland is much less well-understood with many fundamental questions remaining

regarding the amount of shortening and the precise relationship between magmatism, metamorphism, and deformation in this region.

The single large tilt block represented by the KMDCR provides an exceptional place to investigate these topics. The ~40° of westward tilting associated with slip on the major range-bounding normal fault on its eastern margin provides an intact cross section of the pre-extensional upper to middle crust, exposing a broad spectrum of late Mesozoic structures. Although this study specifically focuses on the KMDCR, it has implications for several interrelated broader topics on Cordilleran tectonics, including:

a) *What is the magnitude, style and timing of shortening in the hinterland of the Sevier belt?* The lack of a significant angular unconformity between Paleozoic rocks and the Cenozoic section as well as the observation that Cenozoic rocks are almost exclusively deposited on the upper Paleozoic units has led some to argue that the middle to upper crust in the hinterland was only weakly deformed during the Mesozoic as it was transported eastward above a basal décollement without undergoing much internal deformation (e.g., Miller et al., 1983). However, the presence of large-scale shortening structures and well as metamorphic assemblages that suggest deep tectonic burial suggests that at least locally there was significant shortening in the middle to upper crust (Greene, 2014; Harris et al., 2007; Long, 2015; Wrobel et al., 2021).

b) *What was the precise interplay and genetic relationships between metamorphism, magmatism and deformation in the Sevier hinterland?* The hinterland crust experienced both regional and local dynamothermal metamorphism during the Late Cretaceous (Miller et al., 1988) as well as the emplacement of numerous

leucogranite plutons (e.g., Lee et al., 1981) that are often closely associated with increases in both metamorphic grade and penetrative strain. Are the leucogranites best viewed as a cause of the observed metamorphism or as a consequence of the same regional crustal thickening event? Similarly, are the well-developed tectonite fabrics and folds associated with these metamorphic culminations a localized strain—perhaps associated with pluton emplacement or diapirism, or do they document regional shearing and crustal thickening associated with Sevier age hinterland crustal shortening?

This study addresses these topics by integrating detailed geologic mapping, mesoscopic and microscopic structural analysis, petrography, and igneous and metamorphic geochronology of key localities in the KMDCR. Specifically, this paper focuses on:

1) What are the ages, magnitude and character of mesoscopic to map-scale deformation and metamorphism in these range?
2) What are the spatial and temporal relationships between map-scale and outcrop-scale structures, tectonite fabrics and metamorphic mineral growth?
3) What are the spatial and temporal relationships between the metamorphic and deformational features described above and various intrusive bodies exposed in these ranges, and what do these relationships indicate regarding the role of plutonism vs. regional tectonics in producing these observed deformational and metamorphic features?

Of particular interest is the Water Canyon Anticline (WCA), a large recumbent fold in the southern DCR that was previously interpreted to reflect west-directed Sevier age

shortening in the hinterland (Rodgers, 1987). Here, we present an entirely different interpretation that this fold and associated fabrics are instead primarily the result of emplacement of a large Late Cretaceous pluton, the Tungstonia Granite (TG). This paper presents a detailed geologic map of a ~35 km^2 area in the southern DCR spanning the overturned limb of the WCA, as well as detailed maps of the ~7 km^2 northwest and ~16 km^2 southwest flanks of the KM along the margins of TG. This mapping was accompanied by detailed mesoscopic structural analyses of folding, bedding and cleavage orientations, and assessment of strain magnitudes and orientations. Petrographic analysis of samples from both the southern DCR and western KM shed additional light on the nature and conditions of penetrative strain and metamorphism, their relationship to each other and how both are related to map-scale structures. These field and petrographic observations are supplemented with LA-ICP-MS U-Pb geochronology of metamorphic monazite from the southern DCR that constrains the ages of two overprinting Late Cretaceous metamorphic aureoles as well as U-Pb zircon geochronology of eight samples from various locations within TG that constrains the crystallization and emplacement history of this pluton. Together, these datasets document the magmatic, metamorphic, and structural histories of these two ranges with a focus on discriminating thermal and deformational events related to regional tectonism from those more closely associated with the emplacement of the plutons.

Regional Geologic Setting

Prior to Mesozoic deformation, the Sevier hinterland was the site of prolonged Neoproterozoic to Triassic shallow marine deposition along the western margin of Laurentia, resulting in a westward thickening wedge of >15km of passive margin

siliciclastic and carbonate rocks that underlie most of eastern Nevada and western Utah (Stewart, 1976). During the Mesozoic, eastward subduction of the Fallon plate beneath North America resulted in the development of the retroarc Sevier Orogen, characterized by major crustal shortening inboard of the magmatic arc, and broadly analogous to the modern Andes (Armstrong, 1968; Burchfiel & Davis, 1975; Royse et al., 1975). At the latitude of the KMDCR, the Sevier fold-and-thrust belt is located ~150 km to the east in central Utah and is characterized by several large east-directed thrust sheets and associated folds that affect upper-crustal miogeoclinal rocks and are interpreted to merge at depth with a gently west dipping detachment. Estimates of total shortening exceed ~220 km which likely resulted in upper crustal thickening of ≥15 km (DeCelles & Coogan, 2006). In the foreland, these thrusts are highly influenced by stratigraphy, with characteristic ramp flat geometries and slip along rheologically weak horizons. They are "thin-skinned" and detached from the underlying basement. The timing of thrusting is constrained by analysis of synorogenic foreland basin deposits and thermochronology to have begun as early as Late Jurassic but is almost entirely Cretaceous in age and migrated progressively eastward through time, eventually transitioning into Laramide style deformation during the Paleocene (e.g., Armstrong & Oriel 1965; Burtnet & Nigrini, 1994; DeCelles et al., 1995; DeCelles & Coogan, 2006; Fouch et al., 1983; Heller et al., 1986). Upper crustal shortening in the foreland fold-and-thrust belt is interpreted to have been accommodated to the west by mid- to lower crustal shortening and thickening in the hinterland (Miller & Gans, 1989).

Although crustal thickening in the hinterland is geometrically required to accommodate upper-crustal shortening in the foreland fold-and-thrust belt, subsequent large-scale extension during the Cenozoic and limited exposures of deeper (mid-crustal) levels has

made unraveling this earlier contractional history difficult. One endmember model for hinterland deformation is that eastward translation of the middle to upper crust was facilitated nearly entirely by a subhorizontal or gently west dipping mid- to lower crustal shear zone, with little to no deformation in the overlying rock column. This hypothesis is supported by the observation that in many places the earliest Cenozoic rocks in eastern Nevada are deposited on the youngest units of the Paleozoic section with little angular discordance, suggesting minimal structural relief in the upper crust prior to Cenozoic extension (Armstrong 1968, 1972; Gans & Miller 1983; Long, 2012). However, a number of major shortening structures have been identified in various locations within the Sevier hinterland. Immediately to the south of the KM in the footwall of Northern Snake Range metamorphic core complex, the east vergent O'Neill Peak recumbent anticline and syncline affect the entire Middle to Upper Cambrian section and accommodated almost ~5 km of structural thickening during the Cretaceous (Wrobel et al., 2021). When combined with associated supracrustal shortening structures in the hanging wall of the detachment fault in the Confusion Range of western Utah, total shortening appears to be ≥10 km with ≥7 km of structural burial and is likely responsible for the kyanite grade metamorphism in the footwall of the Northern Snake Range décollement (Greene, 2014; Wrobel et al., 2021). Farther west in the hinterland, the central Nevada thrust belt comprises a zone of upper crustal shortening characterized by east vergent thrust faults and map-scale folds that accommodated ~10 km of shortening during the Cretaceous (Bartley & Gleason, 1990; Long et al., 2014; Taylor et al., 2000).

Perhaps the most extensive record of hinterland shortening and tectonic burial is from the Ruby/East Humbolt/Pequop/Wood Hills metamorphic core complex in

northeastern Nevada, where Cenozoic exhumation by detachment faulting has exposed large areas of mid-crustal rocks. Integration of thermobarometry and geochronology with mapping of contractional structures suggests multiple episodes of tectonic burial and metamorphism throughout the Late Jurassic/Early Cretaceous and Late Cretaceous (Camilleri, 1998; Camilleri & Chamberlain, 1997; Hallett & Spear, 2015; Hudec, 1992). These burial events were separated by at least one period of extensional exhumation, possibly resulting from steep topographic gradients related to crustal thickening (Hodges et al., 1992). Late Cretaceous metamorphism was characterized by higher temperatures and the emplacement of syntectonic leucogranites, likely as a result of the progression from a colder to hotter geotherm (McGrew et al, 2000). Work in the Albion/Raft River metamorphic core complex in southeast Idaho reveals a similar history of major tectonic burial, exhumation, and metamorphism throughout the Cretaceous (Cruz-Uribe et al., 2015; Harris et al., 2007; Kelly et al., 2015). These studies highlight the complex and multiphase nature of deformation and metamorphism in the Sevier hinterland.

Crustal shortening and thickening in the Sevier hinterland was accompanied by both regional and localized metamorphism and crustal anatexis that peaked in the Late Cretaceous at ~80 Ma (Miller et al., 1988; Miller & Gans, 1989). Regional greenschist facies metamorphism is observed at the deepest stratigraphic levels in many of the ranges in eastern Nevada. However, there are also numerous more localized upper-greenschist to amphibolite facies metamorphic culminations that typically have steep vertical and lateral temperature gradients and are spatially associated with the emplacement of leucogranite plutons (e.g., the Papoose Flat Pluton in the Inyo Mtns., the Lexington Creek Pluton in the Southern Snake Range, and the Trout Creek Intrusive Complex in the DCR; De Saint-

Blanquat et al., 2001; Law et al., 1992; Lee et al., 1983; Monroe et al., 2023; Paterson et al., 1991; Sylvester et al., 1978;). These Late Cretaceous leucogranites are strongly peraluminous and have an isotopic composition that indicates they are nearly pure crustal melts (Barton & Anderson, 1990; Best et al., 1974; Farmer & DePaolo, 1983; Lee et al., 1981; Lee et al., 2003; Lee & Christiansen, 1983; Miller & Bradfish, 1980, Gottlieb & Miller, 2022). However, the mechanisms for melting in the hinterland and whether the emplacement of these leucogranite plutons is the cause or consequence of mid-crustal metamorphism are debated. Eastward migration of subduction-related magmatism from the main arc into the hinterland is a possibility (Miller & Gans, 1989). Thermal relaxation following crustal thickening has also been invoked by some workers as the primary cause of this metamorphism and anatexis (Douce et al., 1989; Wright & Wood, 1991). However, this model predicts that metamorphism and crustal anatexis would be widespread throughout the hinterland, not localized. This has led some workers to argue that delamination and foundering of a lithospheric mantle and the replacement with hot asthenosphere was the primary driver for these Late Cretaceous thermal anomalies (Blackford et al., 2022; Wells et al., 2012; Wells & Hoisch, 2008). An additional hypothesis is that melting was a consequence of contractional "A-type" subduction, where underthrusting of supracrustal fluid-rich sediments leads to volatiles fluxing into the hot anhydrous overlying hanging wall, resulting in partial melting (Gottlieb et al., 2022).

During the Cenozoic, the overthickened crust of the Sevier hinterland was extended approximately east-west, thinning the crust to its current thickness of ~30 km (Benz et al., 1990; Gans, 1987). Extension may have begun as early as the Late Cretaceous and is hypothesized to have initially been facilitated by slip along low angle detachment faults

(e.g., Coney & Harms, 1984; Davis & Coney 1979). During the middle Miocene the style of extension transitioned to more typical widely spaced high-angle fault systems and block rotation, forming the present topography of the Basin and Range (Stewart, 1971). The geology of the KMDCR reflects this rich geologic history of the Sevier hinterland, and the rocks exposed in these ranges provide insight on the thermal and deformational architecture of the hinterland crust during the Late Cretaceous.

Geologic Framework of the Deep Creek Range and Kern Mountains

The KM and DCR are not separated by any major structural discontinuities and comprise a single structural block with stratigraphic units that can be traced continuously from one to the other (Fig 1). This block was tilted to the west during slip along the Reilly Canyon Fault which bounds both ranges to the east and likely continues southward to merge with the Northern Snake Range Décollement. (Bick, 1966; Miller et al., 1999; Misch & Hazzard, 1962). This fault has an estimated cumulative 25 km of displacement and is interpreted to have formed at a higher angle (~50-60°) and rotated to its current dip of ~15° during progressive slip and westward tilting of both the hanging wall and footwall blocks, such that paleodepth increases to the east (Gans et al., 1990; Rodgers, 1987).

The eastern part of the DCR is underlain by the Neoproterozoic Trout Creek and McCoy Creek groups, which are interpreted to have been deposited during active rifting and early rapid subsidence on the newly formed western margin of Laurentia (Misch & Hazzard, 1962; Stewart, 1976). The Trout Creek Group is ~3.2 km thick and is composed of

interbedded quartzite, schist, metasiltstone, metadiamictite, and minor marble that have been divided into six mappable units (Fig 9; Rodgers, 1984). This stratigraphy is only exposed at deep structural levels in the DCR, so it is unclear if these units were deposited in an isolated rift basin or if they are relatively continuous throughout the region beneath the present exposure level. The McCoy Creek Group overlies the Trout Creek Group and is composed of a ~2.3 km thick succession of interbedded quartzite, schist, metasiltstone and minor marble and is divided into six mappable units (Fig 9). These units are laterally continuous and are present throughout eastern Nevada at deeper levels of exposure but display significant changes in lithology and unit thicknesses between localities (Misch & Hazzard, 1962).

Approximately 8 km of Paleozoic stratigraphy depositionally overlies the McCoy Creek Group and comprises most of the bedrock exposed in the western DCR. It is composed of lower Cambrian quartzite and shale overlain by a

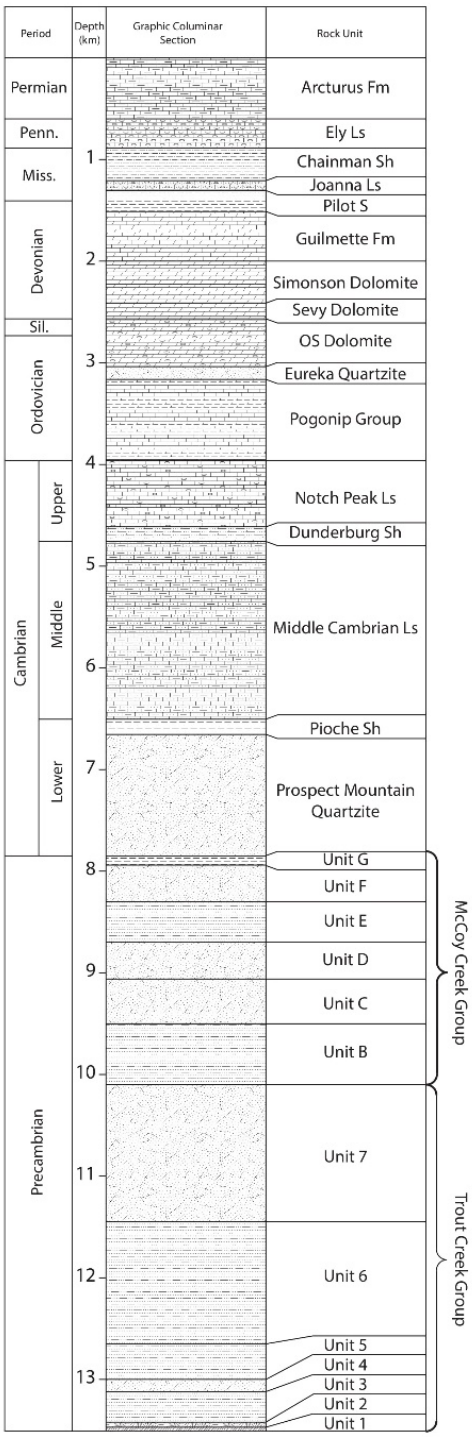

Figure 9: Stratigraphic section of the rock units exposed in the Deep Creek Range. Modified from Rodgers (1987).

succession of middle Cambrian to Pennsylvanian carbonates with minor siliciclastics (Fig 9). The carbonates are dominated by limestone except for the upper Ordovician to Middle Devonian section which is composed primarily of dolomite. These units were deposited slowly on the continental shelf and are laterally continuous for hundreds of kilometers across eastern Nevada. In the westernmost DCR, a succession of Eocene volcaniclastics, ash-flow tuff and andesitic lava flows unconformably overlie the uppermost Paleozoic section with little angular discordance (Nutt & Thorman, 1992). Cenozoic conglomerate and Eocene volcanic rocks are also exposed east of Pleasant Valley in the hanging wall of the range bounding Reilly Canyon fault (Gans et al., 1990).

There are both large plutons and many small undated intrusions in the KMDCR, but all appear to be either Late Cretaceous or Eocene. TG is the largest with an area of >100 km^2 and forms the core of the KM. It is a strongly peraluminous leucogranite that was emplaced at ~70 Ma (U-Pb zircon; Gottlieb et al., 2022; Lee et al., 1986; this study), during the latest stages of crustal shortening in the Sevier hinterland. The Trout Creek Intrusive Complex is exposed on the eastern flank of the DCR at deep structural levels over an area of ~2 km^2 as a few small stocks surrounded by numerous dikes and sills. It was emplaced at 80 ± 2 Ma (U-Pb zircon, Monroe & Gans, 2023) and is a typically aplitic leucogranite with a well-developed solid-state deformational fabric around its margins that is continuous with the country rock and forms the core of a structural dome. The 39 ± 1 Ma (U-Pb zircon; Rodgers, 1987) Ibapah Pluton underlies the central DCR, has a surface exposure of ~80 km^2, and is composed of coarse-grained biotite granite to quartz monzonite. Numerous small, isolated outcrops of granite with a similar mineralogy and texture are scattered throughout the southern DCR. The 37 ± 8 Ma (Rb/Sr; Best et al., 1974) Skinner Canyon Granite (~10 km^2)

and the undated but likely Eocene Uvada Granite (~1 km^2) are exposed in the northeastern KM. All three of these Eocene plutons have sharp and irregular contacts and only narrow static metamorphic aureoles with little to no penetrative deformation along their margins.

Two deformation events affected rocks in the southern DCR during the Late Cretaceous. The first is reflected in a west dipping cleavage (S_1) that is also present in many other nearby ranges and is interpreted to have formed as a result of east-directed layer parallel shear (Miller et al., 1988; Rodgers, 1987). During the second event, rocks on the southern flank of the range were folded into the WCA, a large recumbent fold that closes to the west and has a gently north plunging fold axis. A locally developed cleavage (S_2) that in some areas appears to be axial planar to the WCA also developed during this event. Metamorphism increases down section from unmetamorphosed Paleozoic carbonates in the west to upper greenschist facies within the stratigraphically lowest units and locally to amphibolite facies in several metamorphic culminations.

The overturned limb of the WCA continues southward across Pleasant Valley into the eastern KM, where the stratigraphy dips to the northwest, is overturned, highly attenuated and parallels the margin of TG. This pluton has a well-developed deformational aureole around its margins and intrudes mid-crustal rocks to the east and upper-crustal carbonates to the west. Country rocks in the western KM have structures that appear to be related to both Mesozoic tectonic shortening and deformation associated with pluton emplacement, as well as a variety of normal faults associated with Cenozoic extension.

In order to interpret the original geometry of Cretaceous structures exposed in the KMDCR, it is important to critically evaluate the estimated magnitude and direction of subsequent westward tilting of the ranges during the Cenozoic. Evidence for westward

tilting includes: 1) The general westward dip of stratigraphy with progressively higher stratigraphic units exposed to the west. 2) A systematic increase in metamorphic grade west to east, grading from unmetamorphosed upper-crustal rocks on the western flanks of the ranges to upper-greenschist and locally amphibolite facies mid-crustal rocks along the eastern flanks. 3) The Eocene unconformity and overlying volcanic rocks exposed in the western DCR typically dip westward. 4) $^{40}Ar/^{39}Ar$ thermochronology of potassium feldspar and mica in both TG and the Ibapah Pluton show systemic younging from west to east, with ages that indicate that the western parts of the ranges were exhumed prior to the eastern flanks (P.B. Gans - unpublished data). 5) The present gentle eastward dip of normal faults in the western DCR and consistent bedding to fault angles of 50-60° suggests they formed at a higher angle and were rotated to their present low angles during westward tilting of the ranges. Although the KMDCR is clearly tilted to the west, the magnitude, direction and timing of tilting are only broadly constrained. Rodgers (1987) estimated that the ranges were tilted to the WNW about a horizontal axis with an azimuth of ~030°. This is based on 1) the orientations fault striae, 2) the strike of normal faults, 3) the strike of tilted Eocene volcanic rocks, and 4) the trend of Pleasant Valley (interpreted as a re-entrant or mullion along the Reilly Canyon fault). Rodgers estimated the magnitude of tilting was ~40° based primarily on the average dip of bedding in the Paleozoic section and very limited orientations on volcanic rocks in the western DCR. However, there is significant uncertainty in both the orientation of the axis of tilting and the magnitude of tilting, which could be as little as 20° or as much as 60°.

Previous Work

Early work in the KMDCR by Nelson (1959, 1966, 1969), Misch et al. (1957), Misch & Hazzard (1962), and Bick (1966) first described the stratigraphy, identified the major intrusions, recognized metamorphism, and made initial interpretations on the structural history of the ranges, and their work served as an important framework for later research. Rodgers (1987) focused on the structural and thermal history of the southern DCR by characterizing the geometry of the WCA, describing the character and distribution of cleavages and metamorphism, and conducting $^{39}Ar/^{40}Ar$ geochronology on metamorphic hornblende from the southern flank of the range that suggested metamorphism was Late Cretaceous. He interpreted the WCA to be a major west vergent fold that formed during the Late Cretaceous as a result of tectonic shortening associated with the Sevier Orogeny. He hypothesized that the fold formed over a west-directed ductile shear zone at the base of the overturned limb which resulted in the observed penetrative strain and ductile attenuation of stratigraphy. However, this interpretation is not consistent with several peculiar characteristics of the WCA that will be discussed further.

In the KM, Best et al. (1974) conducted a petrologic study of the Tungstonia, Skinner Canyon and Uvada plutons that characterized their general map relationships, mineralogy, texture, ages, whole rock chemistry and Sr^{87}/Sr^{86} isotopic composition. The high Sr^{87}/Sr^{86} from TG reported by Best et al. (1974) suggests that it formed primarily from a crustal source with little to no mantle input, whereas the Eocene Skinner Canyon and Uvada plutons likely have a significant mantle contribution. Sayeed (1973) and Sayeed et al. (1977) provided a preliminary petrologic, geochemical and structural analysis of TG and surrounding country with similar conclusions as Best et al., (1974). Ahlborn (1977) focused

on the structural history of the KM and provided a framework for the overall deformational history of the range. Extensive unpublished mapping throughout the KM by Gans et al. (1990) documented many of the deformational structures and map relationships in the country rock surrounding TG and was instrumental in guiding the mapping in the western KM presented in this paper.

More recent work in the KMDCR includes a study that focused on the upper-crustal thermal structure of the Sevier hinterland and used Raman spectroscopy of carbonaceous material thermometry and conodont alteration indices to indicate that the southern DCR had elevated thermal gradients of 49 ± 7°C/km (Blackford et al, 2022). Gottlieb et al. (2022) used zircon petrochronology to investigate the petrogenesis of TG and the lithology and structure of the basement and argues that TG was sourced from cratonic basement that was underthrust westward during Sevier shortening.

Deformation and metamorphism in the southern Deep Creek Range

Map relationships and field observations

A geologic map of a ~35 km^2 area on the southeastern flank of the range was produced to build on Rodgers' mapping by documenting in more detail the orientations and character of cleavages, the distribution of map units, the geometry of mesoscopic folds, and the distribution and character of metamorphism (Fig 10). The first period of deformation to affect rocks in the southern DCR is reflected in a cleavage (S_1) in Neoproterozoic to lower Cambrian rocks that dips west with respect to horizontal bedding and increases in intensity and metamorphic grade down section and to the south (Figs 11 & 12a). This cleavage is present throughout the southern DCR in both the upright and overturned limb of the WCA.

Later folding into the WCA resulted in the cleavage having a variety of orientations within the map area, but in general it dips moderately to steeply to the northwest in the upright limb (Fig 11-Z1), gently to moderately to the northwest in the overturned limb in the western half of the map area (Fig 11-Z2-Z5), and moderately to the northeast in the overturned limb in the eastern part of the map area (Fig 11-Z8). The intersection lineation with bedding plunges gently to moderately, with trends ranging from northwest to northeast.

A similar west-dipping cleavage is present in many of the surrounding ranges and thus appears to reflect a relatively widespread deformational event in the Sevier hinterland (Miller et al., 1988, Miller & Gans 1989). Previous workers interpreted this cleavage to be a result of east-directed layer parallel shear when the section was approximately flat lying

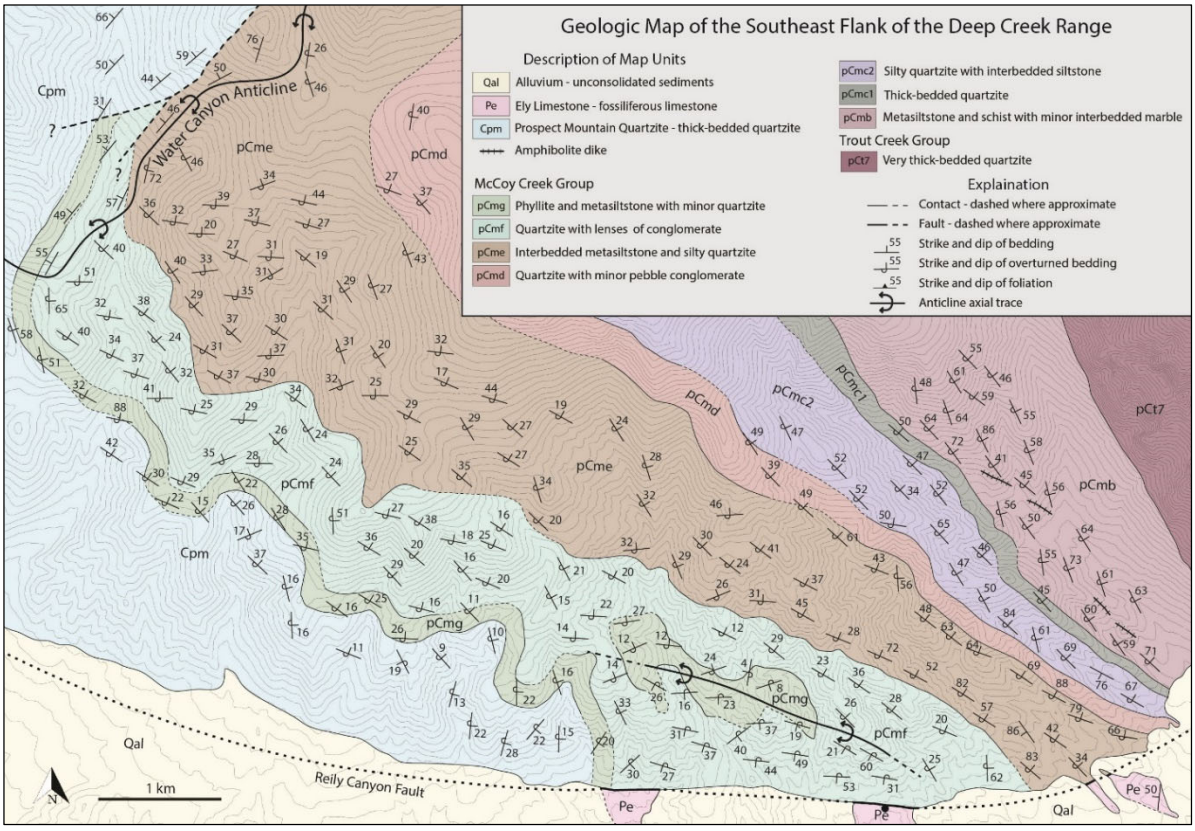

Figure 10: Geologic map of the southeastern flank of the DCR.

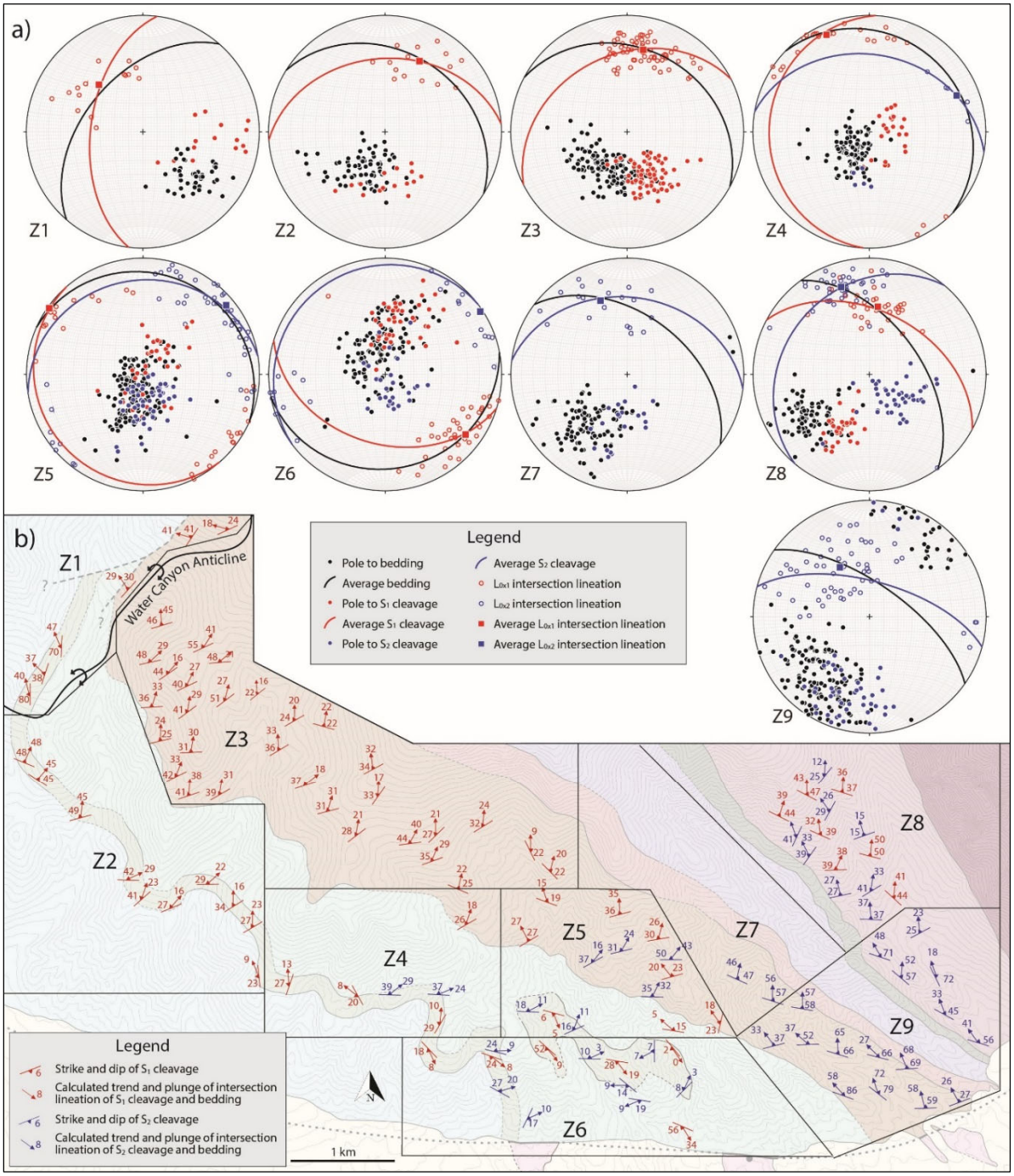

Figure 11: a) Lower hemisphere stereonet projections of poles to bedding and cleavages, intersection lineations and folds in different domains throughout the map area. Great circles illustrate the average bedding and cleavage attitude for each domain (Allmendinger, 2023). b) Map showing outlines of the structural domains summarized in the stereonets (a) and representative orientations of the S_1 (red) and S_2 (blue) cleavages, and intersection lineations.

based on the observations that 1) the cleavage is consistently more west dipping than

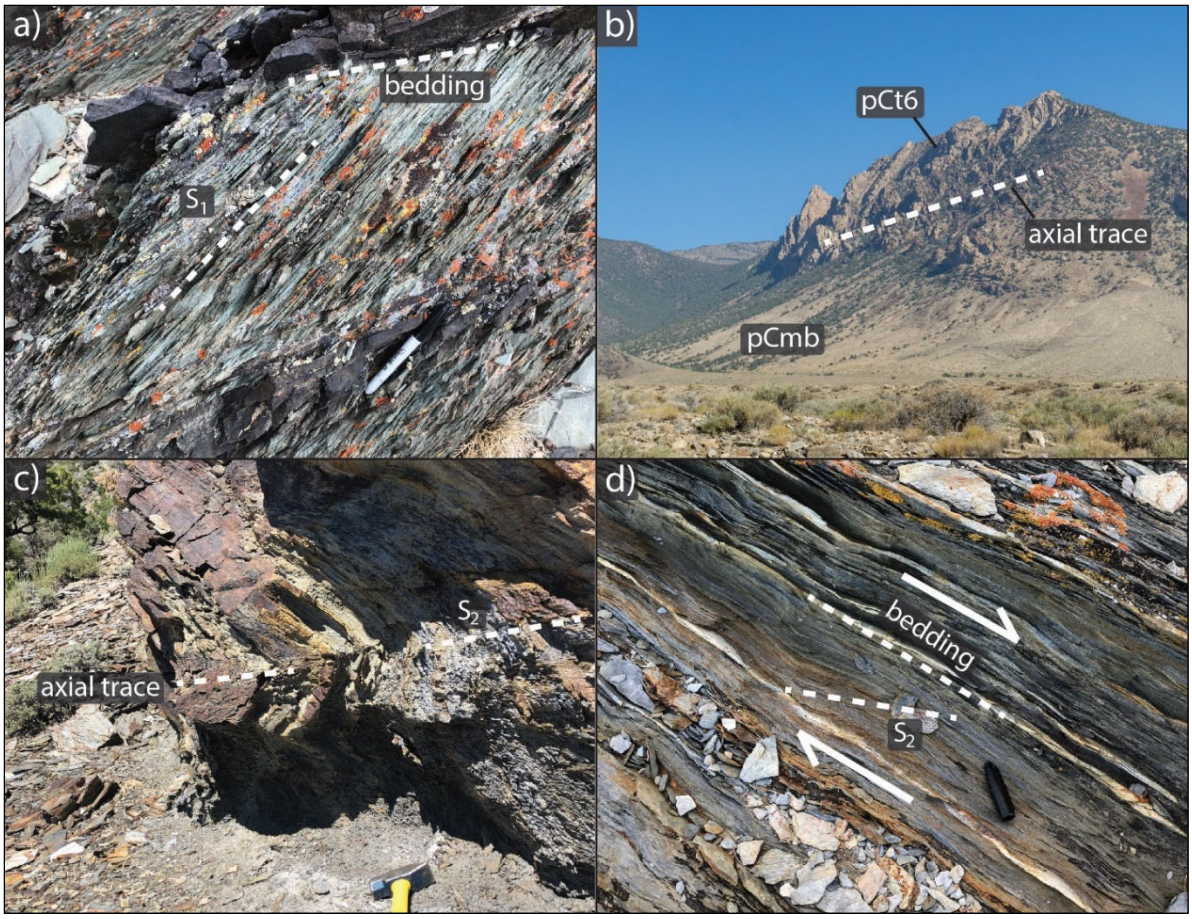

Figure 12: a) Well-developed S_1 cleavage at a moderate angle to bedding in pCme in the northwestern part of the map area. View facing north. b) View of the WCA looking north up the canyon on the eastern side of the map area, approximately parallel to the fold axis. The large cliffs are underlain by thick-bedded quartzite of the upper Trout Creek Group and the valley is underlain by less resistant phyllite and schist of pCmb. c) Outcrop scale fold in pCmb with an axial planar S_2 developed in pelitic layers on the right side of the image. View facing NNW. d) Steeply dipping S_2 cleavage at a low angle to bedding. The relative orientation of bedding and cleavage is consistent with right lateral bedding parallel shear.

bedding and generally intersects bedding at an angle of less than 45 degrees, 2) the cleavage becomes better developed and the intersection angle with bedding decreases with depth, and 3) folds associated with the cleavage are rare, suggesting that bedding was never at a high angle (>45°) to the principal shortening axis. (Miller et al., 1988; Miller & Gans, 1989; Rogers, 1987).

One of the most conspicuous features in the southern DCR is the WCA, which is a major "range-scale" recumbent fold that closes to the west and affects Neoproterozoic to Mississippian strata in the southern DCR and northeastern KM (Figs 1 & 10). Stratigraphy in the upright limb in the northwest part of the map area dips moderately to the northwest (Fig 11-Z1) and as beds roll through vertical in the overturned limb, which is only exposed in the southern DCR and northeast KM, stratigraphy dips gently to steeply to the northeast (Fig 11-Z2-Z8). The calculated fold axis plunges gently to the north and the axial surface dips gently to the north or northwest (Fig 13a). The fold has a subangular hinge with an interlimb angle of ~60° where the hinge is exposed in the northwestern part of the map area. The hinge is more rounded and has an interlimb angle of ~80° farther east, where it is spectacularly exposed in a ~500-meter-high cliff of quartzite of the uppermost unit of the Trout Creek Group (Fig 12b). This fold appears to be relatively local as it cannot be traced northward through the rest of the exposed ~40 km DCR or south into the Northern Snake Range, nor can an offset segment of the fold be identified in the

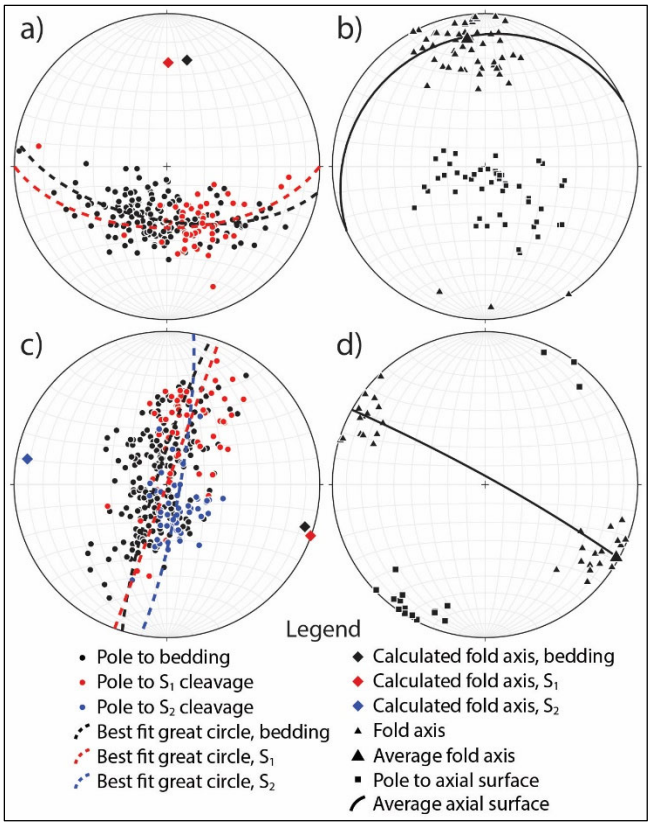

Figure 13: a) Orientations of bedding and the S_1 cleavage around the hinge of the WCA in the northwest part of the map area. b) Orientations of D_2 mesoscopic folds. c) Bedding, S_1, and S_2 orientations from the NNW-ESE trending anticline in the southern part of the map area. d) Orientations of mesoscopic folds associated with the development of the NNW-ESE trending anticline in the southern part of the map area.

presumed hanging wall of the Reilly Canyon Fault in the northern Confusion Range (Greene, 2014; Wrobel et al., 2021).

Middle Cambrian to Mississippian strata in the overturned limb of the WCA continue southward across Pleasant Valley where the same units are present in the eastern KM, where they are highly attenuated and parallel the northeastern margin of TG (Fig 1b). These units have been thinned to as little as 10% of their original stratigraphic thickness and have a strong bedding parallel foliation that parallels the contact of the pluton (Gans et al., 1990). The observation that the intrusive contact follows approximately the same overturned stratigraphic unit over nearly 7 km and that this coincides with the zone of highest strain suggests a genetic relationship between deformation and pluton emplacement or possibly that the pluton was emplaced along a high strain shear zone at the base of the overturned limb. This relationship will be explored further in the following sections.

Pennsylvanian and younger rocks also continue southward from the southern DCR into the western KM but are deflected towards the west, the opposite direction as Mississippian and older strata (Fig 1b). Bedding in the Pennsylvanian Ely Limestone changes from dipping moderately to the west in the southern DCR, to dipping moderately to the NNE in the northern KM, approximately parallel to the margin of TG (Gans et al., 1990). This zone between Mississippian and older rocks and Pennsylvanian and younger rocks thus represents an important discontinuity, where rocks on either side are deflected in opposite directions.

Folding of the WCA was apparently accompanied by the development of a cleavage (S_2) in the southern DCR that is only present in the eastern part of the map area and is most well developed in pelitic horizons of pCmb, pCme and pCmg. In pCmb in the northeastern

part of the map area, the cleavage dips gently to moderately to the north or northwest and appears to be approximately parallel to the axial surface of the WCA and is axial planar to outcrop scale folds (Fig 11: Z8; Fig 12c). However, farther south in pCmb and in pCme, the cleavage becomes much more steeply dipping to the north or northeast and has a very different orientation as the axial surface of the WCA. Here, bedding typically dips steeply to the northeast and the cleavage dips steeply NNE, forming an intersection lineation that plunges moderately to the NW (Fig 11: Z9). The relative orientation of bedding and the cleavages is more consistent with bedding parallel right lateral shear than an axial planar cleavage to the WCA (Fig 12d). This zone coincides with the area of synkinematic metamorphism of the amphibole grade Singleton Creek aureole and here the cleavage is more well-developed and nearly completely overprints the S_1 cleavage. Farther to the west, the S_2 cleavage becomes more shallowly dipping due to folding into a younger NNW-SSE trending anticline and has an intersection lineation with bedding that plunges gently to the northeast (Fig 11: Z5 & Z6).

Mesoscopic folds are locally present with axial surfaces and fold axes approximately parallel with that of the WCA and are best developed in intervals consisting of shale with thin sandstone interbeds and are most common in pCmb (Fig 13b). However, these mesoscopic folds are rare in most parts of the map area and are conspicuously absent in places where they would be most expected (e.g., the same rock types within the hinge region of the WCA). Folds typically have wavelengths of 1-10 m, have rounded to subangular hinges and are generally asymmetric and verge toward the hinge of the WCA (Fig 12c). An axial planar younger (S_2) cleavage is often developed within these mesoscopic folds and is parallel to sub-parallel to their axial surface.

A younger and more localized deformation also affected rocks on the southern DCR and resulted in the formation of a map-scale WNW-ESE trending upright anticline in the southernmost part of the range (Fig 11: Z5 & Z6). This fold has a calculated fold axis of 05, 120, a nearly vertical axial surface, an interlimb angle of ~90°, and a rounded hinge (Fig 13c). Bedding and both the S_1 and S_2 cleavage are folded, indicating that the fold postdates the formation of both cleavages. Mesoscopic folds with nearly identical fold axes and axial surfaces to the main fold are relatively common, and typically have rounded to sub-rounded hinges, interlimb angles of 70-120°, and wavelengths of 3-10 m (Fig 13d). Rodgers (1987) interpreted these structures to be drag folds related to slip on the Reilly Canyon fault; however, their orientation isn't consistent with what would be predicted with models for drag folding. The folding more likely reflects a period of younger NNE-SSW shortening, likely associated with the late-stages of emplacement and ballooning of TG (see below).

Microstructures and metamorphism

Petrographic analysis of deformational fabrics and metamorphic assemblages was performed to characterize the mineral assemblages and porphyroblast-matrix relationships of the S_1 and S_2 cleavages, identify how they change throughout the map area, and determine their relationship to two overprinting amphibolite facies metamorphic aureoles, the Wood Canyon aureole and Singleton Creek aureole. The S_1 cleavage is present throughout the map area but varies greatly in both degree of development and metamorphic grade and is most well-developed in pelitic rocks and absent in quartzites and conglomerates. In the northwestern part of the map area in the upright limb and hinge region of the WCA, S_1 is present as a weakly to moderately well-developed slaty to phyllitic cleavage defined by

aligned microcrystalline micas and a weak grain shape foliation in quartz (Fig 14a). This cleavage becomes more coarse-grained and well-developed to the south, with pelitic rocks on the southern flank of the range having a penetrative S_1 defined by aligned medium- to coarse-grained micas and a weak grain shape preferred orientation in quartz (Figs 14b & 14c). The S_1 cleavage is commonly crenulated by the S_2 cleavage and is nearly completely overprinted by it on the southeastern flank of the range in the zone of metamorphism of the Singleton Creek aureole.

The Wood Canyon aureole was first described by Rodgers (1987) and has isograds that cut across formational contacts and indicate increasing grade to the southeast (Fig 15). The aureole has porphyroblastic biotite, garnet, staurolite, andalusite, and plagioclase, and reaches amphibolite grade along the southern flank of the range. Biotite is medium- to fine-grained, commonly altered to chlorite, and has abundant quartz inclusions that are either randomly oriented or form an internal foliation that is continuous with the external S_1 foliation, indicating growth during or after development of S_1. (Figs 14c & 14d). Garnet is medium- to fine-grained, equant and has aligned trails of quartz and oxide inclusions that are typically subparallel to and occasionally continuous with the S_1 cleavage, suggesting growth happened during or after cleavage development. Garnet is retrograded to aggregates of randomly oriented biotite and chlorite that either form rims or completely replace the garnet porphyroblasts. Relict staurolite is rare but is inferred to have been more common based on abundant staurolite pseudomorphs up to ~5 cm long composed of aggregates of fine-grained quartz and micas that are darker than the matrix. These pseudomorphs are typically subparallel with the S_1 cleavage, suggesting that they are syn- to post-kinematic. Plagioclase occurs as fine-grained equant porphyroblasts with rounded margins and the relative timing

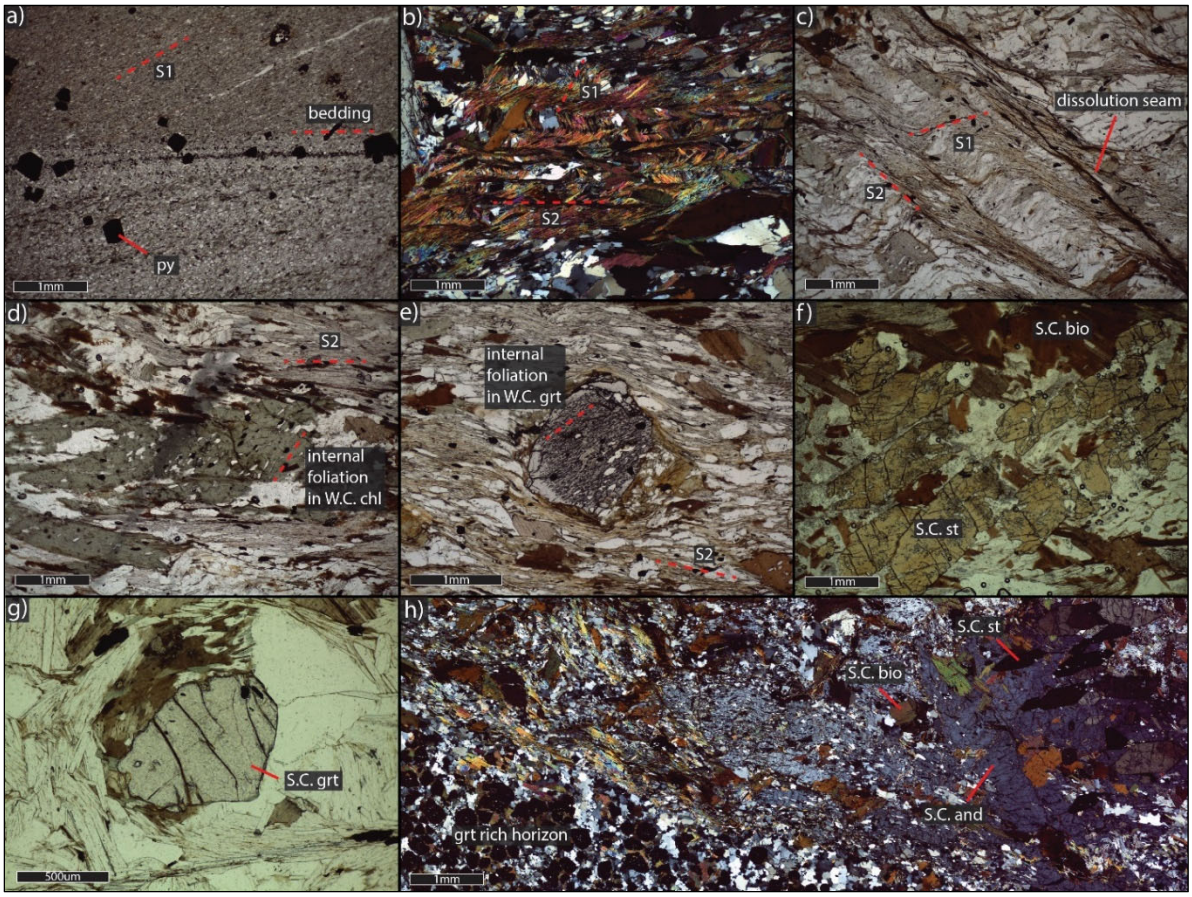

Figure 14: a) pCmg from the western part of the map area with a fine-grained slaty S_1 cleavage and porphyroblasts of pyrite (PPL). b) Schist from pCmb with a well-developed S_1 cleavage defined by penetrative mica growth crenulated by the S_2 cleavage (XPL). c) S_1 cleavage crenulated by the S_2 cleavage. Dissolution seams are present along cleavage domains of the S_2 cleavage (PPL). d) Chlorite from the Wood Canyon aureole with an internal foliation defined by aligned inclusions of quartz that is interpreted to reflect the S_1 foliation (PPL). e) Garnet from the Wood Canyon aureole with an internal foliation defined by aligned inclusions of quartz (PPL). f) Porphyroblasts of staurolite and biotite from the Singleton Creek aureole (PPL). g) Garnet porphyroblasts from the Singleton Creek aureole. h) Schist from pCmb with porphyroblasts of garnet, andalusite, biotite and staurolite from the Singleton Creek aureole (XPL).

of growth and cleavage development is unclear. The Wood Canyon aureole is interpreted to be synkinematic with the S_1 cleavage based on these porphyroblast cleavage relationships and the fact that the S_1 cleavage becomes more coarse-grained and well-developed within the Wood Canyon aureole. However, it is possible that the Wood Canyon aureole formed

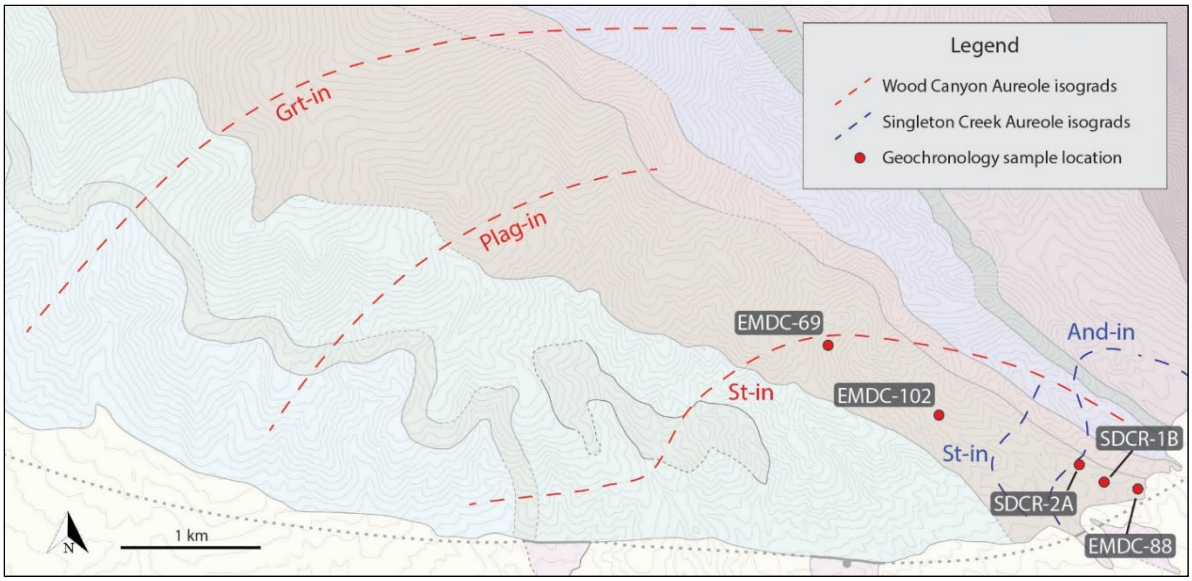

Figure 15: Map showing isograds of the Wood Canyon and Singleton Creek aureoles from Rodgers (1987) and sample locations for monazite geochronology.

after development of the S_1 cleavage and the observed porphyroblast cleavage relationships are due to mimetic growth.

The S_2 cleavage is present in the eastern part of the map area and is variably well developed. Outside the area of synkinematic metamorphism of the Singleton Creek aureole, the S_2 cleavage crenulates S_1, forming a spaced cleavage characterized by asymmetric microfolds of the S_1 cleavage (Figs 14b & 13c). Cleavage domains are typically spaced 1-2 mm and are formed by partial to complete dissolution of quartz on the shorter limbs of these microfolds. In some samples, more extensive dissolution of quartz forms discrete planar to wavy dissolution seams with concentrations of insoluble material (Fig 14c). In the southeastern flank of the range in the area of synkinematic metamorphism of the Singleton Creek aureole, the S_2 cleavage is upgraded and forms a penetrative foliation defined primarily by highly aligned micas (Figs 14d & 14e). In this area, the S_2 cleavage partially to completely overprints S_1, which is only evident as aligned trails of inclusions in garnet and

biotite porphyroblasts of the Wood Canyon aureole or as faint zones of aligned micas in microlithons of the S_2 cleavage (Fig 14d).

Rocks in a narrow zone along the southeastern flank of the DCR are distinctly upgraded to amphibolite facies in the Singleton Creek aureole, which was first identified and described by Rodgers (1987). This aureole is coincident with the highest-grade part of the Wood Canyon aureole, has porphyroblastic biotite, garnet, staurolite, andalusite, and cordierite, and has isograds that cut across formational contacts and indicate increasing grade toward the fault bounded southeastern flank of the range (Rodgers, 1987; Fig 15). Biotite is fine-grained, fresh, has little to no inclusions, and is either randomly oriented or is parallel with S_2, suggesting that it is syn- to post-kinematic (Figs 14f & 14g). Garnet is fine-grained, equant, fresh, hypidioblastic to idioblastic, and contains no inclusions (Figs 14g). It is usually randomly distributed throughout the rock volume but occasionally forms thin garnet-rich layers (Fig 14h). Staurolite is fine-grained, fresh, idioblastic and lacks inclusions (Figs 14f & 14h). It is typically randomly distributed throughout the rock volume but occasionally forms clusters and is sometimes present as inclusions in andalusite (Fig 14h). Andalusite is very coarse grained, fresh, and contains abundant aligned inclusions of quartz and oxide that are parallel with the S_2 foliation, indicating it is syn- to post-kinematic (Fig 14h). The Singleton Creek aureole is interpreted to be synkinematic with development of the S_2 cleavage based on these porphyroblast-cleavage relationships and the fact that the S_2 cleavage becomes penetrative and more well-developed within the aureole. However, it is also possible that it is post-kinematic and the observed porphyroblast-cleavage relationships are due to mimetic growth.

Summary of deformation and metamorphism in the southern Deep Creek Range

Rocks on the southern flank of DCR were affected by an early regional deformation that produced a west dipping cleavage (S_1) in Neoproterozoic to lower Cambrian rocks that is low greenschist grade but is upgraded abruptly towards the south in the amphibolite grade Wood Canyon aureole. Subsequently, the Neoproterozoic to Permian stratigraphy (including the S_1 cleavage in the older stratigraphic units) were clearly folded into the WCA, a recumbent fold that closes to the west and has a fold axis that plunges gently to the N-NNW and a highly attenuated lower (southern) limb. A younger (S_2) cleavage appears to be axial planar to the WCA but becomes more steeply dipping towards the southeast where it is very well-developed and nearly completely overprints S_1. Here, syn- to post-kinematic amphibolite facies metamorphism affected a localized area along the southeastern flank of the range (Singleton Creek aureole). Stratigraphy in the overturned limb of the WCA continues southward into the northeastern KM where it is highly attenuated and parallels the intrusive contact of TG. New constraints on the timing of metamorphism in the southern DCR are discussed below.

Deformation and metamorphism in the western Kern Mountains

The western KM expose the western potions of TG in contact with upper-crustal Ordovician to Pennsylvanian country rock on the northwestern and southwestern flanks of the range. The pluton has a conspicuous deformational and metamorphic aureole around its margins in both the country rock and the marginal parts of the pluton that coincides with a transposition of stratigraphy into parallelism with the intrusive contact. Integration of geologic mapping and structural analysis with petrographic observations of tectonites from

within the pluton's deformational aureole indicate that both penetrative deformation and the transposition of stratigraphy occurred synchronously with and was a direct result of emplacement of the pluton.

Map scale structures and relationships

Detailed geologic maps and cross sections of areas immediately adjacent to the pluton where it is in a clear intrusive relationship were made to characterize pre-, syn- and post-pluton emplacement structures in TG's country rock (Figs 16 & 17). Because of westward tilting of the range, these maps are intended to cover the upper sides and roof of the pluton. Here, TG intrudes upper-crustal dolomite, limestone and siltstone that now display evidence for multiple deformational events, including folds, faults and penetrative strain, at least some of which is associated with the emplacement of the pluton. There is a conspicuous deformational aureole along the margins of TG with a foliation in both the pluton and country rock that decreases in intensity and eventually dies out approximately 1 km outward from the contact, and within a few hundred meters inward into the core of the granite. This foliation is always parallel to the pluton margins and systematically tracks the intrusive contact around the western side of the range, outlining the shape of the pluton (Fig 18: P1-P6). In the distal parts of the aureole, a cleavage is only weakly developed and is at a high angle to bedding in the country rock, but towards the margin of the pluton, bedding is transposed into parallelism with the intrusive contact within a few hundred meters of the pluton, forming a single bedding-parallel high-strain fabric.

The oldest structures exposed in the western KM appear to be N to NE trending map-scale folds that have been subsequently deflected by emplacement of TG and cut by faults. The most obvious of these is the north-trending upright anticline in the southern map area (F5) that separates an eastern limb composed of a conformable section of OS through Dg that dips moderately to the east from a western limb of Dsi, OS, and Dse that dips moderately to the west but has been dismembered by two high angle faults (Fig 16: F5; Fig

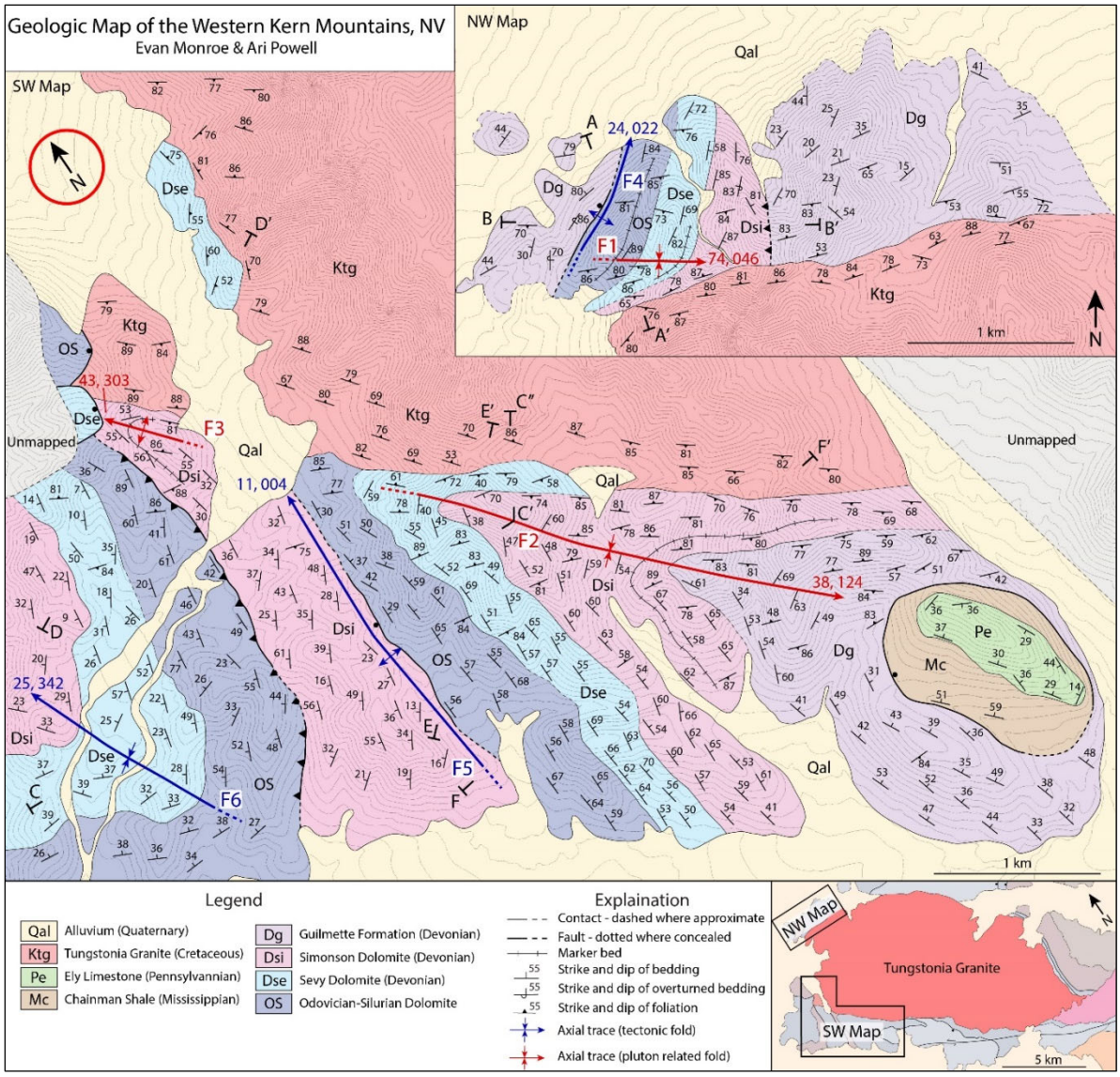

Figure 16: Geologic map of the northwestern and southwestern flanks of the KM. The location of each map area is shown in the inset map in the bottom right corner.

17: C-C"). This fold has a fold axis of 11, 004, a subvertical axial surface and an interlimb angle of ~90° (Fig 18: S3). Prior to westward tilting of the range during the Cenozoic, the western limb would have been approximately horizontal and the eastern limb approximately vertical or overturned, and the fold would have had an axial surface that dipped to the west (i.e., east vergent), similar to other asymmetric folds that have been recognized in the

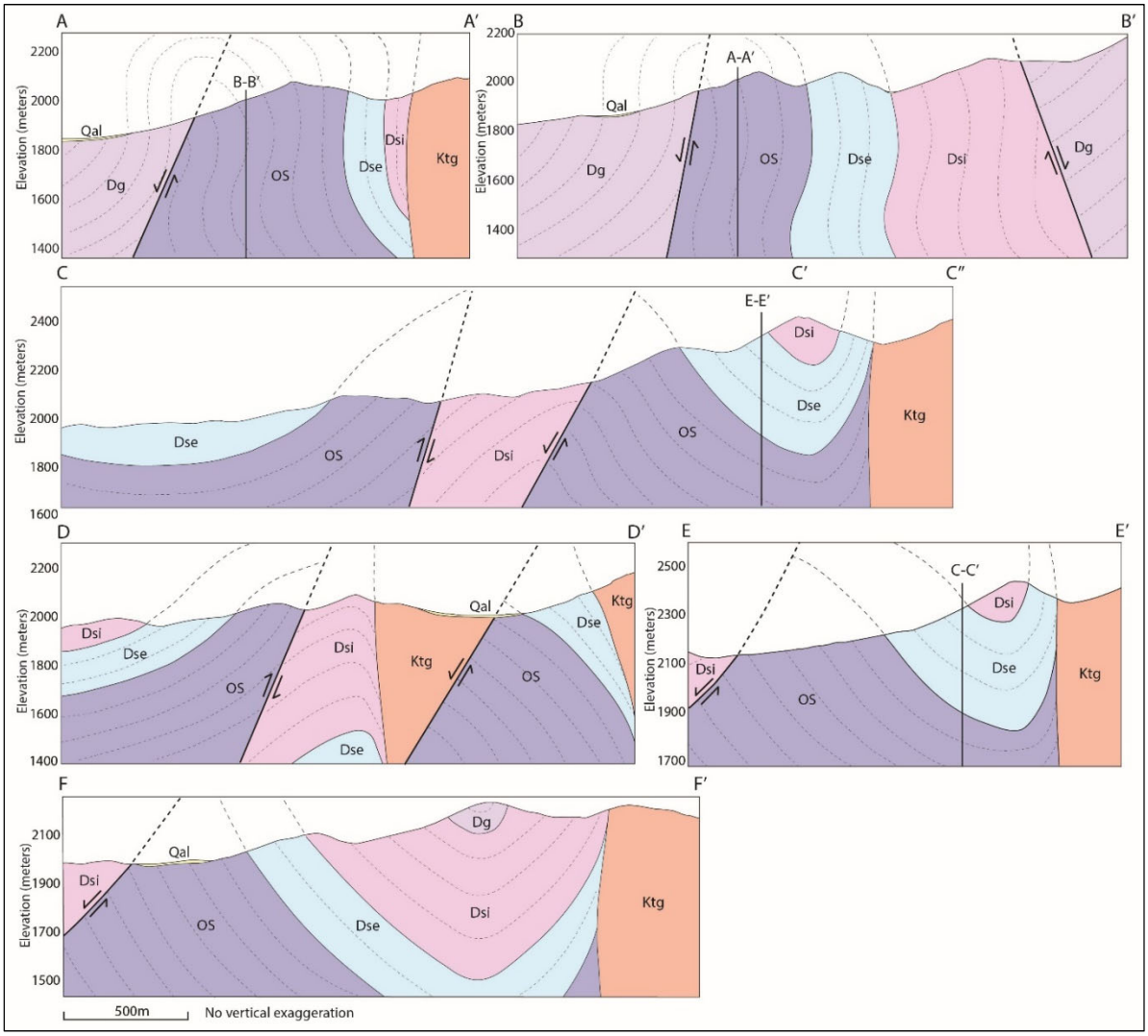

Figure 17: Cross sections from maps of the northwestern (A-A' and B-B') and southwestern (C-C'' through F-F') map areas.

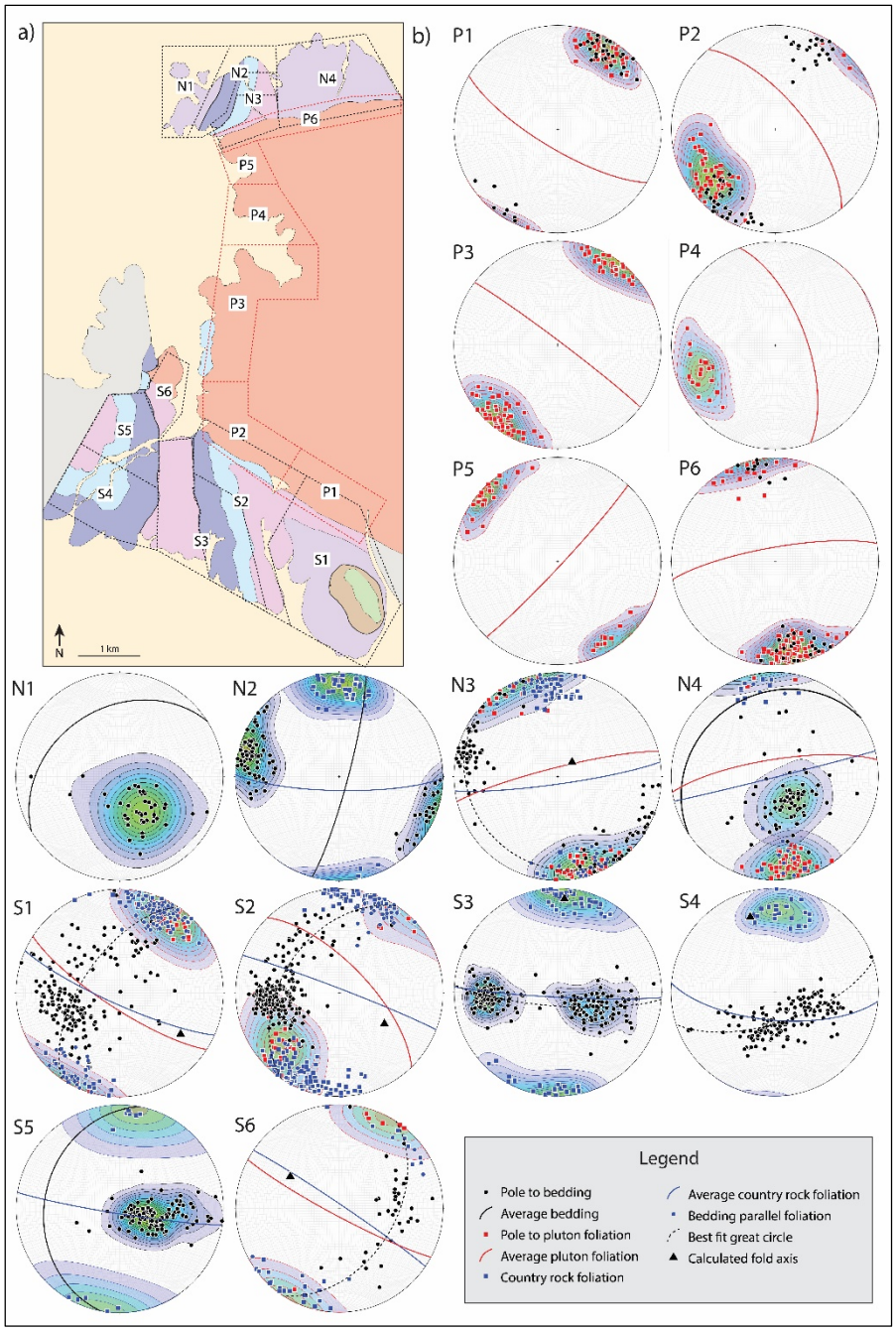

Figure 18: a) Map showing the geographic extent of stereonets. b) Zoned stereonets showing orientations of bedding, foliation, and folds in the northwest and southwest map areas and intervening exposures of TG.

Confusion Range and Snake Range. The geometry of the hinge is obscured by two high angle faults—one that is interpreted as a west-dipping thrust fault that was perhaps synchronous with folding, and the other that is interpreted as a younger west-dipping normal

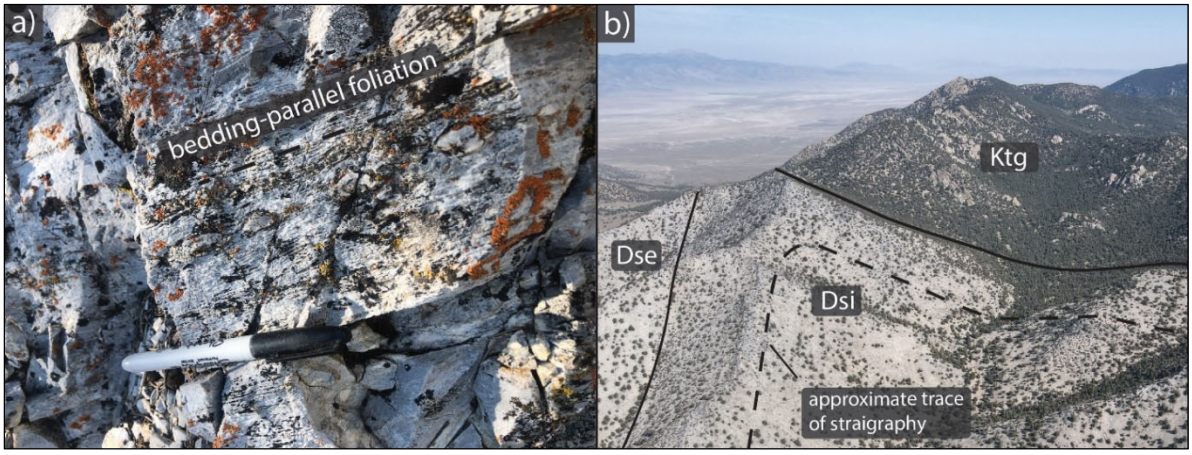

Figure 19: a) Bedding-parallel foliation in Dse ~150 m from the intrusive contact. View facing north. b) Drone image looking north across part of the southern map area. Stratigraphy rotates from being at a high angle to the pluton margin to being sub-parallel to it within a few hundred meters of the contact (F3).

fault. A similar anticline is present in the northern map area (F4) that has a fold axis that plunges gently to the NNE, with bedding of the Guilmette formation in the western part of the map area dipping moderately to steeply to the west and beds to the east of the Ordovician through Devonian dolomites dipping steeply to the east (Fig 16: F4; Fig 17: A-A' & B-B'; Fig 18: N1 & N2). On the eastern side of the northern map area, exposure is poor and bedding is inconsistent but appears to primarily be dipping to the northwest (Fig 18: N4), likely due to the synclinal closure of the associated anticline to the west. However, these folds have been obscured by subsequent normal faulting so their precise geometry is difficult to determine. TG cuts both of these early folds so folding must have occurred prior to emplacement. A gentle syncline (F6) is exposed in the southwestern corner of the southern map area that has a fold axis that plunges gently to the northwest (Fig 16: F6; Fig 17: C-C''; Fig 18: S4). It has a similar orientation to folds exposed in the southwestern DCR (Rodgers, 1987) and is interpreted to be unrelated to pluton emplacement.

Perhaps the most interesting map patterns of the western KM are the conspicuous deflections of stratigraphy into parallelism with the pluton margins. Stratigraphy rotates from being at a high angle to the pluton contact to being sub-parallel to the contact within 100-500 m of the pluton. These abrupt deflections spatially coincide with the zone of penetrative deformation and development of a high strain tectonite fabric near the pluton margins, with the limbs that are adjacent to the pluton being highly strained and attenuated.

In the southern map area, there are two map-scale folds with distinct orientations that reflect the deflection of bedding into parallelism with the pluton contact. The largest of the two is a southwest plunging syncline (F2) that affects the east-facing section of OS through Dg and underlies most of the eastern part of the map (Fig 16: F2; Fig 17: C-C'', E-E' & F-F'; Fig 19b). Bedding orientations around this deflection yield a calculated fold axis of 38, 124, a subvertical axial surface that strikes NW-SE, an interlimb angle of ~50°, and a rounded hinge (Fig 18: S1 & S2). The axial surface of this fold and the pluton margin have a ~10° difference in strike, such that the limb adjacent to the pluton increases in thickness from ~100 m to ~500 m from west to east. Prior to westward tilting of the range, the fold axis and both limbs would have been approximately vertical with the N-S trending limb of the older anticline (F2) being deflected eastward (i.e., dextrally; Table 1).

The second deflection of stratigraphy in the southern map area is a northwest plunging anticline (F3) exposed near the western edge of the map immediately south of the westernmost exposure of TG. Here, Dsi rotates from dipping moderately to the west to dipping very steeply to the northeast, approximately parallel to the pluton margin and foliation, over a distance of ~100 m (Fig 16: F3; Fig 10: D-D'). This anticline has a fold axis of 43, 303, an axial surface that dips steeply to the southwest and an interlimb angle of ~80°

(Fig 18-S6). Prior to westward tilting of the range, the fold axis would have been approximately horizontal, with the limb away from the pluton dipping gently to the southwest or subhorizontal and the deflected limb dipping vertically and striking NW-SE (Table 1). The difference in orientation between the two pluton-adjacent folds in the southern map area clearly reflects the preexisting structure from the earlier N-S trending anticline, such that the eastern fold was affecting rocks that were near vertical and the western fold was affecting rocks that were approximately horizontal. The sense of deflection in both cases is dextral or downward in a pre-tilt orientation. The spatial coincidence of all three folds with the pluton margins and the zone of ductile deformation suggests they formed in response to emplacement of TG.

In the northwest map area, the steeply east-dipping OS through Dsi stratigraphy north of the pluton is deflected to the west starting ~200 m from the intrusive contact and is transposed into parallelism with the

Fold Number	Fold Axis	Transposed Bedding	Limb away from Pluton
F1	74, 046	260, 88	014, 84
F1 Pre-tilt	52, 325	264, 64	191, 58
F2	38, 124	298, 79	352, 54
F2 Pre-tilt	78, 135	306, 80	000, 88
F3	43, 303	302, 89	171, 48
F3 Pre-tilt	03, 303	122, 89	122, 28

Table 1: Orientations of the three folds that transpose bedding into parallelism with the intrusive contact in both their present-day orientation and orientation after restoring for westward tilting of the range. A 40° rotation about a horizontal axis trending 030° was used as a best approximation to restore tilting, however there is significant uncertainty in this estimate. The "Transposed Bedding" column shows the average strike and dip of bedding in the limb adjacent to the pluton, which is approximately parallel to the intrusive contact and foliation. The "Limb away from Pluton" column shows the average strike and dip of bedding in the other limb. The locations of each fold are shown in Fig 9.

WSW striking pluton margins and foliation within ~100 m of the pluton (Fig 16: F1). The fold produced by this deflection (F1) is very steeply plunging with a calculated fold axis of 74, 046 (Fig 18: N3), an axial surface that dips steeply to the north, an interlimb angle of ~130°, and a sub-rounded hinge. Prior to westward rotation of the range during the Cenozoic, this fold would have plunged moderately to the northwest and been defined by an abrupt upward deflection of moderately west-dipping stratigraphy adjacent to the more steeply dipping pluton margins (Table 1). To the east in the Guilmette formation, bedding is inconsistent away from the pluton due to smaller scale folds but still becomes approximately parallel with the pluton margins within 100-400 m of the contact.

At least two distinct normal faulting events affected rocks in the western KM. The earliest period of normal faulting is reflected in a gently east-dipping normal fault exposed in the eastern part of the southern map area that juxtaposes Mississippian Chainman shale in the hanging wall against Devonian Guilmette limestone in the footwall omitting the entire Mississippian Joanna Limestone and Pilot Shale and likely some of the Guilmette as well. The fault is approximately parallel to bedding in both the footwall and hanging wall and possibly represents a bedding parallel segment of an old normal fault with a ramp-flat geometry. This fault projects into TG and the same fault is well-exposed to the north of TG (Gans et al., 1990), indicating it must predate emplacement and likely formed as a somewhat higher angle east-dipping normal fault that rotated to its present low angle during westward rotation of the KMDCR. Younger ~N-S striking high-angle normal faults are also present in both the northern and southern map areas and likely reflect a late-stage extensional event that occurred after emplacement of TG and either during or after westward tilting of the range.

Tectonite fabrics in the deformational aureole of the Tungstonia Granite

TG has a conspicuous deformational aureole around its margins in both the country rock and within the marginal part of the pluton that decreases in intensity inward and outward from the contact. At deeper structural levels in the northeastern KM, this fabric strikes NW and dips moderately to the NE, is parallel to bedding in the overturned limb of the WCA and is continuous throughout all exposures of the country rock northward into Pleasant Valley. At shallower structural levels in the western KM, the cleavage is much more localized and dies out rather abruptly away from the pluton into undeformed Paleozoic carbonates and clastic rocks. Excellent exposures of both the marginal parts of the pluton and the country rock in this area allow for a detailed investigation of the nature and distribution of this strain.

Nineteen oriented samples of carbonate country rock and granite were collected along two transects perpendicular to the pluton margin in the northwest and southwest map areas, as well as a variety of other samples, to assess how the magnitude, mechanisms and conditions of strain vary within the pluton's deformational aureole (Table 2). In hand specimen, most samples within the deformational aureole have a strong foliation and occasionally a very weak lineation, and thin sections were cut where possible perpendicular to the foliation and parallel to the lineation (X-Z face). When no lineation was evident, a

best approximation of the X-Z cut was made by estimating the relative strength of the foliation from various angles.

Samples of country rock were collected from the Devonian Sevy Dolomite and Simonson Dolomite, which are the main wall rocks to the western exposures of TG.

Sample	Distance from Contact (m)	Rock Unit	Average Grain Size (um)	Estimated X/Z	Bedding Orientation	Foliation Orientation
N1	190	Dse	12	1.1	014, 83	086, 78
N2	147	Dse	26	1.7	062, 88	062, 88
N3	126	Dse	21	1.7	066, 87	066, 87
N4	115	Dse	159	1.3	233, 88	233, 88
N5	106	Dse	136	1.8	233, 88	233, 88
N6	86	Dse	25	1.9	245, 82	245, 82
N7	64	Dsi	61	1.9	237, 88	237, 88
N8	50	Dsi	94	3.0	239, 82	239, 82
N9	1	Dsi	138	3.0	246, 78	246, 78
S1	565	Dsi	45	1.1	010, 51	098, 84
S2	300	Dse	14	2.1	333, 55	297, 75
S3	201	Dse	15	2.0	307, 80	307, 80
S4	58	Dse	42	2.2	299, 78	299, 78
S5	5	Dse	41	2.4	317, 61	317, 61

Table 2: Samples collected from TG's country rock in the northern (N) and southern (S) transects. Four samples from TG were also collected from 1 to 50 m from the contact in the northern transect and one sample of TG from ~5 m from the contact in the southern transect.

Undeformed and unmetamorphosed Sevy has an average thickness of 180-200 m and is composed of very fine-grained (10-15 um) light-gray dolomite with thin laminations. Beds typically range in thickness from 20 to 50 cm and occasional coarse-grained horizons are present as well as a few distinct marker horizons that contain abundant detrital quartz. The Simonson Dolomite is 150-175 m thick, has highly variable color (dark brown to light grey), bedding thickness (thin to massive), and grain sizes, and can be divided into three sub-members. The lowest member is ~30 m thick and is composed of light gray to brown, thick-bedded, medium- to coarse-grained dolomite that forms small cliffs and ledges. The dominant member is a thin- to medium-bedded medium- to coarse-grained dolomite with well-developed planar laminations defined by alternating light and dark brown bands. The uppermost part of the Simonson has uniform, very well-developed planar laminations. Minor clay and silt are common throughout both the Sevy and Simonson.

Outside of the pluton's deformational aureole, the country rock is undeformed and unmetamorphosed and is indistinguishable from typical Sevy and Simonson found in other parts of eastern Nevada. In the distal parts of the pluton's deformational aureole, up to 1.5 km from the intrusive contact, a spaced disjunctive pressure solution cleavage begins to appear that is at a high angle to bedding and produces parting planes that are approximately parallel with the pluton margin. In the microlithons between the cleavage domains the rock is largely undeformed. The foliation becomes more pronounced within a few hundred meters of the pluton contact and is defined by both pressure solution seams and the development of a continuous grain shape foliation. Within 100 to 150 m of the pluton contact, the foliation becomes well developed, the dolomite is more coarsely recrystallized, and bedding is transposed into parallelism with it. This foliation increases in grade toward the pluton

margin and is defined by a strong grain-shape-preferred orientation of elliptical dolomite grains, growth and alignment of metamorphic micas, pressure solution seams and compositional layering.

The country rock samples examined for this study are composed primarily of dolomite (~80-98%) with minor to trace amounts of both diagenetic minerals (calcite, quartz, pyrite, oxides) and metamorphic minerals (tremolite, phlogopite, muscovite). Average grain size of dolomite within each carbonate sample ranges from 12-160 um and greatly increases with proximity to the pluton, with the grain size of samples far from the pluton reflecting the original diagenetic recrystallized grain size and samples proximal to the pluton reflecting metamorphic recrystallization (Figs 20a, 21a, 21b & 21c). However, two samples are more-coarse grained than expected for their distance from the pluton. The Sevy Dolomite is known to have conspicuous horizons of more coarse-grained material and it is likely that these anomalously coarse-grained samples are from an originally coarse-grained horizon. Also, the three samples closest to the contact in the northern transect are from Dsi so some of this increase in grain size may reflect the original diagenetic grain size. Some of the samples have a bimodal grain size distribution, with pods and lenses of coarse-grained dolomite occupying 5-20% of the rock volume in a groundmass of fine-grained recrystallized dolomite (Fig 21e). Many of these pods and lenses appear to have originally been carbonate veins that were extensively folded and boudinaged so that they are now disaggregated, or were areas where fluids affected the recrystallized grain size. For these bimodal samples, only the finer grained groundmass was used to measure grain size and ellipticity.

To estimate the magnitude of strain, the ellipticity of ~100 recrystallized dolomite grains per sample was measured from enlarged photomicrographs using the measuring tool in Adobe Illustrator. The average ellipticity ranges from approximately 1 to 3 (long axis over short axis) and increases with proximity to pluton (Fig 20b). It is important to emphasize that these ellipticities are an absolute minimum estimate of the total accumulated strain because of the probability that continuous recrystallization occurred during deformation. This strain estimate only reflects the penetrative grain shape foliation and does not account for volume loss shortening perpendicular to the foliation by pressure solution. In addition, it is unlikely that all thin sections are perfectly parallel to the X-Z face so many of these ellipticities have likely been calculated from an oblique cut of the strain ellipsoid. However, they still provide a rough indication of the magnitude of strain and the strain gradient, which dramatically increases towards the pluton margin. Most highly deformed samples have a well-developed foliation but not an obvious lineation and we suspect that much of the strain is well into the flattening field. However, marbles that are deformed at

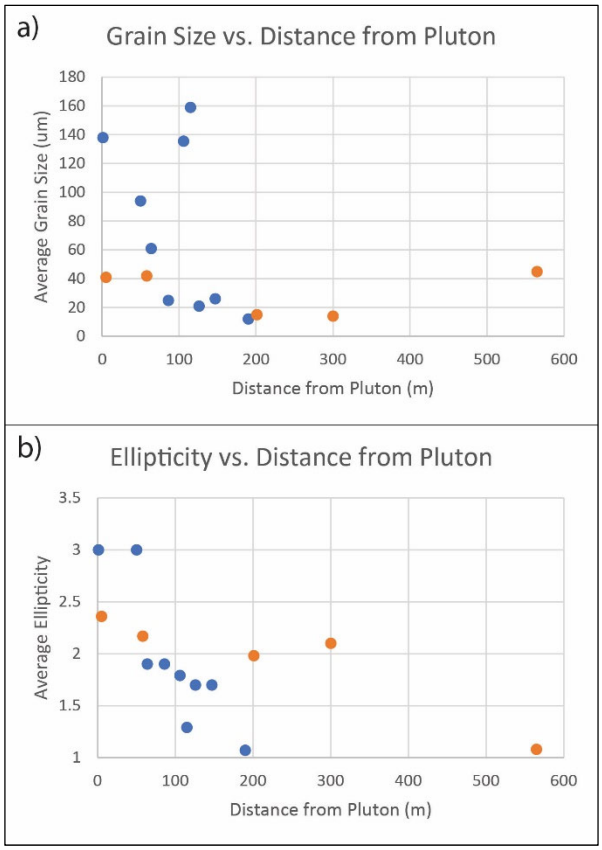

Figure 20: a) Plot showing the average grain size of recrystallized dolomite grains from the northern (blue) and southern (orange) transects plotted against distance from the pluton margin. b) Plot showing the average ellipticity of recrystallized dolomite grains from both transects.

high metamorphic grade typically to not preserve well-developed lineations so it is possible that strain was closer to pure-shear but that the lineation was not preserved.

Dolomite grains within this suite of samples have a variety of textures. For most samples, grains have relatively straight or slightly rounded margins, with well-developed polygonal grain boundaries that typically increase in development toward the pluton margin, indicating that deformation occurred at elevated temperatures towards the intrusive contact, with thermal recrystallization outpacing deformation (Figs 21d). Both type I and type II twins are relatively common and pervasive in the two samples that are proximal to the pluton margin in the northern transect (Fig 21c). Weak to moderate sweeping and patchy undulatory extinction is sometimes present but decreases with distance from the pluton margin. It is common for adjacent grains to have similar/sweeping extinction angles, indicating that they are separated by subgrain boundaries. Incipient subgrain boundaries within larger relict grains are also occasionally present. Many of the coarser grained pods of dolomite have highly irregular/ameboid grain shapes, suggesting a component of grain boundary migration (Leiss & Barber, 1999). These textures indicate that deformation was occurring at elevated temperatures which could only have been caused by heat from TG.

Metamorphic tremolite is present in eight of the samples and makes up 2-10% of the rock volume (Fig 21f). It occurs as euhedral to subhedral porphyroblasts up to 1 cm across but more commonly 200-1000 um and is variably retrograded to very fine-grained aggregates of dolomite, quartz, oxides and muscovite. It occasionally forms radiating and randomly oriented aggregates that cut the foliation but more commonly occurs as isolated porphyroblasts which are usually parallel or subparallel to the foliation but occasionally cut it. Quartz is present in eleven of the samples and typically comprises up to ~8% of the rock

volume, but usually less than 2-3%. Phlogopite and muscovite are present in most of the samples and comprise up to ~4% of the rock volume. Micas are typically very-fine grained

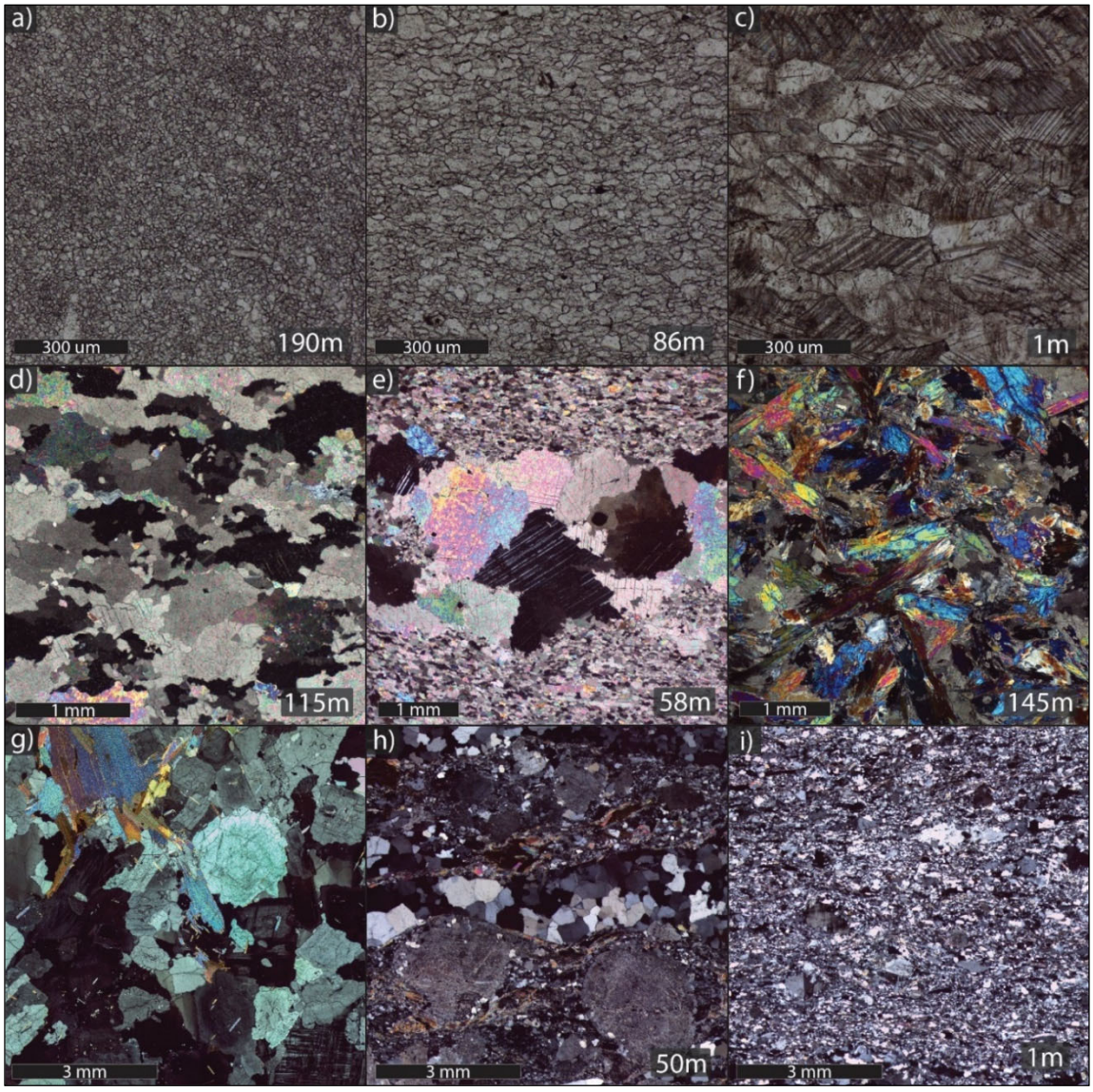

Figure 21: Photomicrographs of rocks from TG's deformational aureole. Distance from the intrusive contact is indicated in the lower right corner of each photo. a) Very fine-grained dolomite with no deformational fabric (PPL). b) Medium-grained dolomite with a weakly developed deformational fabric (PPL). c) Coarse-grained dolomite with a well-developed deformational fabric and pervasive deformation twinning (PPL). d) Coarse-grained dolomite with highly lobate grain boundaries, suggesting grain boundary migration (XPL). e) Fine-grained dolomite with a pod of coarse-grained material. f) Coarse-grained metamorphic tremolite (XPL). g) Undeformed TG from the interior of the pluton (XPL). h) TG collected 50 m from the pluton contact with a moderately well-developed foliation (XPL). i) Highly deformed TG collected 1 m from the pluton contact (XPL).

and occur as platy porphyroblasts, most of which are aligned with the foliation. Small, isolated feldspar grains are present in some of the samples and are usually associated with quartz-rich horizons. Trace oxides are present in nearly all the samples and typically occur as <30 um anhedral grains dispersed throughout the rock volume as well as along dissolution seams.

The unstrained interior of TG is a coarse-grained two-mica granite with an average composition of 40-50% plagioclase, 20-30% potassium feldspar, 25-30% quartz, 3-5% muscovite, 2-3% biotite, and trace oxides, garnet, zircon, titanite, monazite and apatite (Fig 21g). Euhedral books of muscovite up to 5 cm and phenocrysts of perthitic potassium feldspar up to 4 cm are set in a somewhat finer grained matrix of quartz, feldspar and micas displaying a seriate grain size distribution from less than 100 um to 2-3 cm. The interior of the granite has a typical hypidiomorphic granular texture and is isotropic except for occasional aligned books of muscovite, showing no evidence of subsolidus deformation other than undulatory extinction and occasional deformation lamellae in quartz and feldspar.

TG grades from its unstrained interior to a highly strained tectonite near its margins over a distance of ~100-300 m. In the inner portion of the aureole, strain is minimal and primarily accommodated by quartz with little deformation of feldspar. With increasing proximity to the pluton contact, the mesoscopic foliation becomes progressively more well developed and is defined by a strong grain shape preferred orientation of recrystallized quartz ribbons, alignment of synkinematic micas, and an aggregate shape preferred orientation of recrystallized feldspar (Fig 21h). Within a few meters of the contact, the granite is intensely foliated, with highly elongated quartz ribbons, a strong alignment of micas, extensive strain and recrystallization of feldspar, and drastic reduction in

recrystallized grain size (Fig 21i). Some of this reduction in grain size might reflect an original quenching of the granite towards the intrusive contact but the extensive development of quartz ribbons and feldspar porphyroclasts with highly elongated tails showing clear dynamic recrystallization into much smaller subgrains suggests that this conspicuous decrease in grain size associated with the development of an intense tectonite fabric was produced by subsolidus (albeit high temperature) strain and dynamic recrystallization. A qualitative assessment of strain in the most deformed parts of the granite based of ellipticities of quartz ribbons and transposition of aplite dikes is that X/Z is likely >5. Shear sense indicators are relatively ambiguous but asymmetrical tails around feldspar porphyroclasts typically suggest right lateral shear on the northern margin of the pluton and left lateral shear on the southern margin. Because of westward tilting of the range, these shear-senses are pluton-up prior to tilting.

In deformed TG, feldspar occurs as relatively undeformed porphyroclasts surrounded by very fine-grained recrystallized feldspar aggregates which are most common in strain shadows. Larger porphyroclasts are commonly fractured and pulled apart parallel with the foliation. Quartz ribbons range in size from 1 mm to over 5 cm across and commonly have aspect ratios >5 and sometimes > 10. These ribbons used to be single large equant grains prior to deformation and have been stretched out into their current shape. They are now composed entirely of subgrains that have well-developed polygonal boundaries, but are sometimes lobate or ameboid shaped, indicating GBM recrystallization. Muscovite and biotite occur as relatively continuous thin seams or individual grains that commonly wrap around feldspar grains to form an anastomosing network with an average orientation parallel with the foliation.

Relationships between deformation, metamorphism and pluton emplacement in the western Kern Mountains

Analysis of map relationships and petrographic observations in the western KM reveals a few important conclusions regarding the relationships between deformation, metamorphism and the emplacement of TG. First, the tectonite fabrics, localized metamorphism, and deflection of bedding into parallelism with the intrusive contact are interpreted to be synchronous with and directly related to the emplacement of the granite, where deformation in the wall rocks served mainly to make space for the granite and accommodate its upward ascent. In other words, this is not a younger "tectonic" shear zone localized along the margin of a pluton. Second, the types of relationships observed here—high strain fabrics, map-scale folding, abrupt lateral increases in metamorphic grade—are simply smaller-scale versions of what we observe occurring on a much larger scale along the southern flank of the DCR and in the embayment of metasedimentary rocks in the overturned limb of the WCA in the eastern KM. The specific lines of evidence that support these conclusions are:

1) Deformation is restricted to the immediate vicinity of the intrusive contact and decreases rapidly away from that contact in both the pluton and country rock.
2) The tectonite fabrics are dominated by a foliation that appears to be mainly in the flattening field and everywhere parallels the sharp intrusive contact, even though this contact wraps around the western end of TG, such that it ranges from NW to N to ENE striking.

3) The strain in the country rocks is synkinematic with prograde metamorphism whose grade increases abruptly from completely unmetamorphosed country rocks to upper greenschist or amphibolite facies over less than a kilometer towards the exposed contact with the pluton—a metamorphism that can only be interpreted as contact metamorphism.
4) The tectonite fabric in the marginal part of the pluton dies out rapidly inward and is everywhere a high-temperature subsolidus fabric characterized by dynamic recrystallization of feldspar and extensive high-temperature recovery textures including grain boundary migration and complete polygonization of quartz within quartz ribbons. Intensely foliated hand specimens are often disappointing in thin section because of their recrystallized granoblastic texture, with the only evidence for the foliation being the conspicuous alignment of biotite and muscovite grains.
5) A final piece of evidence that this contact is clearly an intrusive contact is that the abundance of leucocratic veins of aplite and pegmatite increases dramatically towards the contact—from quite rare within the interior of TG to an impressive network of dikes and sills within a hundred meters of the contact. Most of these dikes and sills become largely transposed into parallelism with the contact in the intensely foliated area close to the margin, but there are also numerous examples of late aplite dikes cutting across previously deformed and transposed dikes, thereby providing compelling evidence that the emplacement of the shallow levels of the granite was synchronous with the deformation in its marginal facies and contact aureole.

One of the most peculiar attributes of the intrusive contact is the total absence of granite dikes that emanated from the pluton and intruded the adjacent wall rocks, and the lack of any inclusions or pendants of wall rocks within the pluton. We attribute this to the likely very high viscosity of the melt as it was being emplaced largely as a crystal mush and its continued subsolidus ascent to shallower levels driven by the buoyancy of additional magma being emplaced from below—see discussion in following section.

U-Pb Geochronology

U-Pb geochronology was performed to constrain the timing and duration of metamorphism of the Wood Canyon and Singleton Creek metamorphic aureoles as well as the precise age(s) and crystallization history of TG. Both are broadly known to be Late Cretaceous (Gottlieb et al., 2022; Lee et al., 1986; Rodgers, 1987) but it is important to establish more precise ages to determine the duration and timing of both metamorphic and magmatic activity in the area and to assess what relationships, if any, exist between the two. Monazite from five samples of schist from the southern DCR was dated to constrain the age(s) and duration of metamorphism as well as zircon from eight samples from various locations within TG to constrain its crystallization history.

Methods

Analysis took place at UC Santa Barbara's Laser-Ablation-Split-Stream Geochronology facility following the methods described in Kylander-Clark et al. (2013). Zircon crystals were separated using standard magnetic and density techniques, mounted in an epoxy puck, and imaged using the cathodoluminescence detector on UCSB's FEI Quanta 400F field emission source SEM prior to analysis. Monazite was analyzed in thin section to

evaluate the petrographic context of mineral growth. Monazite grains were identified using the cathodoluminescence detector on the SEM and UCSB's Cameca SX-100 electron microprobe was used to make quantitative elemental maps of U, Th, Pr, Gd, La, Y, Nd, Sm, Ce and P to identify zoning patterns to help guide laser spot placement. U-Pb isotopes were measured with a Nu Instruments Plasma HR multi-collector ICP for both zircon and monazite, and element concentrations for monazite were measured concurrently using an Agilent 7700X quadrupole ICPMS. The primary reference material (RM) for zircon U-Pb was 91500 (Wiedenbeck et al., 1995), and GJ1 (Horstwood et al., 2016) and Plešovice (Sláma et al., 2008) were employed for accuracy; both standards yielded dates within 2% of their expected values. Monazite 44069 was used as the primary RM for U-Pb normalization, and Bananiera (Palin et al., 2013), FC-1 (Horstwood et al., 2003) and Trebilcock (Tomascak et al., 1996) yielded U-Pb dates within 2% of their expected values. Bananiera (Kylander-Clark et al., 2013) was used as the primary trace-element RM, assuming 12.9% P in monazite. 60-80 spot analyses were performed on each monazite sample and ~60 spot analyses were performed on individual zircons from each sample of TG. Isotope data was reduced using Iolite software and plotted with Isoplot software (Berkley Geochronology Center, 2012; Paton et al., 2011).

Revised ages of prograde metamorphism in the southern Deep Creek Range

The amphibolite grade Wood Canyon aureole on the southern flank of the DCR contains porphyroblastic biotite, garnet, staurolite, andalusite and plagioclase and has isograds that cut across formational contacts and indicate increasing grade to the southeast (Fig 14). Metamorphic assemblages associated with this aureole are overprinted by the

younger and much more localized Singleton Creek aureole, which is located on the southeastern most flank of the range and also reached amphibolite facies as evidenced by prograde biotite, garnet, andalusite, staurolite and cordierite. Rodgers (1987) analyzed two samples of metamorphic hornblende using the $^{40}Ar/^{39}Ar$ technique to constrain the ages of metamorphism in the Wood Canyon and Singleton Creek aureoles. One was from an amphibolite sill in McCoy Creek unit B that was within the outer portions of the Wood Canyon aureole that yielded an uninterpretable age spectrum. The second sample was from another amphibolite sill in unit B within the outer margin of the Singleton Creek aureole that yielded a plateau of 72.8 ± 0.2 Ma, although most of the gas was released on a single step. It was unclear at this locality whether hornblende was heated beyond its closure temperature during Singleton Creek metamorphism, so its bearing on the age of either of the aureoles is not clear. In any case, the ~73 Ma argon age is best interpreted as a cooling age (or possibly a partially reset older age) and does not likely record the age of peak metamorphism for either event. New U-Pb monazite geochronology on five samples of schist collected along a transect in McCoy Creek unit E was performed in an attempt to determine the ages of both the Wood Canyon and Singleton Creek aureoles. Two samples were collected from within the st + grt zone of Wood Canyon aureole but outside the st-in isograd of the younger Singleton Creek aureole, with three of the samples located within the st ± grt ± and ± cord zone of the Singleton Creek aureole (SDCR-2A, SDCR-1B, and EMDC-88; Fig 23a).

The majority of the monazite grains analyzed are 10-30 um, equant, rounded, and disseminated throughout the rock volume (Fig 22). Rare grains up to 100 um are also present, and multiple spots were put on these larger grains. Elemental maps measured on the EPMA often don't show clear zoning patterns, however some grains–especially the larger

ones–exhibited sector or concentric zoning, which is most evident in Ca and Y. Nearly all the analyses are slightly discordant, indicating a component of common lead which is typical for metamorphic monazite. Projecting these data onto concordia resulted in final dates with errors of ± 2-4 Ma.

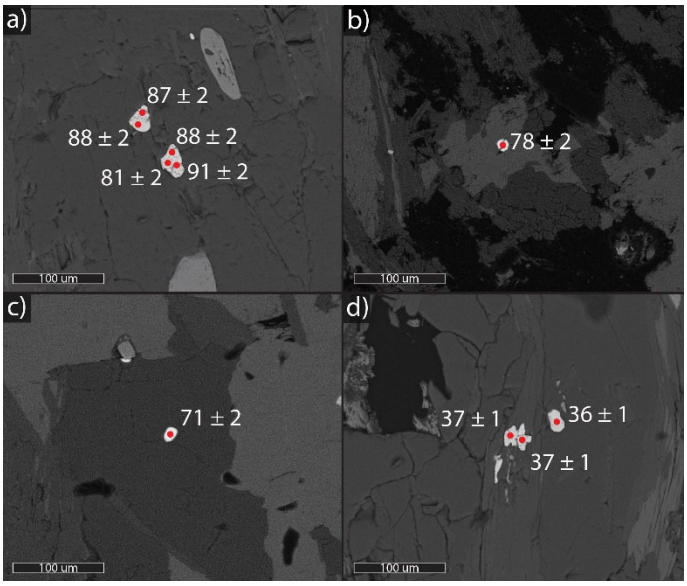

Figure 22: SEM images showing the typical monazite morphologies from the samples analyzed with laser spot locations and associated ages. a) Relatively coarse-grained monazite with multiple Late Cretaceous ages. b-c) Very fine-grained equant monazite that was the most common in these samples. d) Relatively coarse-grained monazite with Eocene ages.

The five samples analyzed have a range of dates from 34 to 108 Ma, with the highest concentration ranging from ~80-90 Ma (Fig 23c). This spread of dates from 80-90 Ma is present in all the samples and it relatively continuous. Sample EMDC-102 and to a lesser extent EMDC-69 and EMDC-88, also show a cluster of Eocene dates from 35 Ma to 42 Ma. The three samples from within the Singleton Creek aureole (SDCR-2A, SDCR-1B and EMDC-88) have a peak at 70 ± 2 Ma, which is absent from the other two samples. There are a small number of older dates (up to 108 Ma) and intermediate dates (between 50 Ma and 78 Ma).

We interpret the spread of dates from ~80-90 Ma to reflect protracted crystallization and recrystallization of monazite during episodic or protracted heating and fluid flow and likely represents the age of the Wood Canyon aureole. The younger 70 ± 2 Ma peak is only

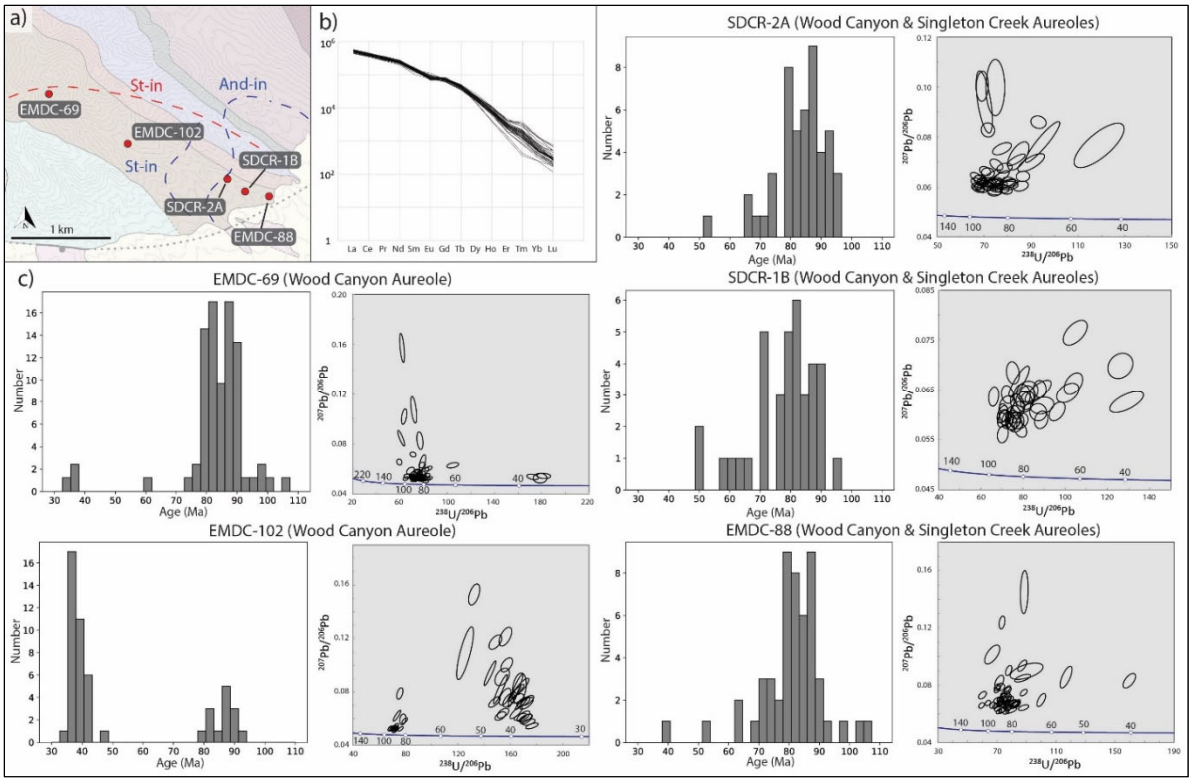

Figure 23: a) Map showing geochronology sample locations and the staurolite-in isograd of the Wood Canyon aureole (red), and staurolite-in and andalusite-in isograds of the Singleton Creek aureole (blue). Isograds from Rodgers (1987). b) Rare earth element spider diagrams for the six samples analyzed. b) Histograms and Tera-Wasserburg concordia diagrams showing the distribution of U-Pb monazite ages from the six samples of schist from the southern DCR that were analyzed. Each age is from a single spot analysis on a monazite grain.

present in samples within the Singleton Creek aureole so we interpret these dates to reflect this younger and much more localized metamorphic event. The Eocene dates overlap with the age of the Ibapah pluton in the central DCR and the Skinner Canyon Granite (and likely the Uvada Granite) in the KM and thus likely reflect heating by Eocene magmas concealed beneath the present exposure surface (Best et al., 1974; Rodgers, 1987). A similar spectrum of Eocene monazite dates was also obtained from the Trout Creek area ~8 km to the north (Monroe et al., 2023). The intermediate dates between the Late Cretaceous and Eocene peaks may reflect minor episodes of monazite (re)crystallization or they could be mixed

analyses between these two domains. Older (~90-105 Ma) dates may represent minor episodes of early monazite (re)crystallization, the significance of which is unclear.

In summary, we interpret with Wood Canyon aureole to represent a protracted period of amphibolite facies metamorphism that occurred over a 10-15 Myr period from ~90 Ma to ~80 Ma. A younger, shorter lived and more localized episode of amphibolite facies metamorphism occurred on the southern tip of the range at ~70 Ma (Singleton Creek aureole). Finally, we see evidence for Eocene monazite (re)crystallization that likely reflects heating and/or fluid flow from Eocene magmas.

Crystallization history of the Tungstonia Granite

U-Pb zircon geochronology was performed on eight samples of TG to assess the age of final crystallization of the pluton and determine whether it was emplaced and rapidly crystallized at all once or if it represents an amalgamation of multiple distinct intrusions separated by significant time intervals. Samples chosen for analysis were collected from different geographic positions within the pluton, including its western, southern, and northern margins as well as its interior. The zircons from each sample show clear igneous textures with concentric zoning patterns and no evidence for metamorphic overgrowths, and laser spots were typically placed near the rims to reflect the latest stage of zircon crystallization.

U-Pb analysis of the eight samples yielded a wide spectrum of zircon dates ranging from 66 Ma to 2.7 Ga, after filtering out discordant (<0.9 concordance value) dates and zircons with a high uranium content (>10,000 ppm) with the potential for lead loss (Figs 24 and 25). Each sample has a fairly continuous spread of dates from ~70 Ma to 80-90 Ma with no clear age breaks, followed by a variety of older Cretaceous and Jurassic ages, as well as

some Proterozoic ages and one Archean age. Older (Proterzoic/Archean) ages and most of the Jurassic and earlier Cretaceous dates were obtained from xenocrystic cores, whereas the majority of younger dates were obtained from rims with some from the interior of grains.

To calculate our best estimate for the final crystallization age of each sample, the TuffZirc algorithm was used in Isoplot which calculates the youngest population of ages that lie within 2σ of each other (Fig 25). Of the seven samples analyzed from the main body of TG, estimated final crystallization ages range from 68.5 ± 0.5 Ma to 70.1 ± 1.2 Ma.

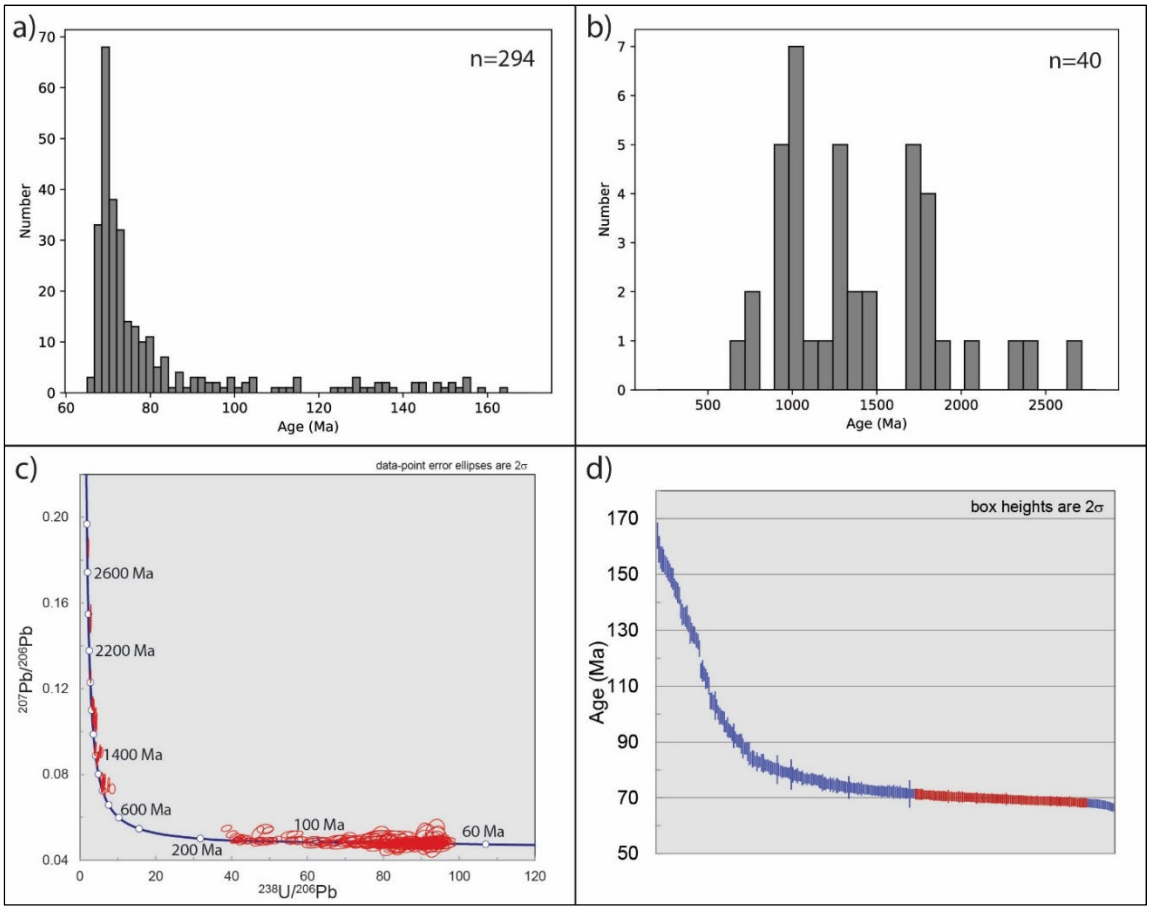

Figure 24: a) Histogram of all ages <200 Ma obtained from the eight samples analyzed from TG. b) Histogram of all ages >200 Ma. c) Terra-Wasserburg concordia plot of all ages from TG. d) Plot showing the spectrum of all ages <200 Ma obtained. Red bars indicate the youngest population that lies within 2σ of each other.

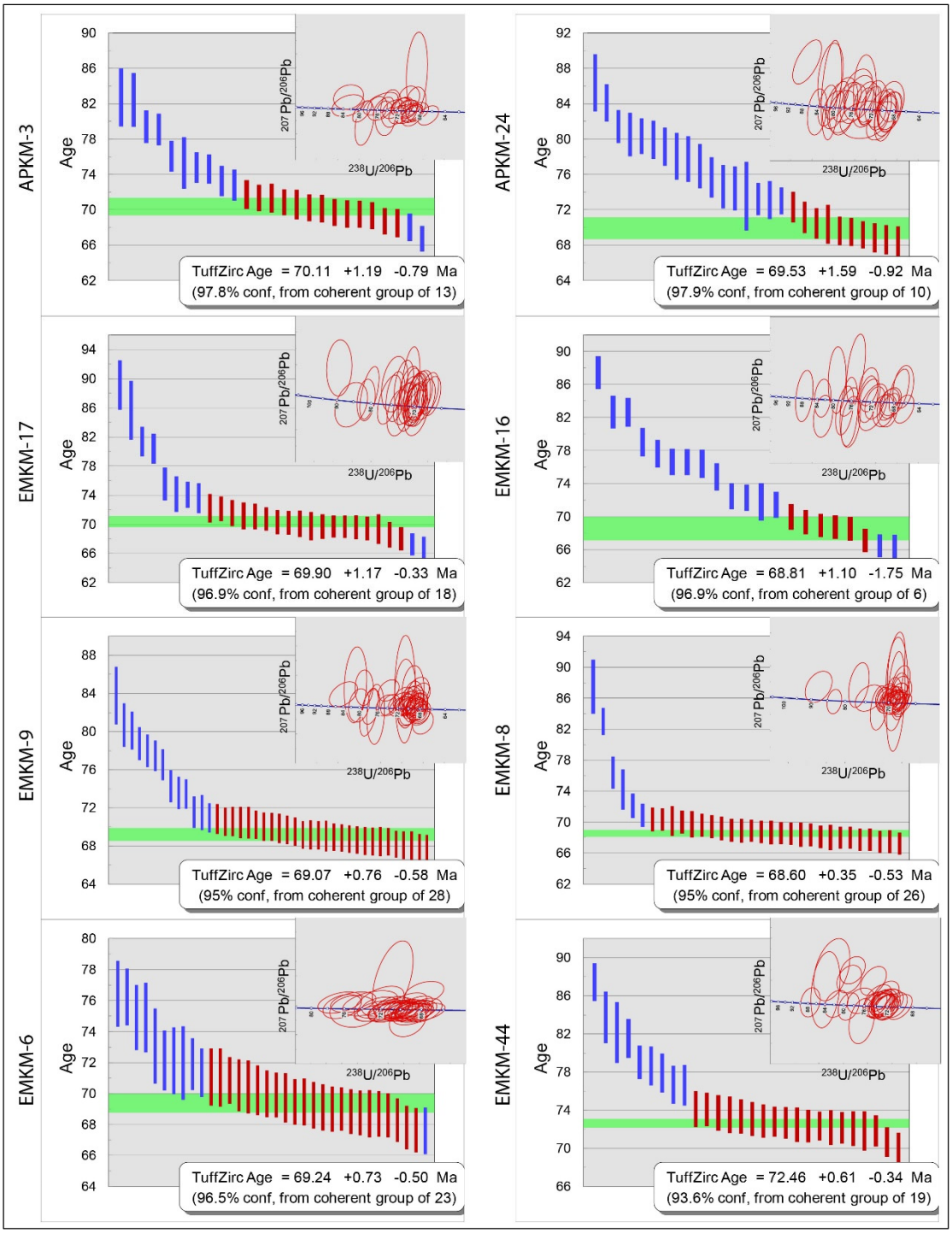

Figure 25: Diagrams showing the ages with errors of individual zircon analyses from each sample of TG. Red bars represent ages that fit within a single population and were used in the final age calculation. Blue bars represent ages that didn't fit into a single population and weren't used in the final age calculation. Tera-Wasserburg concordia diagrams shown on the top right indicate that all U-Pb ratios are concordant or are close to concordia.

Although many of these ages are within error of each other, there is an apparent eastward

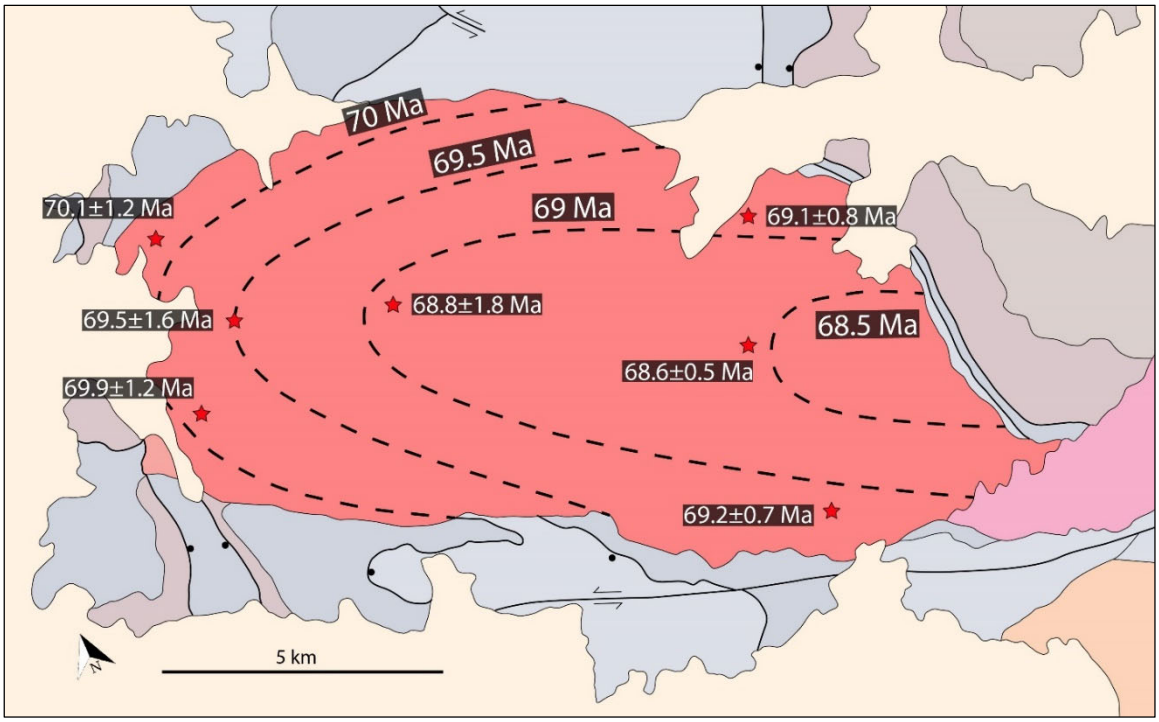

Figure 26: Map of the KM showing the locations and ages of the U-Pb geochronology samples from TG. Interpretive age contours with a 0.5 Ma interval are shown to highlight the inward and eastward younging trend suggested by the ages. Base map modified from Gans et al., (1990).

and inward younging trend within the pluton (Fig 26). Because of westward tilting of the range, this suggests that the uppermost parts of the pluton and margins crystallized before the deeper and interior portions. However, because these ages have significant errors, the precise chronology of emplacement cannot be resolved. In addition to the seven samples analyzed from the main body of TG, a sample from an isolated outcrop of granite that looks both compositionally and texturally identical to the main phase of TG but is located ~10 km to the ESE of the main body (EMKM-24) yielded an age of 72.5 ± 0.6 Ma, ~2 million years older than the ages obtained from the main body.

Given the concentric apparent younging inwards, we believe that TG as it is exposed today reflects the final crystallized product of a prolonged history of melt generation by anatexis and coalescence, crystallization, and ascent of this magma, with final emplacement

at 70 to 69 Ma, perhaps as a crystal mush with a largely crystallized outer rind and still molten interior. This is further supported by the continuous spread in ages from >80 -70 Ma with no clear gaps or inflections, which is interpreted to reflect an even more protracted zircon growth/crystallization history of at least 10-15 million-years, perhaps starting as early as 90 Ma. This crystallization and emplacement history of TG nicely complements the metamorphic history of the southern flank of the DCR, with protracted metamorphism from 90-80 Ma, followed by a ~72 Ma thermal event, perhaps associated with the ascent of TG, and will be explained more in the final discussion.

Discussion

Previous work treated the Deep Creek Range and Kern Mountains as distinct domains, exposing unique and somewhat unrelated geology, with the DCR representing a large tilt block that exposes a large-scale west-vergent tectonic fold associated with Sevier shortening, as well as some peculiar localized metamorphic culminations, and the KM exposing one of the largest Cordilleran S-type granites with a well-developed deformational aureole. Here, we suggest that these two ranges are not only tied together physically, but that the many disparate magmatic and deformational features observed in the KMDCR are genetically related to each other. Specifically, we believe that these ranges document how metamorphism and anatectic melting at deeper levels in the Sevier hinterland locally produced large magma bodies—diapiric mushes—that rose incrementally to shallow crustal levels, and in so doing produced an array of map-scale structures and dynamothermal metamorphic tectonic fabrics that might otherwise be interpreted as a consequence of regional deformation. Salient features of our hypothesis are:

1) The WCA and other folds in the western KM were produced by the downward (or locally upward) deflection of country rocks adjacent to a rising and ballooning pluton.
2) High strain fabrics and prograde dynamothermal metamorphism in the KM and southern DCR are also directly a consequence of thermal weakening and channel flow adjacent to a rising pluton/crystal mush.
3) The melts that produced TG and their subsequent rise and crystallization occurred over a protracted period of time (~10-15 Ma), with final emplacement of the granite at shallow levels as a mostly solidified crystal mush at ~70 Ma.
4) The fairly restricted area now occupied by the Kern Mountains and Deep Creek Range appears to have served as a long-lived ~E-W trending conduit for rising hydrothermal fluids and anatectic melts, derived from deeper crustal levels (>15 km) during Late Cretaceous regional shortening associated with the Sevier Orogeny. A cross-sectional view of this "channel" is now exposed in the KMDCR by Miocene westward tilting and block rotation.
5) Structural geologists and field geologists commonly interpret the presence of map-scale and mesoscopic folding, development of penetrative tectonite fabrics and Barrovian style dynamothermal metamorphism as prima facie evidence for, and a direct response to regional tectonic shortening events. We do not question that much of the magmatism, deformation and metamorphism observed in the KMDCR is indirectly related to Sevier age horizontal crustal shortening, but argue that most of the thermal and deformational features exposed in these ranges are primarily a

response to the vertical (diapiric) ascent and spatial accommodation of anatectic melts from a much deeper Sevier hinterland mid-crustal mush zone.

A reinterpretation of the Water Canyon Anticline

A number of peculiar characteristics of the WCA are not consistent with the interpretation by Rodgers (1987) that it formed as a result of tectonic shortening associated with the Sevier Orogeny:

1. The fold closes to the west not the east, whereas observed shortening structures elsewhere in the Sevier hinterland are almost entirely east vergent, including the closest well-documented Sevier age folds and thrusts in the Northern Snake Range, northern DCR, and Confusion Ranges (Bick, 1966; Greene, 2014; Wrobel et al., 2021).
2. It is a profoundly local structure. There is no evidence that the WCA continues northward from its exposures along the southern flank of the DCR, nor to the south of TG.
3. An axial planar cleavage and higher order parasitic folds are conspicuously absent in areas of the WCA where they would be most likely to form (e.g., in the hinge region and rheologically favorable interbedded sandstone and shale intervals). The absence of these associated features would be most peculiar in mid-crustal metasedimentary rocks of this ilk that were undergoing typical layer parallel shortening. Moreover, the orientation of the steeply dipping S_2 cleavage on the southern limb of the WCA appears to be more more consistent with right-lateral shear than as an axial planar cleavage.

4. Units in the southernmost overturned limb are highly strained and ductily thinned to ~10% of their original stratigraphic thickness in the northeastern KM, whereas most of the upright limb to the north in the DCR is unstrained and at full thickness. These relations suggest that the WCA primarily reflect a deflection of the southern limb in response to a passive shear folding mechanism, rather than layer parallel shortening and passive amplification. One possibility is that this reflects a superimposed ductile shear zone in the overturned limb, perhaps as a part of a west-directed ductile fault propagation fold. However, the lack of continuity of either the fold or hypothesized thrust along strike make this scenario unlikely, whereas the close spatial and temporal association of this highly attenuated limb with the intrusive margin of TG suggests a different cause.

An alternate hypothesis is that the WCA formed primarily in response to ascent of TG and that folding and strain within its thermal and deformational aureole acted as a material transfer process that made space for the rising magma. When magmas are emplaced into the crust, the volume that is occupied by the resultant intrusion must somehow be accommodated by displacement of the wall rocks (e.g., Hutton, 1996; Patterson & Fowler, 1993). Some hypothesized mechanisms for creating this extra space include fracturing and diking, stoping, ductile flow and tectonic accommodation along dilational faults or ductile shear zones (Clemens & Mawer 1992; Glazner, 2004; Miller & Paterson, 1999). Downward folding of stratified country rock adjacent to intrusive margins has been observed for numerous plutonic complexes, including in the Ruth pluton of Alaska, the Yerington Batholith of west-central Nevada and the Pachalka pluton of southeastern California

(Paterson and Farris, 2008). They are characterized by a downward deflection or folding of the country rock into parallelism with the steeply dipping pluton margins and ductile attenuation of the limbs adjacent to the pluton. The precise cause(s) and mechanisms that are responsible for these abrupt downward deflection of country rocks adjacent to plutonic margins are not always clear. One "scenario" envisions the emplacement of large thin sill-like intrusions at shallow crustal levels followed by the progressive downward growth of a tabular intrusion by additional melt rising incrementally that effectively displaces the country rocks downward and to the side. Another simply invokes downward (reverse) flow of country rocks along the rheologically weakened thermal aureole of an intrusion to occupy the space left behind by the rising melt—akin to the flow-lines predicted adjacent to a rising buoyant diapir in a higher density viscous fluid (e.g., Cruden, 1990; Marsh, 1982). These mechanisms are not mutually exclusive and any deflections in the wall rock stratigraphy may be further accentuated by a component of flattening in the deformation aureole due to ballooning of the pluton.

We here suggest that the abrupt eastward deflection and attenuation of the Mississippian and older stratigraphy along the southern flank of the DCR and northern flank of the KM—i.e., the map-scale folding that created the WCA—is an outstanding large-scale example of the sort of downward bending and flow of country rocks adjacent to a rising pluton. As illustrated in Figure 27 and discussed further below, we believe that all of the mechanisms discussed above (downward growth of the intrusion, channel-flow, ballooning) played a role in the resultant map-scale architecture, which is superbly displayed as a consequence of later Cenozoic tilting of the ranges.

The folds adjacent to TG in the westernmost KM are interpreted to reflect similar processes, where both folding (deflection) of the country rock and ductile attenuation and shear along the pluton margins facilitated mass transfer of the country rock to make space for the ascending (and possibly expanding) pluton. The close spatial association of these folds with the pluton margins and its deformational aureole, and the observation that one of the limbs is always folded or deflected into parallelism with the pluton margin, despite considerable variation in the orientation of this contact, leaves little double that these structures formed as a direct result of pluton emplacement. These folds have a variety of orientations due to the pre-existing orientation of bedding prior to emplacement and likely reflect a combination of downward flow and ballooning of the pluton.

Although the WCA is much larger than the folds in the western KM, it shares many of the same characteristics and it is difficult to imagine it has a different origin. We envision the ascent and growth of TG and the development of the WCA as follows: Up to ~20 Myr prior to final emplacement of TG (~90 Ma), prograde metamorphism and anatexis at deep crustal levels was forming a network of small bodies of magma, with fluids associated with these processes likely rising higher in the crust (Fig 27a). Both the monazite data from the southern DCR and the spectrum of zircon ages from TG suggest that melt generation/crystallization was occurring for a prolonged (10-15 Myr) period. By ~80 Ma, these magma bodies began coalescing and rising into the middle crust in a “channel”, resulting in elevated isotherms, thermal softening of the country rock, and perhaps minor downward flow of the country rock. By ~70 Ma, these magmas rose to the upper crust and began feeding a sill-like body along the boundary between the Mississippian Chainman Shale and the Pennsylvanian Ely Limestone (Fig 27c). This geometry is consistent with the

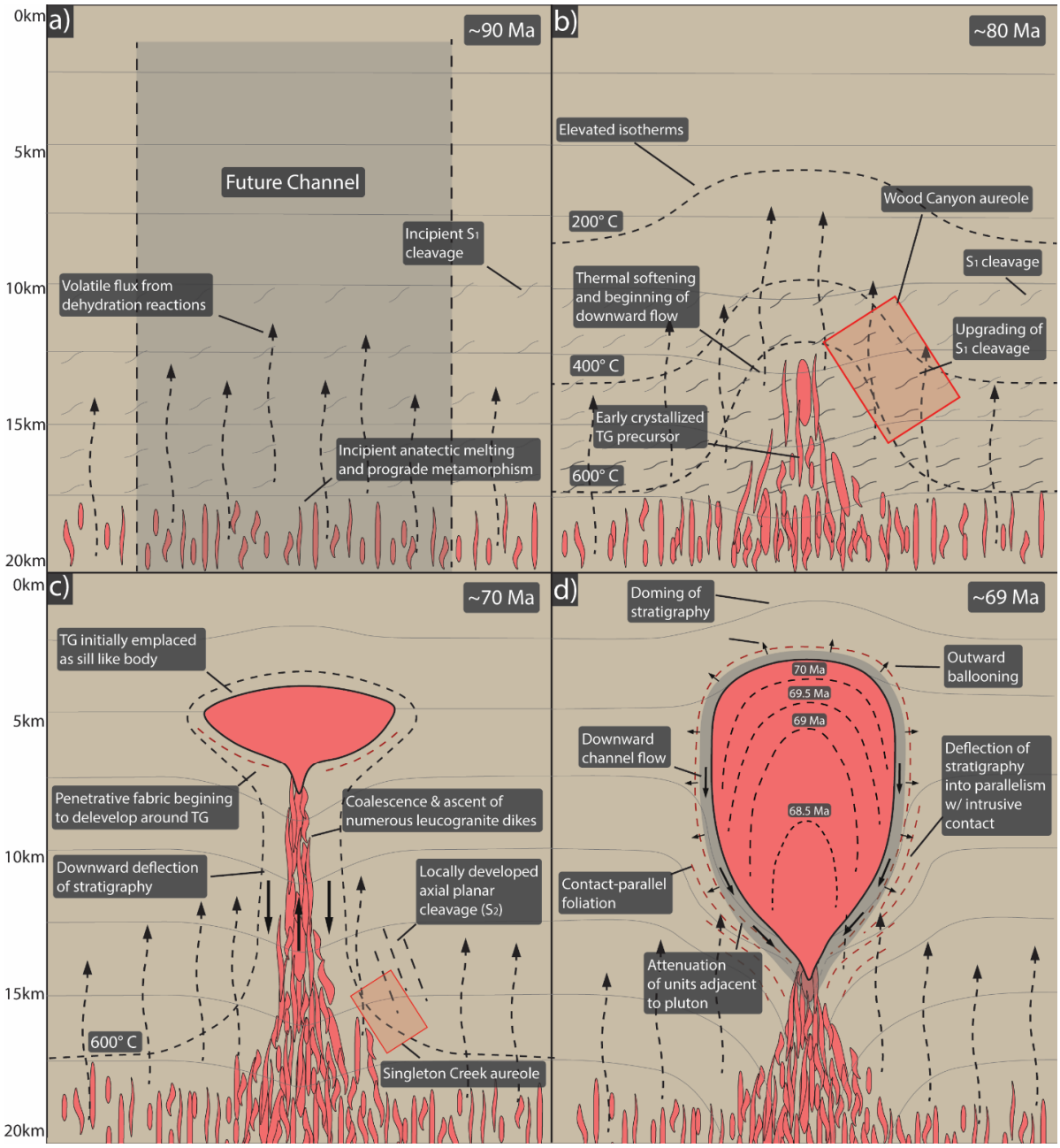

Figure 27: Schematic model of the emplacement of TG. a) 90 Ma - Initial prograde metamorphism and anatexis and melt crystallization at deep crustal levels. b) 80 Ma - Coalescence and ascent of leucogranite bodies to mid-crustal levels. c) 70 Ma - Ascent of magmas to upper-crustal levels and development of a sill-like body. Downward deflection of stratigraphy accommodates the growing pluton. d) 69 Ma - Final stage of emplacement. Progressive downward growth of the pluton transposes stratigraphy into parallelism with the intrusive contact, forming anticlines. Downward channel flow (grey zone) and ballooning result in a high strain fabric and attenuation of units adjacent to the pluton.

observed map relationships in the northern KM and southern DCR, where Mississippian and

older units are deflected to the east (downward) and Pennsylvanian and younger units are deflected to the west (upward). As more magma was injected and the magma body grew downward, the stratigraphy below would have been deflected progressively downward to accommodate the additional volume of the growing magma chamber. Heat from the magma would have reduced the strength of the country rock significantly and localized strain, resulting in a zone of downward channel flow in a narrow zone in the country rock adjacent to the pluton margins. This zone of high strain is reflected in the well-developed contact-parallel foliation around the pluton margins and appears to widen dramatically eastward (downward). Ballooning of the pluton also likely contributed to the high strain fabric, though the importance of this remains unclear. Eventually, after multiple pulses of additional magma and progressive downward growth of the incipient pluton, this sill-like body would have developed into a more spherical/ellipsoidal body and stratigraphy along its northern (and possibly southern) margin would form an anticline (Fig 27d). The overturned limb of the WCA and the northeastern margin of TG restores to being approximately vertical and NW-SE striking after removing ~40° of westward tilting about a horizontal north trending axis. This geometry is consistent with downward folding into parallelism with the approximately vertical side of TG. It is unclear whether a mirror image of this type of large-scale folding occurred on the southern margin of the pluton because younger extensional faulting and eastward directed transport of upper-crustal blocks along normal faults conceals virtually all the southern wall rocks to TG.

The geochronology from the southern DCR and TG provides further support for the general framework outlined above. Correlation of the S_2 cleavage with the Singleton Creek aureole suggests that the WCA formed during this ~70 ± 2 Ma metamorphic event which is

within error of the final crystallization age of TG, suggesting pluton emplacement and folding were coeval. Moreover, the geographic distribution of final crystallization ages within TG suggests the margins of the pluton crystallized first and the interior and deeper portions of the pluton were likely emplaced later as the pluton progressively grew downward while deforming the earlier crystallized outer margins and forcing stratigraphy in the overturned limb of the WCA deeper in the crust.

Ages and significance of metamorphism and plutonism

In the western KM, rocks grade from unmetamorphosed upper-crustal carbonates to highly strained and metamorphosed marble, with evidence for high-temperature recrystallization of dolomite and growth of metamorphic tremolite and micas adjacent to the pluton margins. The spatial coincidence of this zone of metamorphism and penetrative strain with the margins of TG and the abrupt decrease in grade away from the intrusive contact to unmetamorphosed upper-crustal rocks clearly indicates that metamorphism was a direct result of heat from the magma/crystal mush. At these upper-crustal levels, the zone of metamorphism is very narrow (<500m); however, at deeper structural levels in the eastern Kern Mountains, metamorphism is much more widespread and is continuous throughout most of the overturned limb of the WCA northward into Pleasant Valley.

Metamorphism in the southern DCR is characterized by widespread low-grade metamorphism that is distinctly upgraded in two amphibolite facies metamorphic aureoles. The low-grade "background" metamorphism increases systematically down-section from lower-greenschist facies in the McCoy Creek Group and higher units of the Trout Creek Group to upper-greenschist facies in lower units of the Trout Creek Group. This low-grade metamorphism is interpreted to reflect the regional geothermal gradient and is likely

representative of the background thermal conditions throughout much of the hinterland at these stratigraphic levels. The McCoy Creek Group where exposed in many of the surrounding ranges shows similar widespread lower- to mid-greenschist facies metamorphism that increases systematically down-section (Miller et al., 1988; Miller & Gans, 1989).

A protracted period of amphibolite facies metamorphism from ~80-90 Ma affected rocks on the southern DCR prior to the formation of the WCA when the section is inferred to have been approximately flat-lying (Wood Canyon aureole). Porphyroblast-cleavage relationships and upgrading of the S_1 cleavage within the aureole suggests that metamorphism occurred while this cleavage was actively developing. Metamorphism was characterized by an abrupt increase in temperature both down-section and to the south, with isograds cutting across formational contacts, indicating a localized heat source(s)—most likely small bodies of magma and/or fluids circulating in the vicinity of magma bodies that were being emplaced to the south periodically over a ~10-15 Myr period. This is also reflected in the spectrum of zircon ages obtained from the TG that range continuously from ~70 Ma to ~80-90 Ma, which indicates a protracted period of crustal anatexis and crystallization. We hypothesize that this prolonged period of prograde metamorphism and crustal anatexis/crystallization in the KMDCR reflects a "channel" where heat was being advected upward in the crust by the ascent of numerous small bodies of leucogranites and hydrothermal fluids associated with them. This advection of heat resulted in localized metamorphism and high lateral temperature gradients that are not reflective of the broader conditions of the Late-Cretaceous mid-crust in the Sevier hinterland.

The culmination of this prolonged period of prograde metamorphism and anatexis in this "channel" was the final ascent and emplacement of the largest S-type granite exposed in eastern Nevada—TG. This final ascent appears to be reflected in the southern DCR by a more localized and shorter-lived period of amphibolite facies metamorphism occurred on the southeastern tip of the DCR at ~70 ± 2 Ma (Singleton Creek aureole). Porphyroblast-cleavage relationships and upgrading of the S_2 cleavage suggests metamorphism was synkinematic with cleavage development and high strain shearing and attenuation, and therefore also likely occurred during folding of the WCA. We propose that this metamorphism reflects heat from TG magma during its final ascent and crystallization. This hypothesis is supported by the nearly identical ages of the final crystallization of TG and the Singleton Creek aureole. Our interpretation that metamorphism in the southern DCR is primarily a result of Late Cretaceous magmatism suggests that perhaps many of the dynamothermally metamorphosed rocks that are locally exposed at deep structural levels in the Sevier hinterland may be more a reflection of localized magmatic process than regional tectonics.

Summary: A reassessment of the interplay between metamorphism, magmatism and deformation in the Sevier hinterland

The emplacement of TG had a profound impact on deformation in the surrounding country rock and resulted in a high strain deformational aureole around its margins, including folding of the stratigraphy in the western KM and the formation of the WCA. There are other Late Cretaceous plutons in the Sevier hinterland that show a similar intensification of penetrative strain and peculiar folding relationships around their margins,

including the 80 ± 2 Ma Trout Creek Intrusive Complex in the DCR (Monroe et al., 2023) and the 94 ± 2 Ma Lexington Creek pluton in the Southern Snake Range (Gottlieb et al., 2022; Lee and Christiansen, 1983). However, the deformational aureole around TG at deeper structural levels in the northeastern KM appears to be much more extensive than the others and the WCA is far larger than most other documented pluton related deformational structures in the Sevier hinterland. Interestingly, most Jurassic and Eocene plutons in eastern Nevada only have narrow static metamorphic aureoles, even those that are similar in size to TG and were emplaced at similar or deeper crustal levels (e.g., the Ibapah pluton). These contrasts raise some interesting questions: *What was different during the Late Cretaceous that allowed plutons to more easily deform and metamorphose their country rock? Why did TG specifically have such a profound deformational impact on its country rock?*

The Late Cretaceous plutons of eastern Nevada are all 2-mica leucogranites with an isotopic composition that suggests they are nearly pure crustal melts (e.g. Miller & Bradfish, 1980; Best et al, 1974; Wright & Wooden, 1991). These melts are interpreted to have been largely derived from the prograde metamorphism and melting of sedimentary rocks which would result in magmas with a high volatile content. More speculatively, these magmas were likely rising in concert with fluids released from dehydration reactions in the zone of prograde metamorphism. The presence of abundant fluids associated with the rise of these magmas would have drastically reduced rock strength and would allow a pluton to more easily deform the country rock during emplacement.

In the case of TG, it also appears that prolonged metamorphism and crustal anatexis prior to emplacement also played a key role. If our hypothesis is correct that the area now occupied by TG and the overturned limb of the WCA was a long-lived “channel”, where

smaller volumes of leucogranites and hydrothermal fluids generated by prograde metamorphism and anatexis in the lower crust were rising and advecting heat to mid- and upper-crustal levels, this would have weakened this portion of the crust substantially. By the time TG magmas began moving upward in the crust, the surrounding country rock was likely very weak, allowing TG to more easily deform it. We propose that this combination of thermal and fluid-related weakening by the prolonged emplacement of numerous small bodies of leucogranites and associated fluids through this "channel" is what allowed TG to have such a profound deformational impact on its country rock.

The KMDCR provides a sobering example of how the localized ascent of Late Cretaceous anatectic melts and associated fluids were able to produce map-scale structures and extensive metamorphic tectonite fabrics in the Sevier hinterland—deformational features that appear to be primarily accommodating pluton emplacement rather than tectonic shortening. Without the spectacular exposure of these rocks in the KMDCR, it would be easy to interpret much of the penetrative strain, map-scale structures, and metamorphism as reflecting tectonic deformation/burial. This emphasizes the need for caution when interpreting deformational structures and metamorphic assemblages in mid-crustal rocks in the Sevier hinterland as being reflective of broader deformational/metamorphic conditions.

References

Ahlborn, R. C. (1977). *Mesozoic-Cenozoic structural development of the Kern Mountains, eastern Nevada, western Utah.* [Master's thesis, Brigham Young University]

Allmendinger, R. W., Miller, D. M., & Jordan, T. E. (1984). Known and inferred Mesozoic deformation in the hinterland of the Sevier belt, northwest Utah.

Allmendinger, R.W. (2023). Stereonet 11. [Computer Software] Retrieved from www.rickallmendinger.net

Armstrong, R. L. (1968). Sevier orogenic belt in Nevada and Utah. *Geological Society of America Bulletin*, *79*(4), 429-458. https://doi.org/10.1130/0016-7606(1968)79[429:SOBINA]2.0.CO;2

Armstrong, F. C., & Oriel, S. S. (1965). Tectonic development of Idaho-Wyoming thrust belt. *AAPG Bulletin*, *49*(11), 1847-1866. https://doi.org/10.1306/A663386E-16C0-11D7-8645000102C1865D

Bartley, J. M., Gleason, G. C., & Wernicke, B. P. (1990). Tertiary normal faults superimposed on Mesozoic thrusts, Quinn Canyon and grant ranges, Nye County, Nevada. *Basin and Range extensional tectonics near the latitude of Las Vegas, Nevada: Geological Society of America Memoir*, *176*, 195-212.

Barton, M. D., & Anderson, J. L. (1990). Cretaceous magmatism, metamorphism, and metallogeny in the east-central Great Basin. *The nature and origin of Cordilleran magmatism: Geological Society of America Memoir*, *174*, 283-302.

Bendick, R., & Baldwin, J. (2009). Dynamic models for metamorphic core complex formation and scaling: The role of unchannelized collapse of thickened continental crust. *Tectonophysics*, *477*(1-2), 93-101. https://doi.org/10.1016/j.tecto.2009.03.017

Benz, H. M., Smith, R. B., & Mooney, W. D. (1990). Crustal structure of the northwestern Basin and Range Province from the 1986 Program for Array Seismic Studies of the Continental Lithosphere seismic experiment. *Journal of Geophysical Research: Solid Earth*, *95*(B13), 21823-21842. https://doi.org/10.1029/JB095iB13p21823

Berkley Geochronology Center (2012). *Isoplot* (Version 3.7) [Computer software]. https://www.bgc.org/isoplot

Bick, K.F., (1966). Geology of the Deep Creek Mountains, Tooele and Juab Counties Utah: Utah Geological and Mineralogical Survey Bulletin 77, 120p.

Blackford, N. R., Long, S. P., Stout, A., Rodgers, D. W., Cooper, C. M., Kramer, K., ... & Soignard, E. (2022). Late Cretaceous upper-crustal thermal structure of the Sevier

hinterland: Implications for the geodynamics of the Nevadaplano. *Geosphere*, *18*(1), 183-210. https://doi.org/10.1130/GES02386.1

Burchfiel, B. C., & Davis, G. A. (1975). Nature and controls of Cordilleran orogenesis, western United States: Extensions of an earlier synthesis. *American Journal of Science*, *275*(A), 363-396.

Burtner, R. L., Nigrini, A., & Donelick, R. A. (1994). Thermochronology of Lower Cretaceous source rocks in the Idaho-Wyoming thrust belt. *AAPG bulletin*, *78*(10), 1613-1636. https://doi.org/10.1306/A25FF233-171B-11D7-8645000102C1865D

Camilleri, P. A. (1998). Prograde metamorphism, strain evolution, and collapse of footwalls of thick thrust sheets: a case study from the Mesozoic Sevier hinterland USA. *Journal of Structural Geology*, *20*(8), 1023-1042. https://doi.org/10.1016/S0191-8141(98)00032-7

Camilleri, P. A., & Chamberlain, K. R. (1997). Mesozoic tectonics and metamorphism in the Pequop Mountains and Wood Hills region, northeast Nevada: Implications for the architecture and evolution of the Sevier orogen. *Geological Society of America Bulletin*, *109*(1), 74-94. https://doi.org/10.1130/0016-7606(1997)109<0074:MTAMIT>2.3.CO;2

Clark, D. H. (1985). *Tectonic evolution of the Red Hills-southwestern Kern Mountains area, east-central Nevada* (Doctoral dissertation, Stanford University).

Clemens, J. D., & Mawer, C. K. (1992). Granitic magma transport by fracture propagation. *Tectonophysics*, *204*(3-4), 339-360. https://doi.org/10.1016/0040-1951(92)90316-X

Coney, P. J., & Harms, T. A. (1984). Cordilleran metamorphic core complexes: Cenozoic extensional relics of Mesozoic compression. *Geology*, *12*(9), 550-554. https://doi.org/10.1130/0091-7613(1984)12<550:CMCCCE>2.0.CO;2

Cruden, A. R. (1990). Flow and fabric development during the diapiric rise of magma. *The Journal of Geology*, *98*(5), 681-698. https://doi.org/10.1086/629433

Cruz-Uribe, A. M., Hoisch, T. D., Wells, M. L., Vervoort, J. D., & Mazdab, F. K. (2015). Linking thermodynamic modelling, Lu–Hf geochronology and trace elements in garnet: New P–T–t paths from the Sevier hinterland. *Journal of Metamorphic Geology*, *33*(7), 763-781. https://doi.org/10.1111/jmg.12151

Davis, G. H., & Coney, P. J. (1979). Geologic development of the Cordilleran metamorphic core complexes. *Geology*, *7*(3), 120-124. https://doi.org/10.1130/0091-7613(1979)7<120:GDOTCM>2.0.CO;2

DeCelles, P. G., & Coogan, J. C. (2006). Regional structure and kinematic history of the Sevier fold-and-thrust belt, central Utah. *Geological Society of America Bulletin*, *118*(7-8), 841-864.https://doi.org/10.1130/B25759.1

DeCelles, P. G., Lawton, T. F., & Mitra, G. (1995). Thrust timing, growth of structural culminations, and synorogenic sedimentation in the type Sevier orogenic belt, western United States. *Geology*, *23*(8), 699-702. https://doi.org/10.1130/0091-7613(1995)023<0699:TTGOSC>2.3.CO;2

De Saint-Blanquat, Michel, et al. "Internal structure and emplacement of the Papoose Flat pluton: An integrated structural, petrographic, and magnetic susceptibility study." *Geological Society of America Bulletin* 113.8 (2001): 976-995. https://doi.org/10.1130/0016-7606(2001)113<0976:ISAEOT>2.0.CO;2

Douce, P., Humphreys, E. D., & Johnston, A. D. (1990). Anatexis and metamorphism in tectonically thickened continental crust exemplified by the Sevier hinterland, western North America. *Earth and Planetary Science Letters*, *97*(3), 290-315. https://doi.org/10.1016/0012-821X(90)90048-3

Farmer, G. L., & DePaolo, D. J. (1983). Origin of Mesozoic and Tertiary granite in the western United States and implications for Pre-Mesozoic crustal structure: 1. Nd and Sr isotopic studies in the geocline of the Northern Great Basin. *Journal of Geophysical Research: Solid Earth*, *88*(B4), 3379-3401. https://doi.org/10.1029/JB088iB04p03379

Fouch, T. D., Lawton, T. F., Nichols, D. J., Cashion, W. B., & Cobban, W. A. (1983). Patterns and timing of synorogenic sedimentation in Upper Cretaceous rocks of central and northeast Utah. Rocky Mountain Section (SEPM).

Gans, P. B., Miller, E. L., Clark, D. H., and Rodgers, D. W., (1990) Geologic relations in the Kern Mountains–Deep Creek Range, Nevada-Utah and the origin of metamorphic core complex detachment faults: Geological Society of America Abstracts with Programs, v. 22, no. 3, p. 24

Glazner, A. F., Bartley, J. M., Coleman, D. S., Gray, W., & Taylor, R. Z. (2004). Are plutons assembled over millions of years by amalgamation from small magma chambers?. *GSA today*, *14*(5-Apr), 4-11. https://doi.org/10.17615/nspy-zk53

Gottlieb, E. S., Miller, E. L., Valley, J. W., Fisher, C. M., Vervoort, J. D., & Kitajima, K. (2022). Zircon petrochronology of Cretaceous Cordilleran interior granites of the Snake Range and Kern Mountains, Nevada, USA. https://doi.org/10.1130/2022.2555(02)

Greene, D. C. (2014). The Confusion Range, west-central Utah: Fold-thrust deformation and a western Utah thrust belt in the Sevier hinterland. *Geosphere*, *10*(1), 148-169. https://doi.org/10.1130/GES00972.1

Hallett, B. W., & Spear, F. S. (2015). Monazite, zircon, and garnet growth in migmatitic pelites as a record of metamorphism and partial melting in the East Humboldt Range, Nevada. *American Mineralogist*, *100*(4), 951-972. https://doi.org/10.2138/am-2015-4839

Harris, C. R., Hoisch, T. D., & Wells, M. L. (2007). Construction of a composite pressure–temperature path: revealing the synorogenic burial and exhumation history of the Sevier hinterland, USA. *Journal of Metamorphic Geology*, *25*(8), 915-934. https://doi.org/10.1111/j.1525-1314.2007.00733.x

Hodges, K. V., Snoke, A. W., & Hurlow, H. A. (1992). Thermal evolution of a portion of the Sevier hinterland: The northern Ruby Mountains-East Humboldt range and Wood Hills, northeastern Nevada. *Tectonics*, *11*(1), 154-164. https://doi.org/10.1029/91TC01879

Horstwood, M. S., Foster, G. L., Parrish, R. R., Noble, S. R., & Nowell, G. M. (2003). Common-Pb corrected in situ U–Pb accessory mineral geochronology by LA-MC-ICP-MS. *Journal of Analytical Atomic Spectrometry*, *18*(8), 837-846.

Horstwood, M. S., Košler, J., Gehrels, G., Jackson, S. E., McLean, N. M., Paton, C., ... & Schoene, B. (2016). Community-derived standards for LA-ICP-MS U-(Th-) Pb geochronology–Uncertainty propagation, age interpretation and data reporting. *Geostandards and Geoanalytical Research*, *40*(3), 311-332. https://doi.org/10.1111/j.1751-908X.2016.00379.x

Hose, R. K., & Blake Jr, M. C. (1976). *Geology and mineral resources of White Pine County, Nevada* (No. 85). University of Nevada.

Hudec, M. R. (1992). Mesozoic structural and metamorphic history of the central Ruby Mountains metamorphic core complex, Nevada. *Geological Society of America Bulletin*, *104*(9), 1086-1100. https://doi.org/10.1130/0016-7606(1992)104<1086:MSAMHO>2.3.CO;2

Hutton, D. H. (1996). The 'space problem' in the emplacement of granite. *Episodes Journal of International Geoscience*, *19*(4), 114-119. https://doi.org/10.18814/epiiugs/1996/v19i4/004

Kelly, E. D., Hoisch, T. D., Wells, M. L., Vervoort, J. D., & Beyene, M. A. (2015). An Early Cretaceous garnet pressure–temperature path recording synconvergent burial and exhumation from the hinterland of the Sevier orogenic belt, Albion Mountains, Idaho. *Contributions to Mineralogy and Petrology*, *170*, 1-22. https://doi.org/10.1007/s00410-015-1171-2

Kylander-Clark, A. R., Hacker, B. R., & Cottle, J. M. (2013). Laser-ablation split-stream ICP petrochronology. *Chemical Geology*, *345*, 99-112. https://doi.org/10.1016/j.chemgeo.2013.02.019

Law, R. D., Morgan, S. S., Casey, M., Sylvester, A. G., & Nyman, M. (1992). The Papoose Flat Pluton of eastern California: a reassessment of its emplacement history in the light of new microstructural and crystallographic fabric observations. *Earth and Environmental*

Science Transactions of the Royal Society of Edinburgh, *83*(1-2), 361-375. https://doi.org/10.1017/S0263593300008026

Lee, S. Y., Barnes, C. G., Snoke, A. W., Howard, K. A., & Frost, C. D. (2003). Petrogenesis of Mesozoic, peraluminous granites in the Lamoille Canyon area, Ruby Mountains, Nevada, USA. *Journal of Petrology*, *44*(4), 713-732. https://doi.org/10.1093/petrology/44.4.713

Lee, D. E., & Christiansen, E. H. (1983). The granite problem as exposed in the southern Snake Range, Nevada. *Contributions to Mineralogy and Petrology*, *83*(1-2), 99-116.

Lee, D. E., Kistler, R. W., Friedman, I., & Van Loenen, R. E. (1981). Two-mica granites of northeastern Nevada. *Journal of Geophysical Research: Solid Earth*, *86*(B11), 10607-10616. https://doi.org/10.1029/JB086iB11p10607

Lee, D. E., Stacey, J. S., Fischer, L., Peterman, Z. E., & Schnabel, D. C. (1986). Muscovite phenocrystic two mica granites of northeastern Nevada are Late Cretaceous in age. *Shorter contributions to isotope research: US Geological Survey Bulletin*, *1622*, 31-39.

Leiss, B., & Barber, D. J. (1999). Mechanisms of dynamic recrystallization in naturally deformed dolomite inferred from EBSP analyses. *Tectonophysics*, *303*(1-4), 51-69. https://doi.org/10.1016/S0040-1951(98)00258-3

Long, S. P. (2012). Magnitudes and spatial patterns of erosional exhumation in the Sevier hinterland, eastern Nevada and western Utah, USA: Insights from a Paleogene paleogeologic map. *Geosphere*, *8*(4), 881-901. https://doi.org/10.1130/GES00783.1

Long, S. P., Henry, C. D., Muntean, J. L., Edmondo, G. P., & Cassel, E. J. (2014). Early Cretaceous construction of a structural culmination, Eureka, Nevada, USA: Implications for out-of-sequence deformation in the Sevier hinterland. *Geosphere*, *10*(3), 564-584. https://doi.org/10.1130/GES00997.1

McGrew, A. J., Peters, M. T., & Wright, J. E. (2000). Thermobarometric constraints on the tectonothermal evolution of the East Humboldt Range metamorphic core complex, Nevada. *Geological Society of America Bulletin*, *112*(1), 45-60. https://doi.org/10.1130/0016-7606(2000)112<45:TCOTTE>2.0.CO;2

Marsh, B. D. (1982). On the mechanics of igneous diapirism, stoping, and zone melting. *American Journal of Science*, *282*(6), 808-855. https://doi.org/10.2475/ajs.282.6.808

Miller, C. F., & Bradfish, L. J. (1980). An inner Cordilleran belt of muscovite-bearing plutons. *Geology*, *8*(9), 412-416. https://doi.org/10.1130/0091-7613(1980)8<412:AICBOM>2.0.CO;2

Miller, E. L., Gans, P. B., & Garing, J. (1983). The Snake Range decollement: An exhumed mid-Tertiary ductile-brittle transition. *Tectonics*, *2*(3), 239-263. https://doi.org/10.1029/TC002i003p00239

Miller, E. L., & Gans, P. B. (1989). Cretaceous crustal structure and metamorphism in the hinterland of the Sevier thrust belt, western US Cordillera. *Geology*, *17*(1), 59-62. https://doi.org/10.1130/0091-7613(1989)017<0059:CCSAMI>2.3.CO;2

Miller, E. L., Gans, P. B., Wright, J. E., Sutter, J. F., & Ernst, W. G. (1988). Metamorphic history of the east-central Basin and Range province: Tectonic setting and relationship to magmatism. *Metamorphism and crustal evolution, western conterminous United States, Rubey*, *7*, 649-682.

Miller, R. B., & Paterson, S. R. (1999). In defense of magmatic diapirs. *Journal of Structural Geology*, *21*(8-9), 1161-1173. https://doi.org/10.1016/S0191-8141(99)00033-4

Misch, P., Hazzard, J. C., & Turner, F. E. (1957). Precambrian tillitic schists in the southern Deep Creek Range, western Utah, and Precambrian units of western Utah and eastern Nevada (abs.): Geol. Soc. *America Bull*, *68*, 1837.

Misch, P., & Hazzard, J. C. (1962). Stratigraphy and metamorphism of Late Precambrian rocks in central northeastern Nevada and adjacent Utah. *AAPG Bulletin*, *46*(3), 289-343. https://doi.org/10.1306/BC743823-16BE-11D7-8645000102C1865D

Monroe, E.B. and Gans, P.B., 2023. Late Cretaceous magmatic perturbation of the thermal-mechanical architecture of the Sevier hinterland middle crust in western Utah. *Tectonics.* (in review)

Nelson, R. B. (1959). *The stratigraphy and structure of the northernmost part of the northern Snake Range and the Kern Mountains in eastern Nevada and the southern Deep Creek Range in western Utah*. University of Washington.

Nelson, R. B. (1966). Structural development of northernmost Snake Range, Kern Mountains, and Deep Creek Range, Nevada and Utah. *AAPG Bulletin*, *50*(5), 921-951. https://doi.org/10.1306/5D25B605-16C1-11D7-8645000102C1865D

Nelson, R. B. (1969). Relation and history of structures in a sedimentary succession with deeper metamorphic structures, eastern Great Basin. *AAPG Bulletin*, *53*(2), 307-339. https://doi.org/10.1306/5D25C60F-16C1-11D7-8645000102C1865D

Nutt, C. J., & Thorman, C. H. (1994). *Geologic Map of the Weaver Canyon, Nevada and Utah, Quadrangle and Parts of the Ibapah Peak, Utah, and Tippett Canyon, Nevada, Quadrangles* (No. 94-635).

Palin, R. M., Searle, M. P., Waters, D. J., Parrish, R. R., Roberts, N. M. W., Horstwood, M. S. A., ... & Anh, T. T. (2013). A geochronological and petrological study of anatectic paragneiss and associated granite dykes from the Day Nui Con Voi metamorphic core complex, North Vietnam: constraints on the timing of metamorphism within the Red River shear zone. *Journal of Metamorphic Geology*, *31*(4), 359-387. https://doi.org/10.1111/jmg.12025

Paterson, S. R., & Farris, D. W. (2008). Downward host rock transport and the formation of rim monoclines during the emplacement of Cordilleran batholiths. *Earth and Environmental Science Transactions of The Royal Society of Edinburgh*, *97*(4), 397-413. https://doi.org/10.1017/S026359330000153X

Paterson, S. R., Brudos, T., Fowler, K., Carlson, C., Bishop, K., & Vernon, R. H. (1991). Papoose Flat pluton: Forceful expansion or postemplacement deformation?. *Geology*, *19*(4), 324-327. https://doi.org/10.1130/0091-7613(1991)019<0324:PFPFEO>2.3.CO;2

Paterson, S. R., & Fowler Jr, T. K. (1993). Re-examining pluton emplacement processes. *Journal of Structural Geology*, *15*(2), 191-206. https://doi.org/10.1016/0191-8141(93)90095-R

Paton, C., Hellstrom, J., Paul, B., Woodhead, J., & Hergt, J. (2011). Iolite: Freeware for the visualisation and processing of mass spectrometric data. *Journal of Analytical Atomic Spectrometry*, *26*(12), 2508-2518.

Price, R. A., & Mountjoy, E. W. (1970). Geologic structure of the Canadian Rocky Mountains between Bow and Athabasca Rivers: A progress report. *Geological Association of Canada Special Paper*, *6*, 7-25.

Rodgers, D. W. (1984). Stratigraphy, correlation, and depositional environments of Upper Proterozoic and Lower Cambrian rocks of the southern Deep Creek Range, Utah. *Geology of Northwest Utah, Southern Idaho and Northeast Nevada,* 79-92.

Rodgers, D. W. (1987). *Thermal and structural evolution of the southern Deep Creek Range, west central Utah and east central Nevada* (Doctoral dissertation). Stanford, CA: Stanford University.

Royse Jr, F., Warner, M. T., & Reese, D. L. (1975). Thrust belt structural geometry and related stratigraphic problems Wyoming-Idaho-northern Utah.

Sayeed, U. A. (1973). Petrology and structure of the Kern Mountains plutonic complex, White Pine County, Nevada and Juab County, Utah. The University of Nebraska-Lincoln.

Sayeed, U. A., Treves, S. B., & Nelson, R. B. (1977). Geochemistry and hydrothermal alteration of the Kern Mountains plutonic complex, White Pine County, Nevada and Juab County, Utah. *Geologische Rundschau*, *66*, 614-644. https://doi.org/10.1007/BF01989595

Sláma, J., Košler, J., Condon, D. J., Crowley, J. L., Gerdes, A., Hanchar, J. M., ... & Whitehouse, M. J. (2008). Plešovice zircon—a new natural reference material for U–Pb and Hf isotopic microanalysis. *Chemical Geology*, *249*(1-2), 1-35. https://doi.org/10.1016/j.chemgeo.2007.11.005

Stewart, J. H. (1971). Basin and Range structure: A system of horsts and grabens produced by deep-seated extension. *Geological Society of America Bulletin*, *82*(4), 1019-1044. https://doi.org/10.1130/0016-7606(1971)82[1019:BARSAS]2.0.CO;2

Stewart, J. H. (1976). Late Precambrian evolution of North America: plate tectonics implication. *Geology*, *4*(1), 11-15. https://doi.org/10.1130/0091-7613(1976)4<11:LPEONA>2.0.CO;2

Sylvester, A. G., Ortel, G., Nelson, C. A., & Christie, J. M. (1978). Papoose Flat pluton: A granitic blister in the Inyo Mountains, California. *Geological Society of America Bulletin*, *89*(8), 1205-1219. https://doi.org/10.1130/0016-7606(1978)89<1205:PFPAGB>2.0.CO;2

Taylor, W. J., Bartley, J. M., Martin, M. W., Geissman, J. W., Walker, J. D., Armstrong, P. A., & Fryxell, J. E. (2000). Relations between hinterland and foreland shortening: Sevier orogeny, central North American Cordillera. *Tectonics*, *19*(6), 1124-1143. https://doi.org/10.1029/1999TC001141

Tomascak, P. B., Krogstad, E. J., & Walker, R. J. (1996). U-Pb monazite geochronology of granitic rocks from Maine: implications for late Paleozoic tectonics in the Northern Appalachians. *The Journal of Geology*, *104*(2), 185-195. https://doi.org/10.1086/629813

Wells, M. L., Dallmeyer, R. D., & Allmendinger, R. W. (1990). Late Cretaceous extension in the hinterland of the Sevier thrust belt, northwestern Utah and southern Idaho. *Geology*, *18*(10), 929-933. https://doi.org/10.1130/0091-7613(1990)018<0929:LCEITH>2.3.CO;2

Wells, M. L., & Hoisch, T. D. (2008). The role of mantle delamination in widespread Late Cretaceous extension and magmatism in the Cordilleran orogen, western United States. *Geological Society of America Bulletin*, *120*(5-6), 515-530. https://doi.org/10.1130/B26006.1

Wiedenbeck, M. A. P. C., Alle, P., Corfu, F. Y., Griffin, W. L., Meier, M., Oberli, F. V., ... & Spiegel, W. (1995). Three natural zircon standards for U-Th-Pb, Lu-Hf, trace element and REE analyses. *Geostandards newsletter*, *19*(1), 1-23. https://doi.org/10.1111/j.1751-908X.1995.tb00147.x

Wright, J. E., & Wooden, J. L. (1991). New Sr, Nd, and Pb isotopic data from plutons in the northern Great Basin: Implications for crustal structure and granite petrogenesis in the hinterland of the Sevier thrust belt. *Geology*, *19*(5), 457-460. https://doi.org/10.1130/0091-7613(1991)019<0457:NSNAPI>2.3.CO;2

Wrobel, A. J., Gans, P. B., & Womer, J. B. (2021). Late Cretaceous Crustal Shortening in the Northern Snake Range Metamorphic Core Complex: Constraints on the Structural Geometry and Magnitude of Pre-Extensional Footwall Burial. *Tectonics*, *40*(8). https://doi.org/10.1029/2020TC006460

Zuza, A., & Cao, W. (2022). Metamorphic Core Complex Dichotomy in the North American Cordillera Explained by Buoyant Upwelling in Variably Thick Crust. *GSA Today*. https://doi.org/10.1130/GSATG548A.1

III. Virtual field exercises for Structural Geology and Volcanology classes: New approaches to enhancing undergraduate geology field instruction at the upper division level

Introduction

Field experiences and field exercises are widely recognized as an indispensable part of a geologic education. Not only are courses in geologic mapping and field methods an integral part of most undergraduate curricula, but field exercises and field trips are typically an important component of upper division geology courses (structural geology, sedimentology, igneous and metamorphic petrology, volcanology, etc.). Many geoscience educators have stated that students learn best when they are required to apply what they have learned in theory to solving real world problems (e.g. Elkins & Elkins 2007), and in geology this involves careful integration of lecture/topical material, with laboratory exercises, problem sets, and most importantly practical field exercises. When the COVID-19 pandemic emerged in 2020, many geology departments had to quickly adjust to an online education model where in-person field trips were not possible.

This paper describes in detail how we tried to solve this problem by creating virtual field exercises and field trips for upper division courses in Physical Volcanology and Structural Geology – virtual exercises that we believe were successful substitutes for our regular field exercises associated with these classes. These were done under severe time pressure and were our first attempt at field education in an "online world" – attempts that improved steadily as we gained experience and from which we have learned what is effective and what is not. Going forward, we will undoubtedly have ideas about how to do this even better. More importantly we have learned that there are a few things that the

students actually learn better in this format, even as we continue to believe that there is no substitute for a real field experience. In the future, we will use these same videos and associated virtual field instruction modules in conjunction with actual field trips to strengthen the overall experience, better prepare students for the actual trips, devote less time to lecturing in the field, and as a way of making the field experiences available to those who, either for physical disabilities, medical reasons, or family situations cannot attend the actual field excursions. We also suspect these virtual field exercises might be very useful for students attending universities that are far removed from outcrop exposures of the type of geologic features that are being covered in equivalent structural geology and volcanology classes. We believe that the types of videos we present here are far more effective at communicating information and clarifying concepts than simply using a series of still photos in a PowerPoint presentation – photos taken by the professor during travels to far flung places. This paper is less about a pedological philosophy and more about providing concrete examples of virtual field instruction in two upper division courses in Structural Geology and Physical Volcanology. We did this by integrating videos filmed in the field with follow up exercises that could be carried out online to simulate as closely as possible what the students would have been doing in a pre-COVID world.

Statement of the problem: how does one give students a realistic field experience, one where they get a very good sense for what the rocks look like in nature, their textures, scales, appearance from different angles and at different distances, while also providing a "how to" tutorial on what kinds of data and observations they should be making if they were at the field site. The challenge is figuring out how to do this while adequately:

- Emphasizing the ambiguity of real rocks, in contrast to textbook illustrations and photographs that tend to show only flagrantly obvious relationships.
- Recognizing the difference between what they actually see versus what they infer - i.e. learning to describe things as they are, instead of seeing what they think they should be seeing.
- Providing guidance on the types of observations and measurements they could and should be making if they were present at the site.
- Keeping the students engaged and thinking deeply about how field observations and data can be used to solve problems. Encouraging students to develop multiple working hypotheses.

Our approach was to couple carefully crafted field videos with rigorous assignments and problem-solving exercises and thus engage the students to do more than just watch a "show and tell" type video.

Background

Fieldwork is widely considered an essential part of undergraduate education in the earth sciences and for good reason; geology is fundamentally a field science where nature has already performed innumerable experiments, and our role as observational scientists is to carefully reconstruct the parameters of the experiment, how it proceeded, and what the final results tell us about processes. Examining rocks in their natural setting is often far more effective for learning than watching a lecture or reading a textbook (Elkins & Elkins, 2007; Mogk & Goodwin, 2012; Petcovic et al., 2014). Fieldwork provides the opportunity for students to see different rock types and geologic relationships in person, make their own observations, collect their own data, and make their own interpretations. This type of direct

interaction with the natural environment has been shown to be important in facilitating cognition, critical thinking and spatial-reasoning skills (Hutchins & Renner, 2012; Kastens & Ishikawa, 2006). Field trips also play an important role in inspiring budding geologists by kindling their scientific curiosity and passion for the study of geology while at the same time exposing them to enjoyable outdoor/wilderness experiences, often in places of great natural beauty. Moreover, fieldwork skills are often valuable after graduation as many academic and industry careers in geology involve significant fieldwork and many job listings require prior fieldwork experience. Most state "professional geologist" credentials require extensive coursework in geologic mapping and field investigation.

It is clear that fieldwork is a critical component of an undergraduate education in the earth sciences; however, field learning experiences are often unavailable or severely limited to many undergraduates due to the logistical and financial challenges of in-person field trips. Field trips require a significant time commitment for both professors and students and can be disruptive of students' class and work schedules. They can also present difficulties with budget constraints, liability issues and transportation logistics (Behrendt & Franklin, 2014). These problems are exacerbated by the recent trend of increasing class sizes and tightening budgets at many U.S. universities (Diette & Raghav, 2015; Mitchell et al., 2016). Moreover, many schools face a lack of good field localities close to campus, making it nearly impossible to run effective in-person day or weekend trips.

A particularly acute problem with in-person geology field trips as they have traditionally been taught is their inaccessibility for people with disabilities. Geoscience is the least diverse STEM field and has one of the lowest rates of participation by persons with disabilities (Huntoon & Tanenbaum, 2015; Locke, 2005). Field-focused disciplines can be

intimidating to students who don't have prior experience in remote outdoor settings, and unfortunately this is particularly common amongst minorities and marginalized groups (Ghimire et al, 2014; Schwartz & Corkery, 2011; Sherman-Morris & McNeal, 2016). Students with disabilities are especially affected by this problem as there are often physical barriers preventing them from engaging in the outdoors (Carabajal et al., 2017; Hall et al., 2002). A lack of flexible and accessible learning environments and opportunities appears to be one of the principal factors in the underrepresentation of students with disabilities in geoscience (Atchison and Libarkin, 2016). Most existing literature on this problem suggests modifying field trips to make them accessible for disabled students. However, many of the projects and localities for higher-level geology field trips simply don't afford the option of making them accessible for students with mobility disabilities.

We believe that virtual field trips are an effective means of mitigating the logistical and financial challenges of in person field trips, providing an accessible alternative for disabled students, and maximizing the amount of field experiences students can have. They broaden access to field learning to schools that otherwise wouldn't have the funding or resources to run their own trips. They also allow students with disabilities to travel virtually to the best field sites, work with real datasets and analyze real-world geologic problems without impacting the educational experience for the rest of the class. We are not advocating that virtual field trips should totally replace in-person field trips. Rather, we believe they can be used to broaden access to field learning and also be used in conjunction with in-person trips to maximize the amount of field experiences students can have with limited time and budgets. They can also enhance in-person trips by allowing students to become familiar with

the geology of the area by watching a field video before they visit, thus reducing lecture time in the field, or watch it after to reinforce the concepts learned on the trip.

There are many published examples of geology virtual field trips made by other authors that have a range of teaching styles and use various technologies (e.g. Dolphin et al., 2019; Mead et al., 2019; Bursztyn et al., 2015; Lenkeit Meezan & Cuffey, 2012). Most use a combination of photos and short videos from field areas with some using more high-tech methods such as 3-D computer models, rotatable 360° images, and mobile learning games on smartphones. These virtual field trips appear to be quite effective, however the vast majority are for introductory geology courses and don't cover higher-level topics or require significant data analysis and interpretation on the part of the student. Our virtual field trips take a somewhat different approach as they are geared toward upper division students, opting for longer, more in-depth videos, giving the students real datasets from the field areas, and typically requiring fairly extensive data analysis and interpretation based directly on the field videos.

Design and Implementation

The virtual field trips presented in this paper were all originally in-person field trips and field exercises in upper division courses taught by Gans, and were adapted to be virtual during the lockdowns of the COVID pandemic in Fall 2020 and Winter 2021. Normally students would go to these field sites in person, be given an overview lecture and some guidance by the professor (Gans) at the beginning, and then make their own observations, collect their own data, and make interpretations based on these data and observations. Obviously, this was no longer possible for a virtual field trip. Instead, we attempted to

replicate this experience by providing high-quality videos from the field areas and combining them with exercises that give students experience analyzing and interpreting field data and observations. The style of trip varies depending on the topic being covered, with some being more "show-and-tell" and others requiring more data analysis and interpretation.

In addition to their application for an entirely virtual class, the field videos were also used the following year when the structural geology and physical volcanology classes were back to being in-person. In this case, students watched the videos prior to the in-person field exercises to familiarize them with the geology of the field locality and to show them how to collect the appropriate data for the project. The goal was to have the students be better prepared to hit the ground running and to minimize the amount of lecture time needed in the field so more time could be spent looking at the rocks. For the extended 4-day trip near the end of the class, students watched the field video after returning to solidify the concepts learned in the field and help them complete a worksheet and prepare for an exam on topics covered on the field trip.

Video production

The field videos were filmed on a consumer grade interchangeable-lens DSLR camera in 4k resolution using both a standard zoom and a wide-angle zoom lens (Figure 28a & 28b). Exposure settings were set manually for consistent results and both manual and auto focusing were used depending on the type of shot. Of particular importance was accurate representation of color and contrast so a white balance card was used during filming and minimal color and contrast adjustments were made when editing the footage (Figure 28c). Audio was recorded using a clip-on lavalier microphone with a remote transmitter for clear

real time in-camera audio recording (Figure 28d). A microphone wind-muff proved to be very helpful for reducing wind noise in outdoor environments. A tripod with a fluid head was typically used to ensure the footage was stable and allow for smooth panning (Figure 28f). The footage was edited in Adobe Premiere Pro and involved trimming clips, aligning them in the timeline, fine-tuning white balance and contrast, adjusting audio levels, and adding titles, annotations, animations, and figures.

Figure 28: Camera equipment used for filming the field trip videos. a) Mirrorless DSLR camera body. b) Wide angle and standard zoom lenses. c) White balance card. d) Clip-on lavalier microphone and remote audio transmitter. e) Lens filters. f) Tripod with fluid head.

Video content

The virtual field trips can be broadly divided into two types based on whether they are project-based or a "show-and-tell" style. For the project-based field trips, the videos focus on how to collect specific types of data or make specific types of observations relating to the project that the students then complete with data from the field area. Examples of this include how to collect orientations of joints and interpret their relative ages, how to collect data on fault surfaces and interpret slip sense, or how to interpret the relative ages and flow direction of lava flows. The "show-and-tell" style trips don't have a project associated with

them but instead aim to provide a detailed overview of the geology of an area, often focusing on concepts learned in the lecture material from the class.

In all the field videos we aim to walk students through how to approach each outcrop as if they were there: *What relationships are illustrated by the outcrop and what questions are raised by what you are seeing? What types of observations can be made to answer these? What types of data can be collected?* It is important that the students think critically about these types of questions rather than just being fed the answers. Of particular importance is differentiating between factual observations and interpretations, and clearly explaining what types of data and observations can support various interpretations. Additionally, many of the localities visited on the virtual field trips aren't "textbook" examples but instead provide real-world examples of typical rocks where the key features and relationships are usually much less apparent. This forces students to learn how to interpret geological relationships that aren't entirely obvious and gives them practice recognizing subtle clues and features.

A main goal of these virtual field trips was to provide students with as much of a real-world field experience as possible and a key component of fieldwork is the ability to look at the rocks at many different scales. To replicate this, we combined wide panoramic shots with footage of outcrops as well as close-up macro shots of hand-samples and in some cases even inserted photomicrographs from petrographic thin sections. The close-up macro shots have a particular advantage over in-person trips in that they allow the entire class to synchronously look closely at the same rock while being guided through its important features (Figure 29a). This is nearly impossible to do effectively in-person with a large class all trying to see fine details in a small hand-sample.

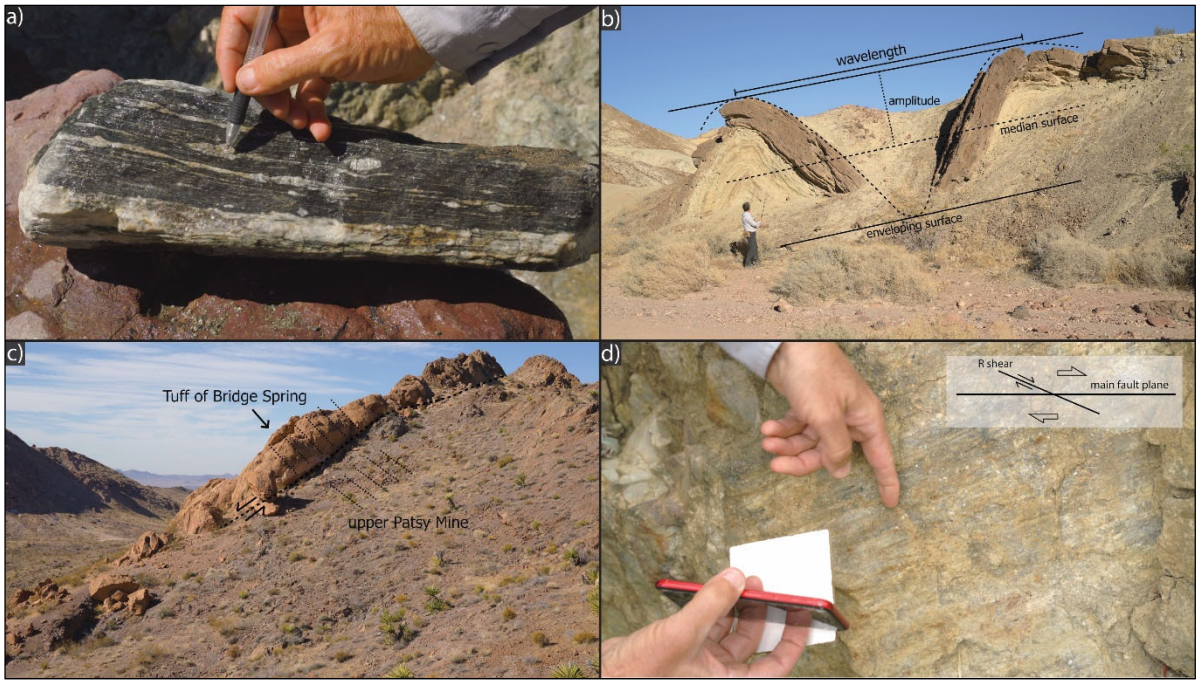

Figure 29: Screenshots from various virtual field trip videos that highlight some of the techniques used. a) Closeup shot of a hand sample. b) Annotations of a series of folds. c) Labels showing the different rock units, highlighting stratigraphy, and showing the location and sense of slip of a fault. d) Inset diagram showing the relationship of R-shears to the main fault plane.

The majority of the video footage was filmed in the field looking at the rocks, but interleaved PowerPoint style Zoom recordings were used to provide background and context to the field sites and to show maps, satellite imagery, photomicrographs, and other figures. This effectively replaces the use of posters in the field and provides the ability to quickly change perspective and "zoom out" to look at satellite imagery or maps or "zoom in" to look at photomicrographs of the rocks from the field areas. Annotations over the video footage are also used extensively to label features and areas of interest, show the traces of faults and folds, and highlight key points (Figure 29b). Particularly effective is their use in pointing out features in wide panoramic shots that would otherwise be hard to identify (Figure 29c). Figures and diagrams are also commonly inset directly into the videos to help clarify the material and relate it back to concepts learned in lecture (Figure 29d).

The videos are hosted on Vimeo for ad-free 4k open access viewing and can be accessed at https://vimeo.com/user130110709. The assignments and associated datasets can be accessed via the supplementary files of this paper and answer keys can be obtained by emailing the authors.

Assignments and deliverables

The assignments and deliverables associated with each virtual field trip vary considerably according to whether they fall into the into "show-and-tell" or project-based categories. The show-and-tell style field trips typically require students to fill out a simple worksheet or questionnaire while watching the video to motivate them to pay attention, reinforce the most important concepts, and encourage them to think critically about the topics being covered. They are designed to be relatively straight forward and don't require much more time than just watching the video itself. Timestamps for each of the questions are used to indicate where in the video each question is referring to, preventing confusion and making it easier for the students to navigate.

The project-based virtual field trips typically require that students analyze and interpret a dataset from the field area that is provided by the instructor and present their results as figures, maps or tables accompanied by a short report (Figure 30a and 30b). For the structural geology labs, the datasets that are provided to the students usually consist of tabulated structural data, such as orientations of bedding, joints, faults, fold axes etc. These data are georeferenced and thus can be easily plotted in Google Earth or stereonet software (Figure 30c). Project-based volcanology virtual field trips don't typically use structural datasets, but instead have the students interpret the field relationships from the videos, make

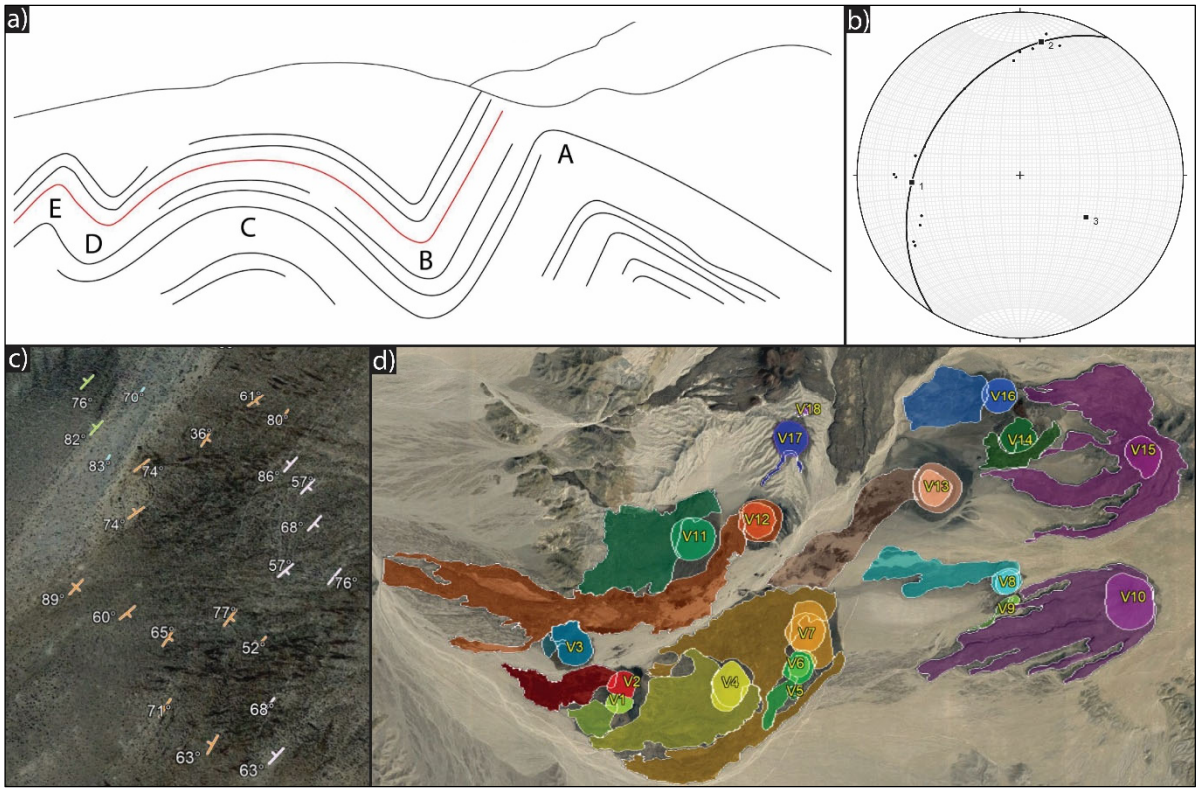

Figure 30: Examples of the types of deliverables and datasets that are used for the virtual field trips. a) Line drawing of a series of folds that was traced from a photo. b) Stereonet showing poles to bedding with a calculated cylindrical best fit fold axis. c) Georeferenced bedding orientations plotted in Google Earth. d) Geologic map of a portion of the Cima Volcanic Field made using Google Earth.

maps using Google Earth, examine photomicrographs of samples from the field areas, and so on (Figure 30d).

Field based exercises for Structural Geology

1) Structural analysis of the Monterey Formation at Ellwood and Hendry's Beaches

This virtual field exercise is designed to be an introduction on how to collect basic structural data in the field and use it to solve simple geologic problems. For the first part of the lab, students travel virtually to Ellwood Beach in Santa Barbara, California and are shown how to use a Brunton compass to collect bedding attitudes as well as how to calculate the thickness of a tilted stratigraphic section by constructing a simple map and cross section

(Figure 31a). The second part of the lab examines folds exposed in the wave cut terraces along Ellwood and Hendry's beaches. The field video includes various shots of the folds and discusses the types of structural data to collect and observations to make when working with folds in the field. Students are given real georeferenced datasets of bedding and fold axis orientations from the two field areas and tasked with 1) plotting the data on lower hemisphere stereographic projections (stereonets), 2) calculating fold axes from a cylindrical best fit to poles of folded bedding, 3) making simple geologic maps showing fold axis orientations and representative bedding attitudes, and 4) making a schematic cross section of one of the fold trains. By the end of this lab, students should be able to make observations in the field, collect basic structural data, calculate the true thickness of a tilted stratigraphic

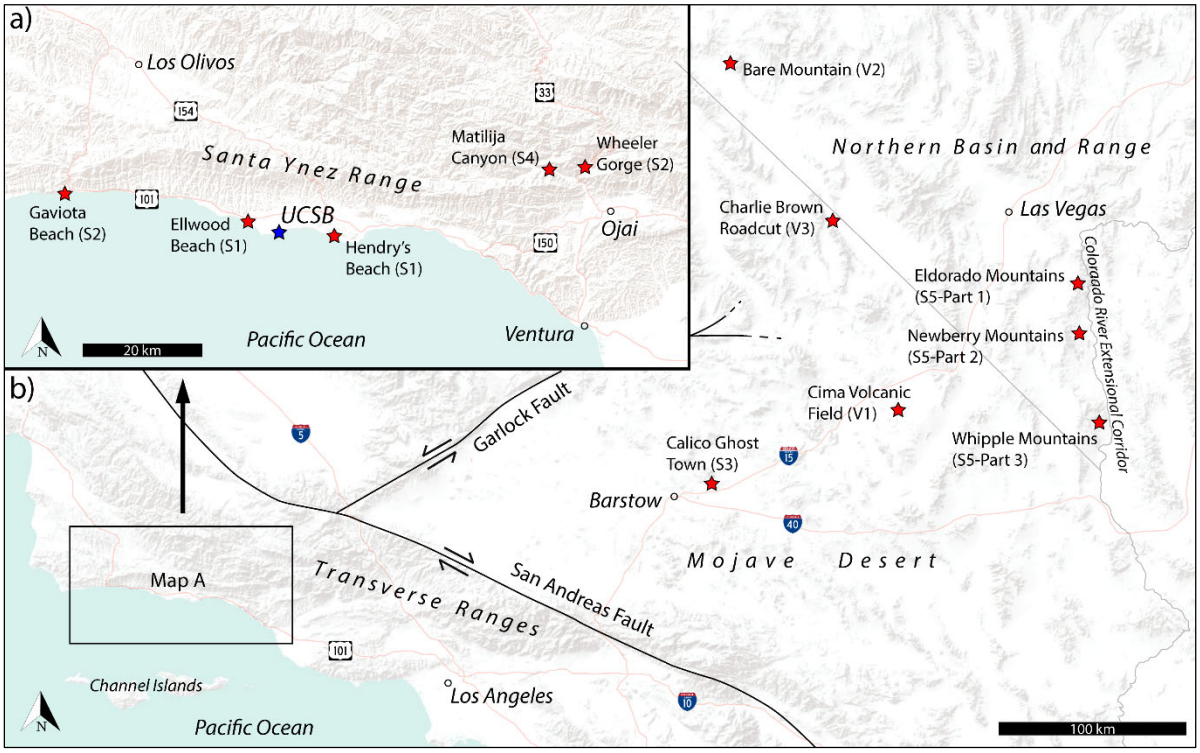

Figure 31: Maps showing the locations for each of the virtual field trips (red stars). Structure virtual field trips are labeled with (S-field trip number) and volcanology field trips are labeled with (V-field trip number). a) Map of the Santa Barbara area. b) Map of southeastern California and southern Nevada.

section, present structural data in stereonet format, calculate the orientation of a fold axis, and make a simple geologic map and cross section. The field video can be viewed at https://vimeo.com/664454133.

2) Analysis of joints in the Santa Ynez Range

This virtual field exercise investigates jointing in the Santa Ynez Range of the California Transverse Ranges and is designed to familiarize students with collecting joint data in the field and using this data to interpret joints in the context of a regional geologic framework. In the field video, students travel virtually to two localities in the Santa Ynez Range and are shown how to identify systematic joints, group them into distinct sets, collect their orientations, and interpret their relative ages (Figure 31a). The video also includes a brief tectonic history of the area and a discussion on how joints form and what they can tell us about paleo-stress fields. Students are given datasets of bedding and joint attitudes from the two localities and are tasked with 1) plotting the data in stereonets, 2) categorizing the joints into distinct sets, 3) rotating joint attitudes to determine their orientations prior to tilting of bedding and clockwise rotation of the range, 4) making an interpretation of the sequence of geologic events, and 5) writing a short report presenting their data and interpretations. The field video can be viewed at https://vimeo.com/670764679.

3) Structural analysis of folds near Calico Ghost Town, western Mojave Desert, CA

This virtual field exercise is focused on folds exposed near the Calico Ghost Town in the west-central Mojave Desert and teaches students the types of data to collect and observations to make when working with folds in the field and how to analyze and interpret this data (Figure 31b). The field video shows a number of outcrop scale folds with a variety

of morphologies and discusses the terminology that can be used to fully describe them (fold axis and axial surface orientations, interlimb angle, hinge angularity, wavelength and amplitude), the types of structural data that can be collected, and how to calculate the amount of shortening. For the lab exercise, students are given high-resolution images of an exceptionally well exposed train of folds as well as datasets of bedding orientations around the fold hinges and are tasked with 1) providing a complete description of each fold using all the appropriate fold parameters terminology, 2) calculating fold axis and axial surface orientations using stereonets, 3) making a simple line drawing overlay of the folds to calculate the amount of shortening, 4) interpreting the kinematic mechanisms of folding, and 5) writing a short report summarizing their observations and interpretations. The field video can be viewed at https://vimeo.com/682563005.

4) Kinematic analysis of fault slip-data associated with the Santa Ynez Fault

This site exposes a plethora of variably oriented small-scale faults with beautifully developed slickenlines in a Cretaceous conglomerate adjacent to the left-lateral/reverse Santa Ynez Fault near Ojai, California (Figure 31a). The virtual field trip is designed to familiarize students with recognizing assorted features on fault surfaces and collecting various data from faults, including fault plane and slickenline orientations and sense of slip criteria (Riedel shears). They then analyze the data from a large number of small-scale faults in the area using the FaultKin program (Allmendinger, 2019), and make interpretations on fault kinematics to determine if the small-scale faults are related to the nearby much larger Santa Ynez Fault. The video introduces the regional geology of the area and the slip history of the Santa Ynez Fault, and shows how to identify faults and slickenlines in the field,

measure their orientations, and interpret their senses of slip, and includes a short lecture on using FaultKin to perform a kinematic analysis of fault slip data. Students are given a dataset of fault plane and slickenline orientations and slip senses and tasked with making stereonet plots showing faults and striae, P and T axes, kinematic tensor axes, the best-fit fault plane solution, and tangent lineations. Students use these plots as figures in a geologic report that discusses the data and provides an interpretation on the kinematics of small-scale faulting at the site and how it relates to slip on the Santa Ynez Fault. The field video can be viewed at https://vimeo.com/672558015.

5) A virtual field trip through the lower Colorado River Extensional Corridor: Examining the interplay between magmatism and large magnitude extension in a failed continental rift

The Colorado River Extensional Corridor (CREC) is an area of large-magnitude extension along the California-Arizona border south of Las Vegas and is a world-class study site for investigations into extensional tectonics (Figure 31b). This three-part virtual field excursion to the CREC is designed to tie together many of the concepts covered throughout the structural geology course and apply them to a classic real world geologic/tectonic study area. The video consists of three parts ranging in length from 50 to 100 minutes and is mostly of a "show-and-tell" style. Some of the major topics covered include domino style rotational normal faulting, detachment faults and metamorphic core complexes, and the interplay between magmatism and extension in this failed continental rift. Not surprisingly, this wide-ranging virtual field excursion covers many additional topics, including tilted calderas, overturned unconformities, dike swarms and magmatic foliations as paleo stress and tilt indicators, and even what burros like to eat! Students are not required to complete

any major projects or reports but instead must fill out a lengthy questionnaire while watching to ensure they are understanding the concepts and engaged in the geology. By the end of this virtual field trip, students should have an in depth understanding of the geology of the CREC, have seen a wide array of brittle and ductile structures in their regional geologic context, and be confident in applying their newly acquired knowledge of structural geology to solve complex geologic problems. Throughout this video, students are forced to think about how various structural and stratigraphic features observed at outcrop scale help inform and constrain the broad geologic context of Miocene extension and magmatism in this part of the Basin and Range. The field videos can be viewed at https://vimeo.com/680624227.

Field based exercises for Physical Volcanology

1) Deciphering eruptive products and eruptive histories in young monogenetic basaltic cinder cones and lava flows of the Cima Volcanic Field, Mojave National Preserve

This virtual field investigation is focused on the southern portion of the Cima Volcanic Field in the eastern Mojave Desert and is designed to familiarize students with mapping and interpreting the products and eruptive histories of small monogenetic basaltic eruptions (Figure 31b). Eleven short georeferenced videos from various key locations in the volcanic field provide insight to what the different types of deposits look like, how to assess the relative ages of different lava flows and which vents they are associated with. Students are directed to carefully synthesize the information provided by the videos and use the site specific information as "clues", in conjunction with extensive analysis of Google Earth imagery at different magnifications and view obliquity to 1) make a geologic map of the

various vents and associated lava flows, 2) estimate the volumes of erupted magma from each vent, 3) determine the relative ages of 18 different vents and associated lava flows, and 4) write a report summarizing the eruptive history of the volcanic field. By the end of this exercise, students should be able to identify the different types of vent facies explosive deposits and effusive basalt flows, identify different vents and assess which lava flows were derived from them, interpret flow directions, relative ages, and evolution of the landscape, estimate volumes of erupted magma, and produce a highly professional geologic report on the physical volcanology of a young basaltic cinder cone and lava field. The field videos can be viewed at https://vimeo.com/822486501.

2) Ignimbrites associated with large-scale caldera forming eruptions and their internal zoning, associated fall and surge deposits, and map relations: An examination of Miocene ignimbrites from the SW Nevada volcanic field, southern Bare Mountain, NV

The southwest Nevada volcanic field is a classic example of multiple nested large-scale silicic caldera systems in the Basin and Range Province, and the outflow sheets from these calderas provide outstanding exposures of the different types of zonation observed in ignimbrites (Figure 31b). This virtual field trip takes students on a transect through four ignimbrites exposed in a canyon in southern Bare Mountain/Yucca Mountain and is designed to familiarize them with the internal stratigraphy of large ignimbrites. The video walks the viewers systemically up-section through the stack of ignimbrites and provides detailed descriptions of each of the different welding, glass preservation/devitrification, vapor phase alteration, and compositional zones in each ignimbrite. This virtual transect helps students appreciate the considerable variations in color, texture and crystal content in a

single ignimbrite and provides a conceptual basis for why these internal variations are observed. Students are given a suite of photomicrographs from the ignimbrites and are tasked with answering various questions about phenocryst assemblages, devitrification, vapor phase alteration, hydration, etc. By the end of this exercise students are familiar with the eruptive history of the southwestern Nevada volcanic field and are very comfortable identifying and describing the different internal zoning patterns of ignimbrites as well as identifying and discriminating other types of pyroclastic deposits. Specifically, students are shown excellent examples of fallout and surge deposits associated with each ignimbrite and learn to recognize the many compositional and textural features that distinguish these different types of pyroclastic deposits. The field video can be viewed at https://vimeo.com/807699601.

3) Geology of the Charlie Brown Roadcut, Resting Springs Range, CA: A virtual field trip and examination of Miocene silicic pyroclastic deposits and Basin-Range faulting in a roadcut along CA hwy. 178

The roadcut along the Charlie Brown Highway near Shoshone, California is an outstanding locality for looking at pyroclastic deposits and Basin and Range faulting and is a classic destination for geology field-trippers in the southwestern United States (Figure 31b). The fresh roadcut exposes a spectacular cross-sectional view of the Resting Spring ignimbrite, with its textbook zonation that would otherwise be covered with a thick coat of desert varnish. The ignimbrite buttresses against and is draped over an aesthetically pleasing normal fault scarp that cuts an older sequence of lakebed and pyroclastic deposits. This show-and-tell style virtual field trip teaches students how to describe ignimbrites, determine

the sense of slip and amount of offset of faults, and reconstruct the geologic history of an area. The field video begins by introducing the general layout of the roadcut, describing the different types of volcanic deposits exposed and characterizing the faults cutting them. Throughout the video, the viewers are challenged to "see what's there" and to think carefully about what the various stratigraphic and structural relations exposed in this outcrop imply about the sequence of geologic events. It then zooms in to thin-section scale and discusses a suite of photomicrographs from the different zones within the ignimbrites, highlighting various key features of each zone. It ends by proposing a sequence of geologic events that emphasizes how to use objective (factual) field observations to reconstruct a plausible interpretive geologic history of this very intriguing area. This exposure is a classic little geologic puzzle and there are many subtle details that are overlooked by most geology groups that stop here. We anticipate that this video will be widely used by many different groups including introductory classes – not just physical volcanology classes. The field video can be viewed at https://vimeo.com/822390940.

Evaluation

Methods

To assess the efficacy of the virtual field trips, students from the 2022 Structural Geology class were asked to complete a short anonymous survey with eleven questions about their general impressions of the videos. This class was taught with a hybrid model, with the first field exercise being fully remote and the others being in-person but with the field videos used to prepare the students prior to going to the field or to solidify their understanding after returning from the trip. The survey was hosted using the online survey

application SoGoSurvey and was given during the last week of class with all twenty-five students participating. It consisted of nine multiple choice and two short answer questions for more open-ended feedback. A shorter, more informal survey was given to the previous year's structural geology class that was fully remote but the volcanology class wasn't able to be surveyed.

Results

The results of the survey confirm that the students generally liked the field trip videos and thought they were effective at teaching them the skills and background (conceptual) material necessary for geologic fieldwork. The first three questions assessed their overall impression of the field videos as well as the quality of the video content and the filming and audio. The overwhelming majority of the students chose "excellent" for all three questions with 12-20% choosing "good" and none choosing neutral, bad or very bad (Figure 32a-c). It also appears that most of the students enjoyed watching the field videos more than a typical in-class lecture, with 64% agreeing with the statement, 28% feeling neutral and 8% disagreeing (Figure 32d). We believe that a big advantage of field videos is that they are more engaging and enjoyable to watch than a typical in-class lecture and this data supports this claim to an extent.

The next question assessed how effective the students thought the videos were at preparing them for collecting data and making observations during the in-person field exercises, and the majority of the students agreed with this statement, highlighting the videos' utility in being used in conjunction with in-person trips (Figure 32e). The majority of students also thought that watching the CREC video after returning from the in-person visit to the area helped solidify their understanding of the concepts learned while in the field

(Figure 32f). The hybrid model of combining in-person field trips with virtual field videos appears to be well received with the students with 96% either agreeing or strongly agreeing that it is an effective way of teaching field geology (Figure 32g).

The students' opinions of whether the field videos are an acceptable substitute for an in-person trip are much more mixed, with 36% disagreeing or strongly disagreeing with that statement (Figure 32h). This highlights that although these videos can be an effective way of teaching field geology to some extent, many students feel strongly that there is no good substitute for actually getting out into the field and interacting with the rocks directly.

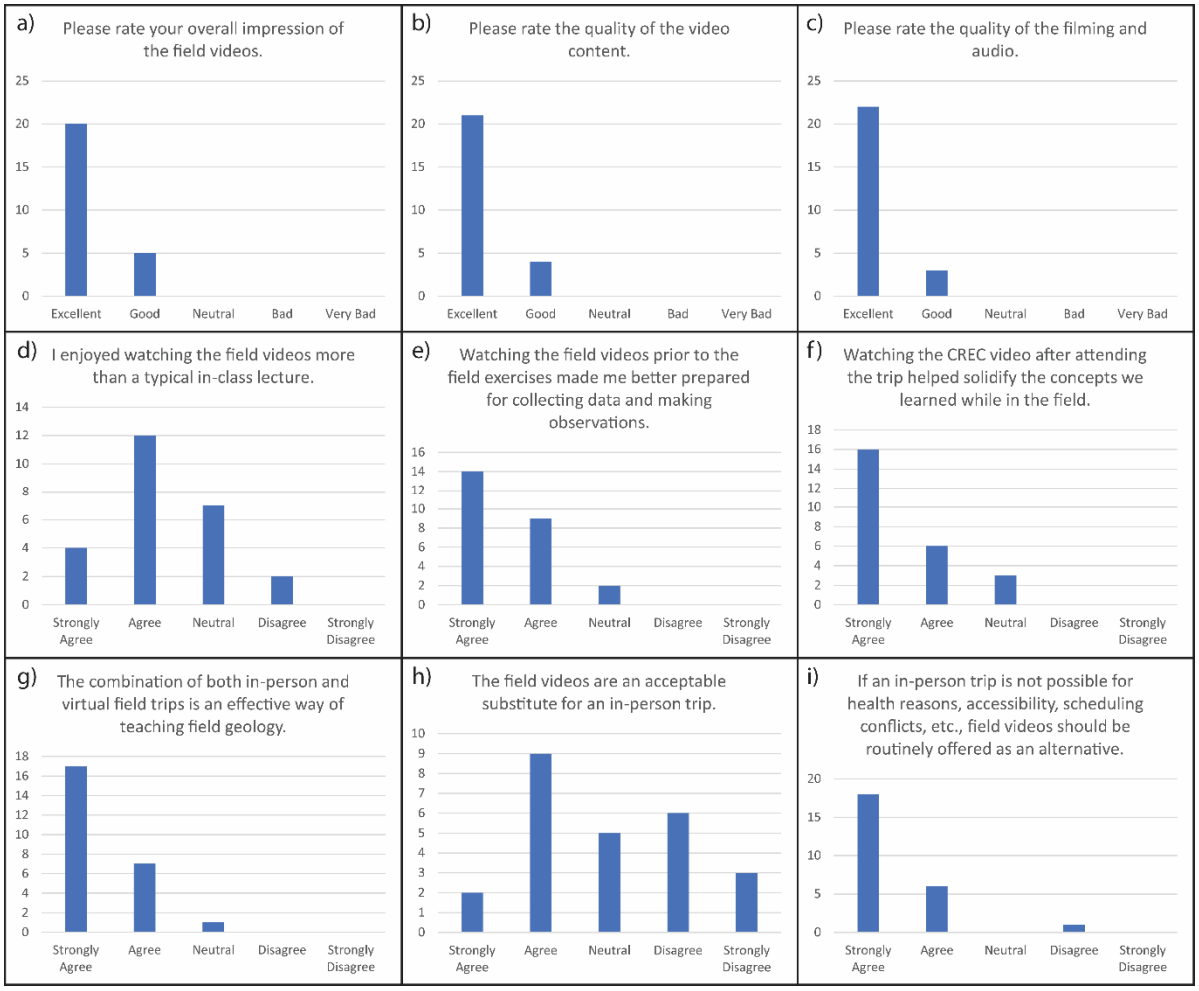

Figure 32: Responses from the survey given to the 2022 Structural Geology class to assess the efficacy of the virtual field trips.

However, the majority of the students do believe that if an in-person trip is not possible, field videos should be routinely offered as an alternative (Figure 32i). We believe that this is one of the biggest advantages and most important applications of these virtual field videos.

Perhaps the most important feedback that was received from the survey was from the two open ended questions. The first asked students what they liked about the field videos, and although there were a variety of responses there were a few common themes. Many students said that the ability to pause and rewind the videos was very helpful and allowed them to work at their own pace and take notes without rushing. The annotations and embedded figures were also viewed as being quite helpful at pointing out features and clarifying concepts, and is something that isn't possible with in-person trips. Students also enjoyed the variety of perspectives shown in the videos, especially the close-up shots of hand samples that pointed out the subtler features that can be easily missed. Many also noted that it was easier to pay attention to the content in the comfort of their home than while hot and tired in the field. The following response from one of the students summarizes much of the positive feedback that was received: "The videos were well produced and the content delivered was in-depth, well-structured and informative. These videos are not quite a full substitute for an in the field experience, but are extremely useful for a follow up to being out in the field. Being able to review the material covered in the field and being able to append notes taken in the field and reinforce concepts that might have not been quite solidified due to typical field work factors, like being hot or tired."

The second open ended question asked students what they thought could be improved with the virtual field trips. Many students thought some of the videos were too long at times and could be shortened a bit. We agree with this and believe the videos should

be as short and concise as possible without sacrificing too much content. As we reviewed the videos ourselves we also felt that they are too long and chalked this up to the fact that they were made at the last minute (under severe time pressure) with almost no preparation, and no prior experience in making such videos. Besides that, the narrator tends to be fairly long winded, or at least his kids say so! Adding more timestamps to make navigating through the videos easier was another common recommendation, especially for the longer videos. Other feedback included adding more figures, annotations and diagrams, transcribing the videos to make it easier to take notes and get the correct spelling of terms, and adding an inset map in the corner to show the location of each field spot and possibly have an interactive map that could be opened in Google Earth. Perhaps the most notable critique was that although the students thought field videos were good, there is no real substitute for being out in the field. This is summarized well by a comment from one of the students: “Field videos are great for just conveying information or teaching a lesson in structure, but we obviously wouldn't have had the experience of what it is really like to do field geology. I think that taking field measurements/camping/hiking/seeing y'all cook in the field is an important component of a field class. That being said, the videos were notably high quality and very informative.” We agree with this sentiment and believe that these videos are best used to augment in-person trips and only to fully replace them when absolutely necessary.

Limitations

Although the survey provided some informative feedback about the students’ impressions of the field videos, there are some limitations to this dataset. Most importantly,

only the hybrid class was able to be surveyed so we are lacking data from the class that did all the field trips completely virtually. This is unfortunate because this is one of the main ways these field trip videos can be used and it remains unclear how that group of students perceived the field videos. However, the hybrid class that was surveyed still did their first field trip completely virtually, so they did get some exposure to that type of application of the field videos. Another potential limitation of the dataset is that although the survey was completely anonymous, some students may have been compelled to answer questions more positively than they truly believe in order to "please" their TA and professor.

Perhaps the biggest limitation is that we had no quantitative way of assessing what the true educational benefit was to online field instruction versus in-person field instruction. Our own judgement based on performance on comprehensive exams following one year of structural geology where the field trips and exercises were entirely remote (virtual) and the subsequent year where they were almost entirely in-person but were supplemented by the virtual field trip videos is that the students had a far superior grasp of the topical material covered by the field trips and exercises when they had in-person experience supplemented by the videos than when it was entirely virtual, even better than previous years when only the in-person option was available. Ideally, we would try both methods independently on large (statistically meaningful) control groups and then assess how much each group learned in terms of concepts and in their abilities to solve field based geologic problems. Our suspicion is that both groups might be fairly similar in terms of their conceptual understanding but that the in-person group would be far better equipped to undertake original geologic investigations in the field. We believe that in-person instruction supplemented by the field videos is the best possible approach.

Discussion

Benefits of virtual field trips

Although virtual field trips will never be a total replacement for in-person trips, they do have a number of unique advantages that make them quite useful in many situations. Most obvious is that they alleviate the issues of insufficient funding, extensive time commitment, and the logistical difficulties of in-person trips. This is especially important for schools with limited budgets or a lack of good field localities close to campus. They also afford the ability to travel virtually to inaccessible places that wouldn't be feasible to take an entire class. They offer greater flexibility than in-person trips and provide an alternative for students with disabilities or for students that can't attend due to illness or family/personal emergencies. When used in conjunction with in-person trips, they allow students to be better prepared prior to going out in the field or can be used to solidify the concepts after returning from a field trip.

In addition to the logistical, financial and accessibility advantages of virtual field trips, they also have a number of pedagogical benefits that aid in teaching field geology. The ability to pause and rewind allows students to work at their own pace and take detailed notes without rushing. Annotations and labels clarify the locations of features that are often hard to point out in person. Moreover, inset figures and text can be seamlessly incorporated into the videos and the interleaved PowerPoint slides allow for quick transitions to map views or photomicrographs of the rocks. A common problem with in-person trips is that it is hard to hear the speaker, especially in windy conditions, or see exactly what they are pointing out. These problems are alleviated with the high-quality audio from the clip-on lavalier microphone and annotations/pointers in the video footage. Lastly, the videos also can always

have the best vantage point for viewing an outcrop and allow for close up descriptions of rocks that aren't possible with an entire class in-person.

Drawbacks of virtual field trips

Although effective in many ways, virtual field trips have a number of drawbacks when compared to in-person trips. Most important is the inability for students to see the rocks in person, explore the area on their own, and collect their own data. Without this first-hand direct interaction with the rocks, students will never be fully prepared to do fieldwork on their own. This problem is inherent to all virtual field trips and can only be mitigated by providing in-person trips in addition to virtual trips. Another issue is that it is difficult to convey the scale and three-dimensional aspects of objects in a two-dimensional video. Providing a variety of perspectives and different scales in the video footage reduces but does not completely eliminate this problem. Students also aren't able to ask questions in real time when watching the field videos. Moreover, virtual field trips generally don't provide the opportunity for students to socialize with their peers, work in teams in the field and have one-on-one interactions with their TAs and professors. This can be mitigated by having open chat room discussions or having students work together in groups. Lastly, virtual field trips aren't as immersive and generally don't provide the same opportunity to appreciate the natural world as in-person trips.

Recommendations for future virtual field trips

After producing these virtual field trips and receiving feedback from our students, there are a number of recommendations that we have for future virtual field trip videos. First, we believe that the videos should be as short as possible without losing an excessive

amount of content. It can be tough for anyone to sit in front of a computer screen and watch someone talk for extended periods of time without losing focus, and many of the students stated that some of the videos were too lengthy. Adding more timestamps to make it easier to navigate the longer videos would also help alleviate this problem. More diagrams, annotations, and labels would also make the videos more engaging to watch and easier to understand. Adding more close-up shots of rocks would also be helpful and allow the students to see the smaller details that they normally would in the field with their hand lens.

Perhaps the most significant improvement on the virtual field trips would be to make them more interactive. Although many of the projects require extensive critical thinking and data analysis, most of the videos that we produced did not require that the students think all that much for themselves or make their own independent observations to solve geologic problems while watching. Observations and data are often described to the viewer and an appropriate interpretation is proposed without providing adequate time for the viewer to make their own hypothesis first. Rather than just feeding the viewer information, future videos could pause and encourage the viewer to come up with their own ideas by asking questions such as “What do you see?” and “How do you interpret what you see?”. This active learning would not only make the videos more engaging to watch, but would also give the students first-hand experience figuring out geologic problems as if they were in the field themselves.

Conclusions

1. Virtual field trips and field exercises for upper division courses in structural geology and volcanology can provide an alternative to in-person trips when an in-person trip

isn’t possible due to logistical issues, insufficient funding, health concerns, accessibility, etc.

2. Field trip videos are effective at augmenting in-person trips by better preparing the students prior to the trip or solidifying what they learned after returning.
3. Virtual field trips have both advantages and disadvantages over in-person trips but will never be a total replacement for in-person trips.

References

Allmendinger, R.W. (2019). FaultKin 8 [Computer software]. Retrieved from www.rickallmendinger.net

Atchison, C. L., & Libarkin, J. C. (2016). Professionally held perceptions about the accessibility of the geosciences. *Geosphere*, *12*(4), 1154-1165. https://doi.org/10.1130/GES01264.1

Behrendt, M., & Franklin, T. (2014). A review of research on school field trips and their value in education. *International Journal of Environmental and Science Education*, *9*(3), 235-245.

Bursztyn, N., Pederson, J., Shelton, B., Walker, A., & Campbell, T. (2015). Utilizing Geo-Referenced Mobile Game Technology for Universally Accessible Virtual Geology Field Trips. *International Journal of Education in Mathematics, Science and Technology*, *3*(2), 93-100.

Carabajal, I. G., Marshall, A. M., & Atchison, C. L. (2017). A synthesis of instructional strategies in geoscience education literature that address barriers to inclusion for students with disabilities. *Journal of Geoscience Education*, *65*(4), 531-541. https://doi.org/10.5408/16-211.1

Diette, T. M., & Raghav, M. (2015). Class size matters: Heterogeneous effects of larger classes on college student learning. *Eastern Economic Journal*, *41*, 273-283. https://doi.org/10.1057/eej.2014.31

Dolphin, G., Dutchak, A., Karchewski, B., & Cooper, J. (2019). Virtual field experiences in introductory geology: Addressing a capacity problem, but finding a pedagogical one. *Journal of Geoscience Education*, *67*(2), 114-130. https://doi.org/10.1080/10899995.2018.1547034

Elkins, J. T., & Elkins, N. M. (2007). Teaching geology in the field: Significant geoscience concept gains in entirely field-based introductory geology courses. *Journal of geoscience education*, *55*(2), 126-132. https://doi.org/10.5408/1089-9995-55.2.126

Ghimire, R., Green, G. T., Poudyal, N. C., & Cordell, H. K. (2014). An analysis of perceived constraints to outdoor recreation. *Journal of Park and Recreation Administration*, *32*(4), 52-67.

Hall, T., Healey, M., & Harrison, M. (2002). Fieldwork and disabled students: discourses of exclusion and inclusion. *Transactions of the Institute of British Geographers*, *27*(2), 213-231. https://doi.org/10.1111/1475-5661.00050

Huntoon, J. E., & Tanenbaum, C. (2015). Increasing diversity in the geosciences. *Eos*, *96*(5). https://doi.org/10.1029/2015EO025897

Hutchins, E., & Renner, N. (2012). Situated and embodied learning in the field. In K. A. Kastens & C. A. Manduca (Eds.), *Earth and mind II: A synthesis on research on thinking and learning in the geosciences: Geological society of America special paper 486*. (Vol. 2, pp. 181–182). Geological Society of America. https://doi.org/10.1130/2012.2486(30)

Kastens, K. A., & Ishikawa, T. (2006). Spatial thinking in the geosciences and cognitive sciences: A cross-disciplinary look at the intersection of the two fields. In C. A. Manduca & D. W. Mogk (Eds.) *Earth and mind; how geologists think and learn about the Earth: Geological society of America special paper 413.* (pp. 53-76). Geological Society of America. https://doi.org/10.1130/2006.2413(05)

Lenkeit Meezan, K. A., & Cuffey, K. (2012). Virtual field trips for introductory geoscience classes. *The California Geographer, 52,* 71-88.

Locke, S. (2005). The status of persons with disabilities in the geosciences. In *Regional Alliance for Science, Engineering, and Mathematics Squared (RASEM2) Symposium. Las Cruces, NM: New Mexico State University*.

Mead, C., Buxner, S., Bruce, G., Taylor, W., Semken, S., & Anbar, A. D. (2019). Immersive, interactive virtual field trips promote science learning. *Journal of Geoscience Education*, *67*(2), 131-142. https://doi.org/10.1080/10899995.2019.1565285

Mitchell, M., Leachman, M., & Masterson, K. (2016). Funding down, tuition up: State cuts to higher education threaten quality and affordability at public colleges. Center on Budget and Policy Priorities.

Mogk, D. W., & Goodwin, C. (2012). Learning in the field: Synthesis of research on thinking and learning in the geosciences. In K. A. Kastens & C. A. Manduca (Eds.), *Earth and mind II: A synthesis on research on thinking and learning in the geosciences: Geological society of America special paper 486*. (Vol. 2, pp. 131–163). Geological Society of America. https://doi.org/10.1130/2012.2486(24)

Petcovic, H. L., Stokes, A., & Caulkins, J. L. (2014). Geoscientists' perceptions of the value of undergraduate field education. *GSA Today*, *24*(7), 4-10. https://doi.org/10.1130/GSATG196A.1

Schwartz, A., & Corkery, M. R. (2011). Barriers to participation among underrepresented populations in outdoor programs. *Recreational Sports Journal*, *35*(2), 130-144. https://doi.org/10.1123/rsj.35.2.130

Sherman-Morris, K., & McNeal, K. S. (2016). Understanding perceptions of the geosciences among minority and nonminority undergraduate students. *Journal of Geoscience Education*, *64*(2), 147-156. https://doi.org/10.5408/15-112.1